University of Alberta

Implementation of MR Image-Guided Adaptive Brachytherapy for Cervix Cancer

by

Jiyun Ren

A thesis submitted to the Faculty of Graduate Studies and Research
in partial fulfillment of the requirements for the degree of

Master of Science
in
Medical Physics

Department of Physics

Fall 2011
Edmonton, Alberta

Abstract

Currently, the Cross Cancer Institute uses CT imaging in conjunction with the traditional Manchester system, which prescribes dose to a defined point, for cervix cancer brachytherapy. To take advantage of MRI for enhanced definition of soft tissue including the cancerous tissue itself, this thesis focuses on a study of MR image-guided cervix brachytherapy. Firstly, the geometric distortions of an applicator in an MR image and the accuracy of CT-MRI registration were quantitatively evaluated with a custom-made phantom, which provides one measure of the MRI distortion and indicates a CT-MRI registration method for cervix brachytherapy. The remaining part of the thesis describes an optimization method - simulated annealing (SA) - for automatically determining the dwell time configuration based on a set of specified dose-volume constraints. Application to a computer simulation model showed that SA was effective when the model structure sizes and distances are in a normal range. The effects on the optimization of different initial dwell times and a different initial number of dwell positions were also investigated. In general, optimization conformed dose to the target and significantly reduced dose to surrounding normal tissue.

Acknowledgements

I would like to thank my supervisors Dr. Ron Sloboda and Dr. Geetha Menon for all their support, encouragement, and patience along the way. They were very generous with their time and always ready to offer assistance. Huge thanks to Dr. Sloboda for his guidance and great assistance in writing the thesis and the conference abstracts. Talking with Dr. sloboda from project overview to physics principle to algorithm details always benefited me greatly. His guidance and encouragement were vital to my ability to complete this research. Huge thanks to Dr. Menon for her comments on writing the thesis and help with the BrachyVison treatment planning system. Geetha was also a great person to talk to about any subject be it physics, career, or personal. Without her support the research would not have been possible.

Thanks to Kieth for his help in acquiring MR image of the phantom which took a long time for scanning. Thanks to Lori for her help in acquiring CT image of the phantom. Lori was always ready to offer assistance. Thanks to Gary in the machine shop for making the special phantom for this research.

I would like to thank to the students and the staff of the Medical Physics department at the Cross Cancer Institute, especially Lori, Katie, and Jennifer, for their friendship, making this an enjoyable period of my life.

And finally, I am grateful to my family members, for their continuing support over the years.

Table of Contents

List of Tables

List of Figures

List of Abbreviations

2D	Two-dimensional
3D	Three-dimensional
AP	Anterior-Posterior
BED	Biologically Effective Dose
BT	Brachytherapy
CCI	Cross Cancer Institute
COIN	Conformal Index
CN	Conformation Number
CT	Computed Tomography
CTV	Clinical Target Volume
D90	The isodose that includes 90% of an anatomic structure
D100	The isodose that includes 100% of an anatomic structure
$D_{0.1cc}$	Minimum dose in the most exposed 0.1 cm^3 of an anatomic structure
D_{2cc}	Minimum dose in the most exposed 2 cm^3 of an anatomic structure
DVH	Dose Volume Histogram
EBRT	External Beam Radiation Therapy
EMBRACE	An Int**E**rnational study on **M**RI-guided **BRA**chytherapy in Locally Advanced **CE**rvical Cancer
ESTRO	European Society for Therapeutic Radiology and Oncology
EQD_2	Equivalent dose in 2 Gy fractions
FSD	Fletcher Suit Delclos
GEC	Groupe Européen de Curiethérapie

GTV	Gross Tumour Volume
GYN	Gynecology
HDR	High Dose Rate
HR-CTV	High Risk-Clinical Target Volume
HS	Henschke Shielded cervix applicator
HVL	Half-Value Layer
ICRU	International Commission on Radiation Units and Measurements
IGBT	Image-Guided Brachytherapy
IR-CTV	Intermediate Risk-Clinical Target Volume
LDR	Low Dose Rate
LQ	Linear-Quadratic
MRI	Magnetic Resonance Imaging
NCRP	National Council on Radiation Protection and Measurements
PMMA	Polymethyl Methacrylate
SA	Simulated Annealing
SLDR	Selectron LDR
OAR	Organ at Risk
PDR	Pulsed Dose Rate
PTV	Planning Target Volume
TRAK	Total Reference Air Kerma
T&O	Tandem and Ovoid
V100	Percentage of an anatomic structure receiving 100% of the prescribed dose

Chapter 1 Introduction

1.1 Cancer Treatment

1.1.1 Overview

The primary choice for treating solid tumors is surgery as it can eradicate the whole tumor under some circumstances. Two other commonly used treatment methods, radiation therapy and chemotherapy, also play important roles in assisting the curative treatment of many forms of cancer, as well as controlling disease and relieving symptoms when surgery is not applicable. These methods can be used alone or in combination with one another. The selection depends on several factors such as type of cancer, stage of the disease, general health of the patient, and involvement of other treatments.

Radiation therapy uses ionizing radiation to kill cancer cells, or impede their growth. This type of treatment can be given in two ways: external beam radiation therapy (EBRT), applied with the use of a radiation therapy machine; and internal radiation therapy, also called brachytherapy (BT), applied with one or more small sources of radioactive material inserted or implanted in the body.

Although not as widely used as EBRT, BT has its own advantage in that, with the radioactive sources placed in proximity to the tumor volume (or even within the tumor), it allows a very high central dose concentrated in a small area / tumor, while there is a rapid dose fall-off in the surrounding normal tissue. This technique is commonly used for treatment of prostate and gynecological (cervix, uterus or vagina) cancers.

1.1.2 Three Types of Brachytherapy

Depending on the different methods of source application, there are three types of brachytherapy [Khan 2003]:

a. Surface application (rarely used now), where plastic molds are prepared to conform to the surface to be treated and the sources securely positioned on the outer surface of the mold; used to treat small superficial areas.

b. Interstitial implantation, in which the radioactive sources are fabricated in the form of needles, wires, or seeds, which can be inserted directly into the tissue; utilized when the tumor is well-localized. Interstitial implants can be temporary or permanent, depending on the radioactive half-life of the radionuclide.

c. Intracavitary insertion, in which applicators containing radioactive sources are introduced into body cavities (such as the vagina, uterus, or nasopharynx) to irradiate the walls of the cavity or nearby tissues. Usually the radioactive source is loaded into a previously inserted applicator. Intracavitary brachytherapy used in gynecology will be described in the following section.

1.1.3 Intracavitary Brachytherapy in Gynecology

Since the first treatment of uterus cancer with radium in 1908 [Johns and Cunningham 1983], intracavitary brachytherapy has evolved into the treatment of choice for cancers of the uterine cervix, uterine body, and vagina [Khan 2003]. Concomitant chemoradiation followed by brachytherapy represents the standard of care in patients with locally advanced cervical cancer (tumors larger than 4 cm, i.e. stage IB2 through stage IVA). For stage IB1, brachytherapy is used as a treatment option in combination with external beam RT, or as a preoperative treatment in combination with colpohysterectomy and lymphadenectomy. If radiotherapy is considered, brachytherapy is generally a major part of the

treatment, delivering substantial dose to the tumor in the central pelvis while sparing the surrounding organs at risk [Haie-Meder *et al.* 2005].

1.2 Brachytherapy Treatment Techniques

Technical developments have played essential roles in the evolvement of gynecological brachytherapy: the introduction of artificial isotopes, afterloading devices to reduce personnel exposure, and automatic devices with remote control to deliver controlled radiation exposure from high-activity sources [Khan 2003].

1.2.1 Radionuclides for Intracavitary Insertion

Since its discovery in 1898, ^{226}Ra (radium) has been used in brachytherapy until fairly recently. In consideration of radiation protection, ^{226}Ra was replaced by γ–emitters of lower energy. With these radium substitutes, shielding issues are reduced and the risk of radon contamination is avoided. One of the substitutes most commonly used is ^{137}Cs, because the scattering and attenuation characteristics of ^{137}Cs γ rays in tissue balance one another similarly to ^{226}Ra γ rays, providing very nearly the same relative dose distribution [Khan 2003]. By proper choice of activity of the ^{137}Cs sources, the ^{226}Ra dose distribution could be well approximated.

At our institution an ^{192}Ir source is used for pulsed dose rate (PDR) treatment. ^{192}Ir has a complicated γ ray spectrum with an average energy of 0.38 MeV. Because of the substantially lower energy compared to ^{226}Ra (HVL of 14 mm lead) and ^{137}Cs (HVL of 5.5 mm lead), an ^{192}Ir source requires less shielding for personnel protection (HVL of 2.5 mm lead). ^{192}Ir has the disadvantage of a short half-life (73.8 days). However, the half-life is long compared to the average treatment time such that the sources can be used in temporary implants, similar to radium and cesium [Khan 2003]. The activity varies by only a few percent over

the duration of an average treatment. The exposure rate constant Γ_δ is 4.69 $R \cdot cm^2 \cdot h^{-1} \cdot m \cdot Ci^{-1}$ [Glasgow and Dillman 1979].

1.2.2 Dose Rates: LDR, HDR, and PDR

1.2.2.1 LDR

In conventional brachytherapy with ^{226}Ra or ^{137}Cs sources, the dose rate at the point or surface, where the dose is prescribed, lies between 0.4 and 2 Gy/hour and is referred to as low dose rate (LDR) brachytherapy [ICRU 1985]. Compared to EBRT, LDR brachytherapy allows additional sparing of normal tissues and maximizes the therapeutic ratio (ratio of the maximally tolerated dose to the minimally curative or effective dose) by taking advantage of a radiobiological principle known as the dose-rate effect: as the dose rate is lowered, there is a reduction in the cell mortality from a given dose of radiation. This reduction in cell mortality occurs preferentially in normal tissues and allows higher doses of radiation to be given without a concomitant increase in normal tissue complications [Logsdon and Eifel 1999].

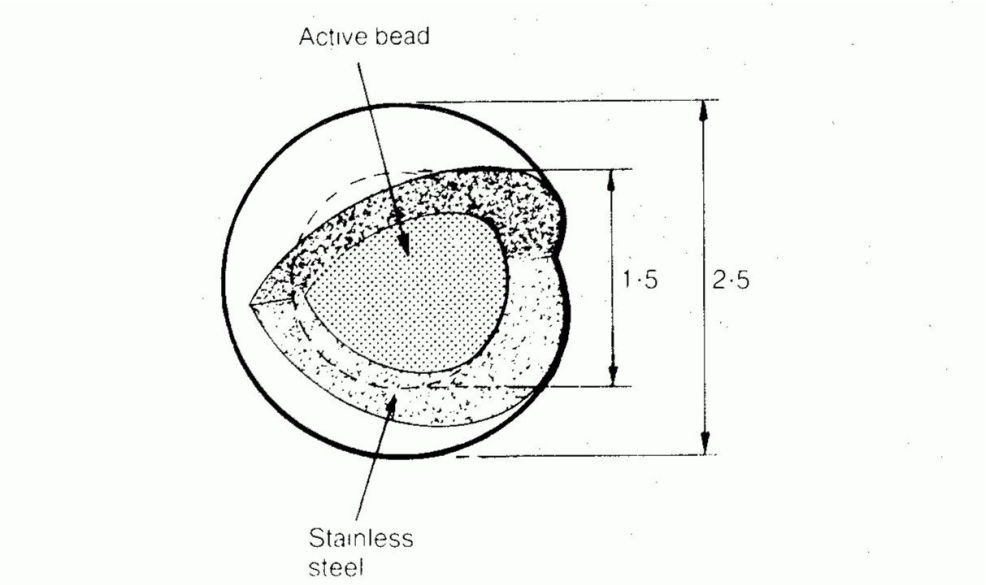

Figure 1-1. Spherical ^{137}Cs source as used in the Selectron afterloading system (distances in mm).

1.2.2.2 HDR

With the introduction of remote afterloading devices (see Section 1.2.3), it is possible to deliver treatment at a very high dose rate (HDR), which is classified by ICRU Report 38 [ICRU 1985] to be 20 cGy/min or higher. The total treatment time is hence significantly reduced with HDR.

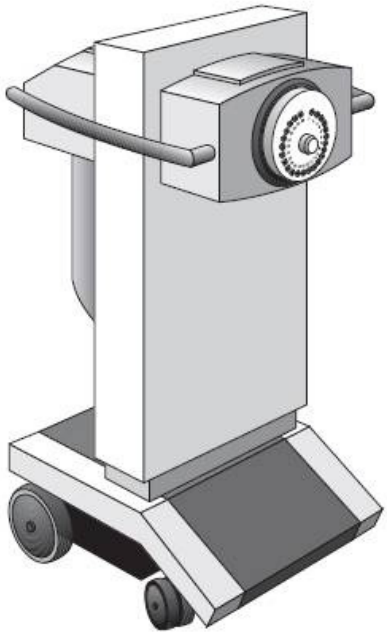

Figure 1-2. Varian GammaMed-Plus HDR and PDR afterloader.

HDR remote afterloading, with its shorter treatment time, has the advantage of allowing for better patient immobilization, treating a larger patient population (which would otherwise require prolonged hospitalization if treated by LDR brachytherapy) and providing the convenience of treating on an outpatient basis. However, the question of how HDR compares with LDR in terms of clinical outcomes is a rather controversial issue, because the outcome data, i.e. survival rates and early and late tissue complication rates, are not yet sufficiently complete for the HDR technique to date to draw definitive conclusions [Khan 2003].

1.2.2.3 PDR

As the majority of clinical experience in brachytherapy has been obtained with LDR brachytherapy, PDR brachytherapy has been developed to simulate continuous LDR treatments by means of delivering the same total dose in the same total time, and thus provides a radiobiologically equivalent treatment as LDR. With a higher activity source (typically 1 Ci) than used for conventional LDR brachytherapy, PDR treatment is accomplished by exposing the source from the afterloader for only a fraction of the time, termed the pulse time, during a repeated period, termed the pulse interval. The most commonly used pulse interval is one hour.

PDR allows for nursing care during the time between treatment pulses, and also permits visitation without extending the treatment time. Another advantage is the ability to achieve greater conformation of the dose to the treatment volume than is possible with LDR [Horton *et al.* 2005a]. The principal difference between PDR and HDR remote afterloading units is the lower activity of a PDR source (approximately 0.5-2.0 Ci) at installation compared to a HDR source (approximately 10 Ci at installation) and the fractionation scheme.

1.2.3 Afterloading Techniques

Brachytherapy is nowadays mostly practiced with afterloading techniques, in which unloaded applicators or catheters are placed in the patient prior to treatment, according to a chosen plan. Sources are inserted later, after the position of the applicators has been radiographically checked using dummy sources. The dose distribution can also be computed so that the position of the applicators can be corrected if necessary before the sources are inserted.

Historically, afterloading techniques required manual handling of radioactive material during the preparation and loading of the sources into previously inserted applicators. This resulted in patients and staff being exposed to radiation hazards

[Khan 2003]. Later, restrictions on radiation exposure resulted in the development of remote afterloading techniques, which are most commonly achieved by moving a single radioactive source, welded to the end of a flexible wire, through the applicator channels. Source insertion and removal are controlled by a remote control panel, thus eliminating direct handling of the radioactive source. In addition, the source can be rapidly loaded and unloaded, making it possible to provide patient care with the source retracted into its shielded position [Khan 2003]. While either manual or mechanical afterloading techniques may be used for LDR applications, remote afterloading techniques are mandatory for HDR or PDR applications. The introduction of remote afterloading techniques resulted in a significant improvement in radiation protection for staff [ICRU 1985].

1.2.4 Uterine Cervix Applicators

To maintain the proper geometrical positioning of sources, the traditional Manchester system (see Section 1.3.1) used a rubber uterine tandem to hold one to three radium tubes, and rubber ovoids separated by a rubber spacer to each hold a radium tube [Khan 2003]. Modern LDR tandem and ovoid applicators (see Figure 1-3(B)) utilize ^{137}Cs in the form of tubes or pellets as radiation sources. Because of the large physical source sizes, the applicators themselves were bulky and uncomfortable for the patient to endure [Rownd 2005].

The relatively smaller size of ^{192}Ir HDR/PDR sources allowed the physical size of the applicators to be reduced, specifically the tandem diameter, from approximately 6 mm in LDR applicators to 3 mm in HDR/PDR applicators (Figure 1-3(B)) [Rownd 2005]. At present, Fletcher Suit Delclos (FSD), Henschke shielded (HS), and Manchester-style applicators are the most commonly used applicator systems [Horton *et al.* 2005b, Thirion *et al.* 2005] (see Section 2.2.3 and 2.4.4 for Manchester-style and HS applicator details). Generally in these applicators the tandem and ovoid catheters are made of stainless steel and permit remote afterloading of the sources [Khan 2003]. To be compatible with

Figure 1-3. Tandem & ovoid applicators: (A) Manchester-style; (B) Fletcher LDR (lower part) and HDR (upper part) applicator (from Rownd 2005); (C) Henschke applicator (designed for Nucletron low-dose-rate Selectron afterloading system, from Thirion et al. 2005).

both MRI and CT, titanium or composite fiber tubing is recommended because it is neither ferromagnetic nor produces serious artifacts in CT images (low atomic-number material with less photoelectric interactions) [Thomadsen 2005]. The source is movable within the tandem with the remote afterloader, but normally dwells at the geometric center of each ovoid. The dwell positions and dwell times of the source are programmable to achieve the planned dose distribution.

1.2.5 Imaging for Cervix Brachytherapy

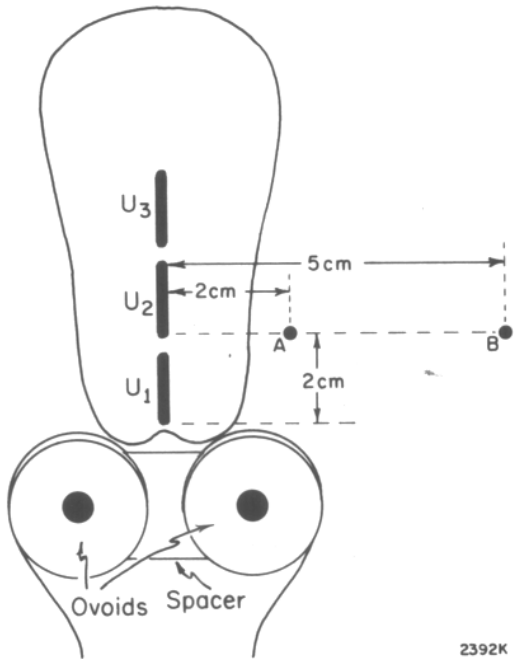

Figure 1-4. Schematic diagram of the uterus showing the use of an intrauterine tube and ovoids in the treatment of cancer of the uterus. Radiation sources U_1, U_2, and U_3 lie within the intrauterine tube. A single radiation source within each ovoid is oriented with its axis perpendicular to the plane of the page. From Johns and Cunningham 1983.

Originally the treatment of cervix cancer was based primarily on clinical considerations, and these were of necessity empirical [Johns and Cunningham 1983]. The treatment technique used an applicator designed to simplify dosage

calculations (Figure 1-4). Without an imaging technique to assist in localizing the radiation sources, the applicator geometry and the isodose distribution were assumed to be "ideal" in the Manchester system [Johns and Cunningham 1983]. The problem with this original treatment approach was that the uterus may be eccentric for reasons of anatomy or as the result of disease. The uterine tube is therefore unlikely to be arranged in the ideal position of Figure 1-4 [Johns and Cunningham 1983]. After x-rays became widely available, conventional radiographic films (Figure 1-5(A)) were used to check the localization of the sources to improve the accuracy of dose calculation (see Section 2.2 for details).

As a 3D imaging technique, computed tomography (CT) offers accurate localization of intracavitary applicators and can show the 3D relationship of the applicators to neighboring anatomic structures, thereby obtaining the dose delivered to the target volume and neighboring organs. However, CT images have significant limitations in visualizing soft tissue. It is very difficult to separate cervical tissue from the uterus, bladder, and rectum or to ascertain where the cervix ends and the vagina begins on CT images [Nag *et al.* 2004]. Target contours on CT can significantly overestimate the tumor width, resulting in significant differences in dose parameters D90, D100, and V100 (see Section 2.4.1.2 for definitions) for the high risk-clinical target volume (HR-CTV) compared with those obtained using MRI [Viswanathan *et al.* 2007].

Magnetic resonance imaging (MRI) offers superior soft tissue contrast, enabling visualization of the cervical tumor size and volume, distinction of tumor from normal uterus and cervix, and definition of parametrial and vaginal infiltration of the disease. MRI remains the standard for CTV definition [Viswanathan *et al.* 2007]. However, a titanium applicator is poorly visualized in MRI due to magnetic susceptibility artifacts arising from this metallic material. Hence CT-MRI fusion is required in this case to define the applicator geometry.

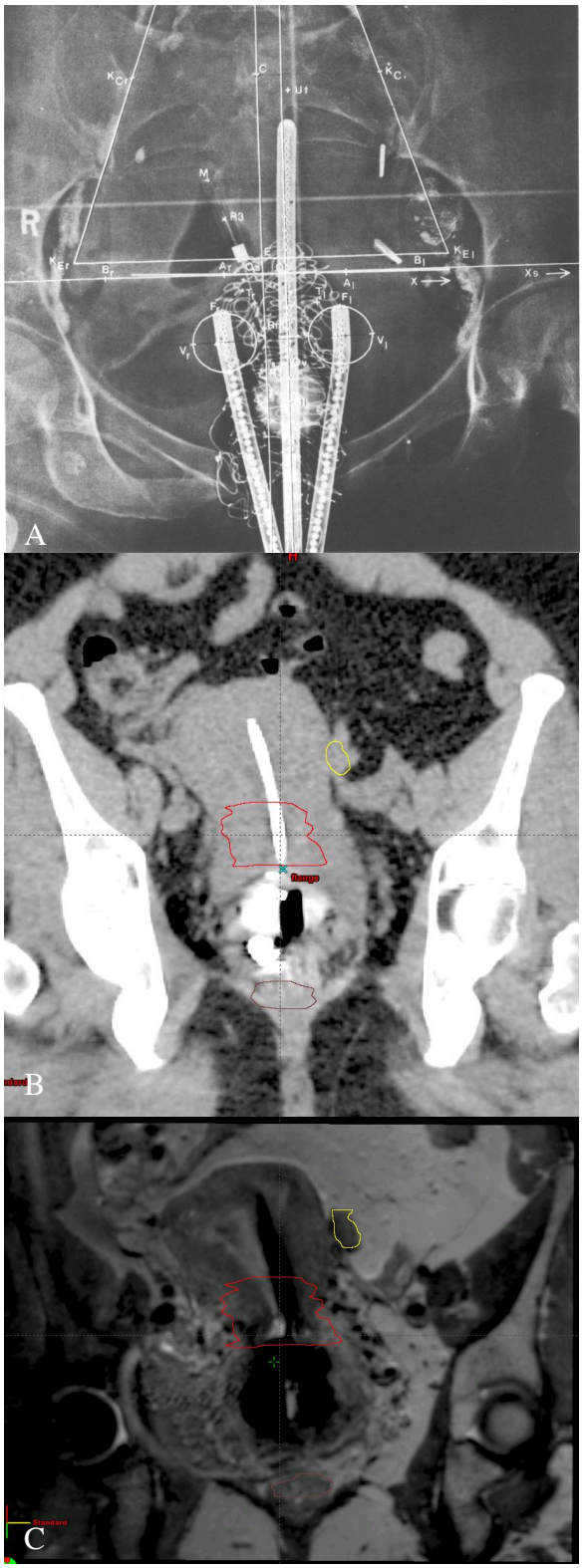

Figure 1-5. (A) A-P radiograph, and (B) CT and (C) MR images of the female pelvis in a para-coronal plane with a treatment applicator in place.

1.3 Dose Quantification and Dose Specification for Cervix Brachytherapy

Different systems of dose specification have been developed for brachytherapy in gynecology. Probably the oldest systems are the Paris system of Regaud and the Stockholm system of Forsell, both based primarily on clinical experience [Khan 2003]. “It is remarkable that these two systems, which differ widely in the amounts of radium used and in the time schedule of their applications, produced similar clinical results” [Khan 2003]. In both systems, applications have been reported in terms of “mg·h” (milligram hours), i.e., the product of the total mass of radium contained in the sources (in mg) and the duration of the application (in hours) [ICRU 1985]. In the 1930s the Manchester group analyzed the Paris technique from a physical point of view so that the dose at points in the pelvis could be expressed in roentgens. They further modified the Paris technique, using applicators designed to simplify dosage calculations [Johns and Cunningham 1983].

1.3.1 Historical Development of Dose Quantification from "mg·h" to "Roentgen" to "Gray"

The strength of a brachytherapy source can be specified in terms of activity, exposure rate at a specified distance, equivalent mass of radium and air kerma strength. Early experiments with radium indicated that one gram of radium underwent 3.7×10^{10} disintegrations per second. This led to the definition for the first unit of **activity** (A), the curie (Ci) [Johns and Cunningham 1983].

The quantity **exposure** (X) is a measure of ionization produced in air by photons, defined as $X = dQ/dm$, where dQ is the absolute value of the total charge of the ions of one sign produced in air when all the electrons (negatrons and positrons) liberated by photons in air of mass dm are completely stopped in air. The unit of exposure is roentgen (R). $1R = 2.58\times10^{-4}$ C/kg air. The exposure rate at any particular point is proportional to the product of activity and the source’s

exposure rate constant, Γ_δ. Γ_δ has been defined as $\Gamma_\delta = \frac{l^2}{A} \cdot (\dot{X})_\delta$, where $\dot{X}_\delta$ is the exposure rate from photons of energy greater than δ at a distance *l* from a point source of activity A.

In the case of radium, the source strength was traditionally specified in terms of milligrams of radium instead of mCi. The dosage system developed for radium has proved to be so useful that although other radionuclides have now largely replaced radium, some users, especially the physicians who are accustomed to radium sources, continued to use "mg·h" (milligram hours), the product of the total mass of radium contained in the sources (in mg) and the duration of the application (in hours), for treatment specification [Johns and Cunningham 1983, Khan 2003]. NCRP has suggested [NCRP 1974] that the source strength could be expressed in terms of an "effective" equivalent mass of radium (mg-Ra-eq). The equivalence is judged by equal dose rates at equal distances from the sources. The "effective" equivalent mass of radium of a source of a known activity may be determined from the relation, mg-Ra-eq=A· Γ / Γ_{Ra}, where A is the activity of the (radium substitute) source, Γ is its exposure rate constant, and Γ_{Ra} is the exposure rate constant for radium. Note that such a conversion of units must explicitly specify the radium source in terms of a point source and its filtration.

Although exposure rate at a specified distance is the method of choice in designating source strength, the quantity exposure has now been largely phased out. Most of the standards laboratories have already replaced exposure by the quantity **air kerma strength (S_k)**. Air kerma strength is related to exposure rate at the calibration distance *l* as: $S_k = \dot{X}_l \cdot (\frac{\overline{W}}{e}) \cdot l^2$, where the second factor is the average energy expended per unit charge of ionization produced in air.

As exposure is a measure of ionization in air only, the exposure rate distribution in air considers only the inverse square law and source filtration effects. When a

source is introduced into body, one needs to consider, in addition, attenuation as well as scattering in the surrounding tissue. The quantity **absorbed dose** has been defined to describe the quantity of radiation for all types of ionizing radiation, including charged and uncharged particles, all materials, and all energies [Khan 2003]. The definition of absorbed dose is the quotient of the mean energy $d\varepsilon$ imparted by ionizing radiation to material of mass dm. The SI unit for absorbed dose is the gray (Gy) and is defined as 1 Gy = 1 J/kg. The exposure rate calculated at a point in tissue can be converted into absorbed dose rate via the following relation: $D_{med} = X \cdot \frac{\overline{W_{air}}}{e} \cdot \frac{(\overline{\mu_{en}}/\rho)_{med}}{(\overline{\mu_{en}}/\rho)_{air}} \cdot A$, where $\frac{(\overline{\mu_{en}}/\rho)_{med}}{(\overline{\mu_{en}}/\rho)_{air}}$ is the energy absorption coefficient ratio.

1.3.2 Manchester System

In the original Manchester system, 1 to 3 radium tubes were loaded in a rubber tandem inserted in the uterine canal. Simultaneously, radium tubes were loaded in appropriate-sized rubber ovoids, which were placed against the cervix and held at a constant separation by a rubber spacer. The dose distribution is characterized by the doses to four points: point A (left and right) and point B (left and right) (see Section 2.2.2.3 for more details).

Point A as originally defined is 2 cm superior to the lateral vaginal fornices and 2 cm lateral to the cervical canal (Figure 1-6). Point B is defined 3 cm lateral to point A. Ideally, point A represents the location where the uterine vessels cross the ureter. It is believed that the tolerance of these structures is the main limiting factor in the irradiation of the uterine cervix, therefore point A remains the point of dose prescription. In clinical practice, the point A dose is determined as the average value of dose at the left and right A points.

The Manchester system is the most extensively used system in the world [Khan 2003]. However, since the system was designed to deliver a constant dose rate to

defined points near the cervix (point A), irrespective of variation in size and shape of the uterus and vagina, the anatomic significance of point A has been questioned.

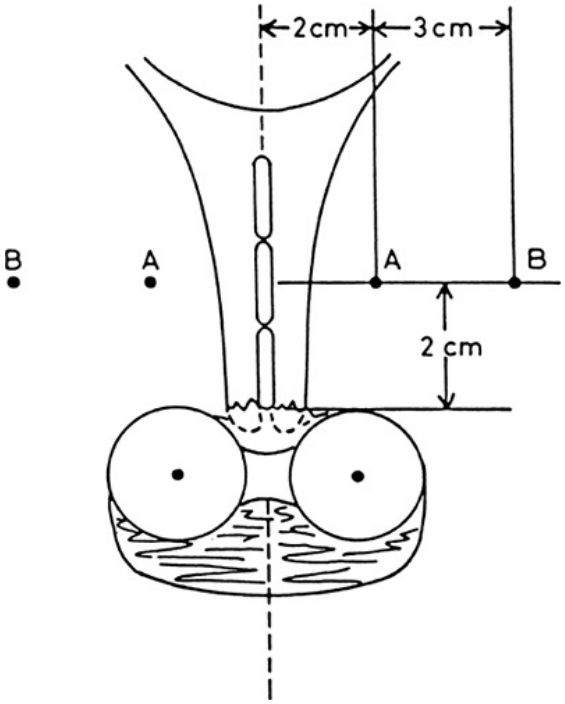

Figure 1-6. Original definition of points A and B, according to the Manchester system. From Meredith WJ. Radium dosage: the Manchester system. Edinburgh: Livingstone, 1967.

Two limitations associated with this system are: (i) point A is governed by the position of the sources in the applicators and not by any specific anatomic structure; (ii) dose to point A is very sensitive to the position of the ovoid sources relative to the tandem sources, which should not be the determining factor in deciding implant duration. Another limitation of the system is that the location of point A relative to the brachytherapy target volume is dependent on the size of the cervix and so may lie inside the tumor (large cervix, underdose) or outside the tumor (small cervix, overdose), that is, dose prescription at point A could risk underdosage of large cervical cancers or overdosage of small ones [Khan 2003] (Figure 1-7). Furthermore, the exact meaning and the definition of point A have

not always been interpreted in the same way in different centers and even in a given center over a period of time. In particular, some centers relate point A to anatomical references in the patient, and others to the geometry of the sources [ICRU 1985].

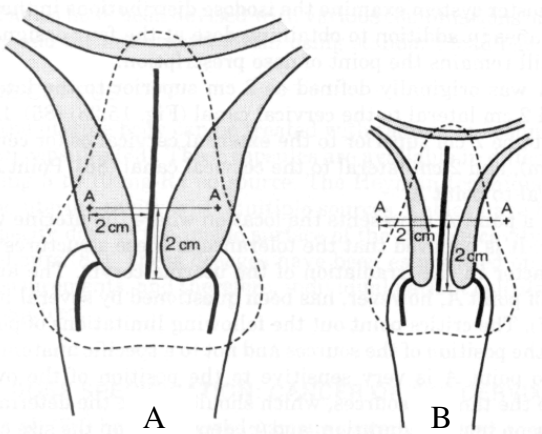

Figure 1-7. Variation of point A relative to anatomy. (A) Point A inside large cervix, resulting in underdosage. (B) Point A outside small cervix, resulting in overdosage. From Pierquin B, Wilson JF, Chassagne D, eds. Modern brachytherapy. New York: Masson, 1987.

With intracavitary therapy and uniform source activity, the dose is maximum adjacent to the sources and at the center of the treated volume, and it falls off continuously with distance from the sources. Consequently, the size of the treatment volume cannot be deduced from a simple inspection of the isodose pattern. Due to the high dose gradient around the sources, it is also not meaningful to specify the target absorbed dose in terms of the dose absorbed at specific point(s) within the target volume [ICRU 1985].

The Manchester system was originally meant for ^{226}Ra as the radioisotope and applicators specially designed to accommodate ^{226}Ra tube sources, and provided a set of rules to deliver almost a constant dose rate to the dose specification point A. Treatment with ^{226}Ra has subsequently been superceded by ^{137}Cs (LDR), ^{192}Ir (PDR and HDR) and ^{60}Co (LDR and HDR). Differences in source design,

applicator geometry, or dose delivery from those associated with the original Manchester system require appropriate adaptation in contemporary applications.

1.3.3 ICRU 38 Dose Specification

ICRU 38 has recommended an approach to dose specification that relates the dose distribution to the target volume, instead of the dose to a specific point [ICRU 1985]. The dose is prescribed as the value of an isodose surface that just surrounds the target volume (called the minimum target dose). The reference volume (defined as the volume enclosed by the reference isodose surface) is subsequently described in terms of the height, width and thickness of the volume enclosed within the 60 Gy isodose surface for low dose rates, obtained as the sum of all brachytherapy and external beam doses. For higher dose rates a dose level lower than 60 Gy has to be selected [ICRU 1985]. Dose to ICRU recommended reference points provides further useful information in regard to the tolerance and adequacy of treatment.

The weakness of the ICRU system until recently was in the difficulty to determine the target volume, due to the inability to visualize the target with radiographic films [Khan 2003]. This drawback is currently overcome with the ability to perform image-guided brachytherapy using MRI or CT. Because the target volume can currently be determined and delineated on the 3D images (more accurately with MRI than CT), and the target volume can be superimposed on the isodose pattern which is solely determined by the source configuration, one can easily determine the minimum target dose (Figure 1-8).

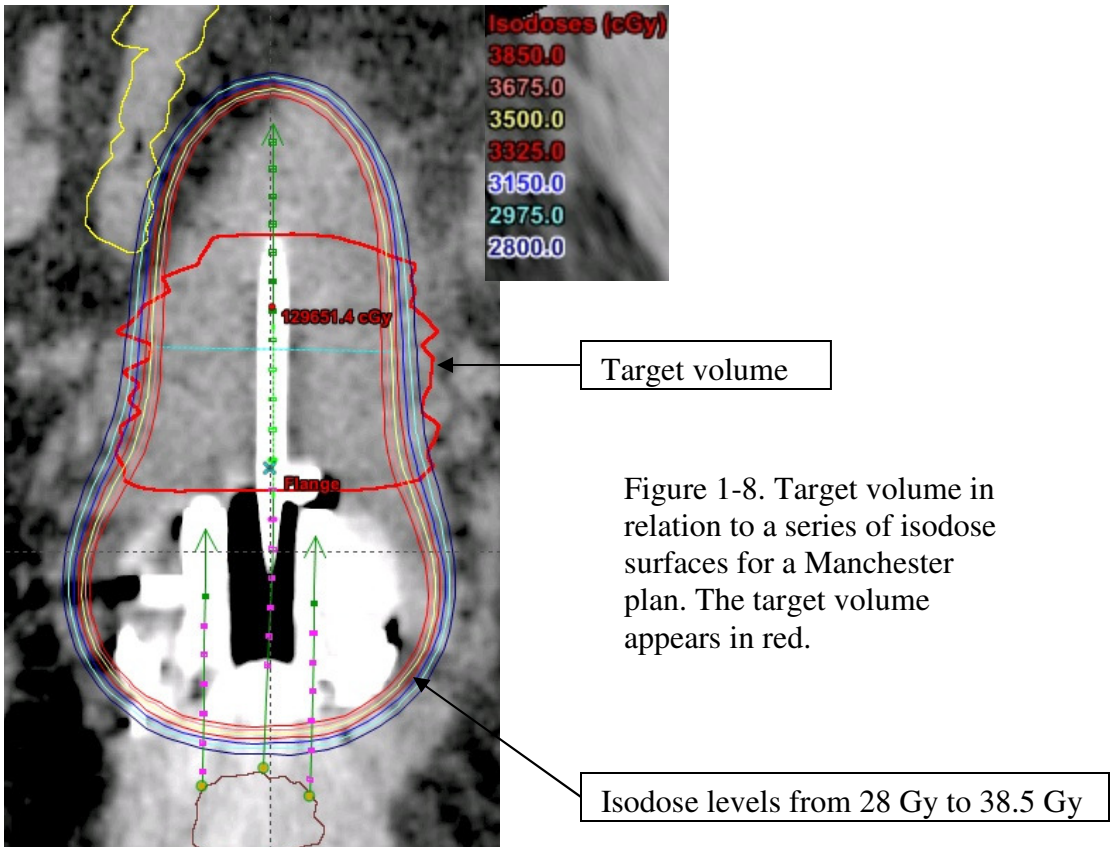

Figure 1-8. Target volume in relation to a series of isodose surfaces for a Manchester plan. The target volume appears in red.

1.4 Thesis Overview

1.4.1 Objective – MRI-guided 3D Image-based Cervix Cancer Brachytherapy

Recently, with the availability of sophisticated remote afterloading and image-based treatment planning capabilities, conformal brachytherapy has become possible. The GEC-ESTRO (Groupe Européen de Curiethérapie – European Society for Therapeutic Radiation Oncology) working group has published recommendations on contouring of the tumor target and organs at risk as well as dose volume parameters to be reported for MRI-guided brachytherapy for cervical cancer [Haie-Meder *et al.* 2005, Potter *et al.* 2006].

The advantage of this technique is the possibility to adapt the dose distribution to the anatomy of each individual patient through 3D imaging performed just prior to BT. This allows for the possibility of delivering a higher than normal dose of radiation to the tumor and also more sparing of the organs at risk, potentially producing greater local control rates. Although 3D image-based dosimetry is now extensively used in prostate brachytherapy [Nag 2006], it has not been implemented in cervical brachytherapy in most centers. As the traditional Manchester system of dose specification is currently used in our institution, and owing to the superior soft tissue contrast offered by MRI over CT, the need arises for us to develop 3D MRI-based brachytherapy treatment planning.

1.4.2 Overview of Content

Chapter 1 provides an introduction to intracavitary brachytherapy in gynecology as well as the treatment techniques. The objective of the thesis has also been presented.

Chapter 2 will highlight the experience of the Cross Cancer Institute (CCI) in moving towards 3D image-guided cervix brachytherapy. Film-based, CT-based, and MRI-based treatment planning and delivery will be compared.

Chapter 3 will evaluate uncertainties inherent in CT-MRI fusion, as well as titanium applicator distortion in MRI. Since MRI is unable to accurately image metallic applicators, CT-MRI fusion provides a means to locate applicators for MRI-guided cervix brachytherapy. A phantom designed to evaluate CT-MRI fusion will first be introduced. Thereafter we will fuse the CT and MR images based on registering the plastic frame of the phantom. Finally, registration error and MRI distortion of the titanium applicator will be quantified in this chapter.

In Chapter 4, traditional Manchester plans and 3D image-based treatment plans obtained using BrachyVision treatment planning system software will be

compared. Using a computer-simulated female pelvis model based on clinical data, a non-linear "stochastic" optimization method, simulated annealing (SA), will be applied to optimize the volume dose for cervix PDR brachytherapy to match specified dose-volume constraints. The effect on the results of optimization due to variations in model structure sizes and number of PDR brachytherapy source dwell positions will also be investigated using the model. Evaluations by dose-volume parameters are shown to demonstrate significant improvement in dose conformation to targets and dose sparing to surrounding organs by 3D dose optimization compared to conventional Manchester planning.

References

Glasgow GP, Dillman LT. Specific gamma-ray constant and exposure rate constant of ^{192}Ir. *Med Phys* 1979; 6(1):49-52.

Haie-Meder C, Potter R, Van Limbergen E, Briot E, De Brabandere M, Dimopoulos J, Dumas I, Hellebust TP, Kirisits C, Lang S, Muschitz S, Nevinson J, Nulens A, Petrow P, Wachter-Gerstner N. Recommendations from Gynaecological (GYN) GEC-ESTRO Working Group (I): concepts and terms in 3D image based 3D treatment planning in cervix cancer brachytherapy with emphasis on MRI assessment of GTV and CTV. *Radiother Oncol* 2005; 74(3):235-45.

Hensley, F.W., Physics of pulsed dose-rate brachytherapy*, Proc. of the 22nd annual EMBS international conference,* July 2000, Chicago IL.

Horton JL, Lawyer A, Mourtada F. Continuous low dose rate and pulsed dose rate remote afterloader units, *Ch8, AAPM Brachytherapy Society Summer School*, July 2005a, Seattle WA; 99-108.

Horton JL, Lawyer A, Berner P, Cunningham M, Mourtada F. Intracavitary brachytherapy applicators and UT M. D. Anderson cancer center intracavitary brachytherapy techniques, *Ch45, AAPM Brachytherapy Society Summer School*, July 2005b, Seattle WA; 815-27.

International commission on radiation units and measurements (ICRU). Dose and volume specification for reporting intracavitary therapy in gynecology. *ICRU report* No.38. Bethesda, MD: International Commission on Radiation Units and Measurements. 1985.

Johns HE, Cunningham JR. *The physics of radiology*. 4th ed. 1983, Springfield, IL: Charles C Thomas. 453-97.

Khan FM. *The physics of radiation therapy*. 3rd ed. 2003, Baltimore: Lippincott Williams & Wilkins. 358-400.

Logsdon MD, Eifel PJ. Low dose rate brachytherapy in the treatment of cervical carcinoma*. Hematol Oncol Clin North Am* 1999; 13(3):577-84.

Nag S, Cardenes H, Chang S, Das IJ, Erickson B, Ibbott GS, Lowenstein J, Roll J, Thomadsen B, Varia M. Proposed guidelines for image-based intracavitary brachytherapy for cervical carcinoma: report from Image-Guided Brachytherapy Working Group*. Int J Radiat Oncol Biol Phys* 2004; 60(4):1160-72.

Nag S. Controversies and new developments in gynecologic brachytherapy: image-based intracavitary brachytherapy for cervical carcinoma. *Semin Radiat Oncol* 2006; 16(3):164-7.
Thirion P, Kelly C, Salib O, Moriarty M, O'Reilly D, Griffin M, Armstrong J. A randomised comparison of two brachytherapy devices for the treatment of uterine cervical carcinoma. *Radiother Oncol* 2005; 74(3):247-50.

National Council on Radiation Protection and Measurements (NCRP). Specification of gamma-ray brachytherapy sources. *NCRP Report* No. 41. Washington, DC: US Government Printing Office, 1974.

Thomadsen BR. Volume imaging in gynecological brachytherapy, *Ch42, AAPM Brachytherapy Society Summer School*, July 2005, Seattle WA; 785-96.

Potter R, Haie-Meder C, Van Limbergen E, Barillot I, De Brabandere M, Dimopoulos J, Dumas I, Erickson B, Lang S, Nulens A, Petrow P, Rownd J, Kirisits C. Recommendations from gynaecological (GYN) GEC ESTRO working group (II): concepts and terms in 3D image-based treatment planning in cervix cancer brachytherapy-3D dose volume parameters and aspects of 3D image-based anatomy, radiation physics, radiobiology. *Radiother Oncol* 2006; 78(1):67-77.

Rownd J. Changing from Low Dose Rate to High Dose Rate Intracavitary Gynecological Brachytherapy, *Ch48, AAPM Brachytherapy Society Summer School*, July 2005, Seattle WA; 853-7.

Viswanathan AN, Dimopoulos J, Kirisits C, Berger D, Potter R. Computed tomography versus magnetic resonance imaging-based contouring in cervical cancer brachytherapy: results of a prospective trial and preliminary guidelines for standardized contours. *Int J Radiat Oncol Biol Phys* 2007; 68(2):491-8.

Chapter 2 Towards Image-Guided Cervix Brachytherapy: The CCI Experience

2.1 Introduction

With the dramatic advances in new technology over the last two decades, the practice of brachytherapy has undergone several changes especially in the areas of treatment planning and treatment delivery. Accurate brachytherapy treatment planning requires correct definition of patient anatomy, reconstruction of applicators, and identification of source positions. In most cases, this is a matter of an effective scan technique with the recognition of all imaging limitations, choice of applicators compatible with the imaging modality, and estimation of source positions within the applicator [Rownd 2005]. This chapter discusses in detail the evolution of brachytherapy for cervix cancer at the CCI from 1982 to the present.

Before the advent of anatomical structure-based treatment, brachytherapy was done with radiographic films and planar 2-D dosimetry. Treatment planning was based on traditional standardized rules and doses to defined prescription points. Prior to 2007, LDR brachytherapy was utilized exclusively at the CCI for cervix cancer treatment using film-based treatment planning. From 1982-2009, treatment was delivered using a Selectron LDR afterloader (Nucletron BV, Veenendaal, The Netherlands) that incorporated multiple ^{137}Cs sources (see Section 2.2.3). Since 2007, this treatment mode has been superseded by PDR brachytherapy delivered using a GammaMed-Plus afterloader (Varian Medical Systems, Palo Alto, CA). With the single stepping source used in PDR, better dose coverage of the treatment volume can be achieved by choosing suitable dwell positions and optimizing dwell times. This afterloader also makes MRI-based treatment planning dose optimization possible [Hensley 2000].

Since 2007, the CCI has been using BrachyVision software (Varian Medical Systems, Palo Alto, CA) for both LDR and PDR brachytherapy treatment planning. This treatment planning system has extensive functionality including image manipulation, 3D dose computation, rules-based dose optimization, dose-volume histogram (DVH) indices display, and 3D image-based planning tools. With this planning system and the clinical availability of 3D imaging modalities, the practice of image-guided cervix brachytherapy planning can be accomplished routinely.

With advances in digital technology, CT and MRI are increasingly being used in brachytherapy treatment planning. CT offers accurate localization of intracavitary applicators. It can show in 3D the relationship of the applicators to neighboring anatomic structures, which cannot be achieved by films. MRI offers superior soft tissue resolution, enables visualization of the cervical tumor and also delineates the tumor from surrounding normal tissue [Viswanathan *et al.* 2007]. 3D imaging is superior for defining target volumes and for guiding and confirming applicator insertion. At the CCI, the ready availability of CT and the introduction of the BrachyVision planning system prompted a transition from film-based to CT-based LDR treatment planning in 2007. A Varian GammaMed-Plus PDR afterloader and MRI-compatible (titanium) Henschke tandem and ovoid (T&O) applicator were also introduced into clinical service in 2007.

At the CCI, dose prescription for cervix cancer brachytherapy treatments has historically been based on the conventional 'point A' of the Manchester system. Although there are decades of clinical experience behind the use of this system, there are also limitations associated with it. Point A can neither be closely related to anatomic structures (it is related to the position of sources) nor can it represent the whole target volume. A number of studies have demonstrated that the hypothetical point A is defined based on an intracavitary applicator which may have a significant variation in geometry [Datta 2005] and that point A does not reliably represent the ureteral position [Potter *et al.* 2001] as originally postulated.

Furthermore, analysis in a locally conducted literature review revealed that no correlation could be found between the biologically effective dose to point A and patient survival, pelvic control or late complications [Petereit and Pearcey 1999]. The ICRU recommends that reference points like point A not be used because, "such points are located in a region where the dose gradient is high and any inaccuracy in the determination of distance results in large uncertainties in the absorbed doses evaluated at these points" [ICRU 1985]. Consequently a working group of GEC-ESTRO recommended that for better cervical tumor control, 3D image-based treatment planning be performed [Haie-Meder *et al.* 2005, Potter *et al.* 2006]. The major advantage of this technique is the possibility to conform the dose with regard to the treatment volume of interest and normal tissues.

With the availability of CT and MRI, a modern treatment planning system, a PDR afterloader, and CT- and MRI-compatible treatment applicators, the CCI embarked on a study of 3D image-based cervix cancer treatment planning in 2008. In this chapter film-based, CT-based, and MRI-based treatment planning and delivery as performed at the CCI will be described.

2.2 Film-based Treatment Planning and Delivery (1982 – 2006)

2.2.1 Imaging

Radiographs of the applicator in treatment position obtained with accurately specified x-ray source and film imaging geometry are required. A minimum of 2 exposures, each with a different viewing orientation, are needed to reconstruct the three dimensional coordinates of the implant points of interest. Several types of localization films have been developed for this purpose, e.g. shift films, orthogonal films, and stereo films. All of these allow sufficiently accurate measurements and calculations to be made. The simplest two-film technique is the one with the film planes orthogonal to each other. Typically these are anterior-

posterior (AP) and lateral films, but can be any two films taken at directions orthogonal to each other.

Prior to 2007, a pair of orthogonal films (AP and lateral) obtained with an x-ray simulator was the essential tool used for planning brachytherapy treatments at the CCI (see Figures 2-1 and 2-2). In the operating room the radiation oncologist, as part of the process of inserting the treatment applicator, would also inject contrast into a Foley catheter inserted in the bladder and placed radioopaque gauze packing around the applicator to facilitate later identification of ICRU bladder and rectal points, respectively. In the simulator a radiation therapist would insert radiographic dummy source markers into the applicator to facilitate source position determination during treatment planning. Film magnification factors required to reconstruct points of interest were determined using a grid of external reference markers embedded in a Lucite sheet placed in the simulator accessory tray, whose image was projected onto the orthogonal films.

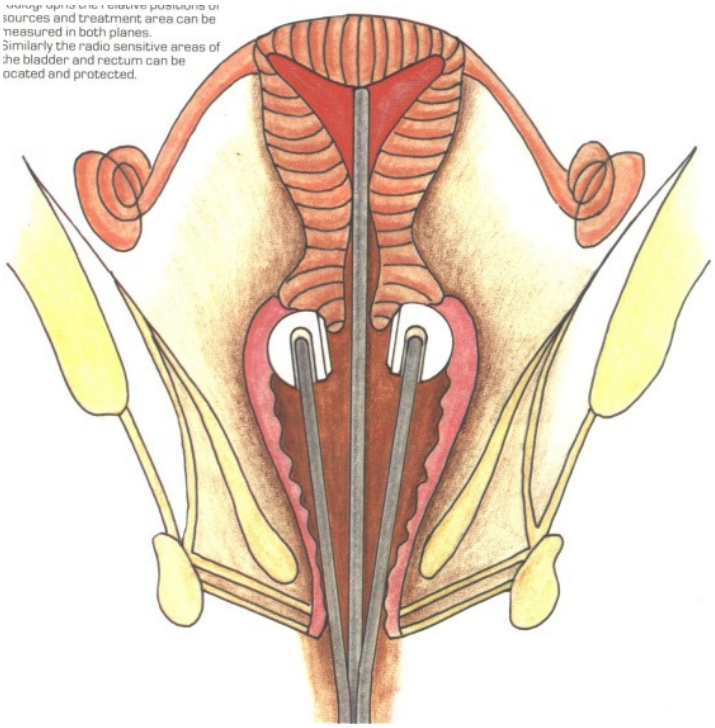

Figure 2-1. Schematic representation of a tandem and ovoid applicator in position for brachytherapy treatment of cervix cancer. From Nucletron product brochure.

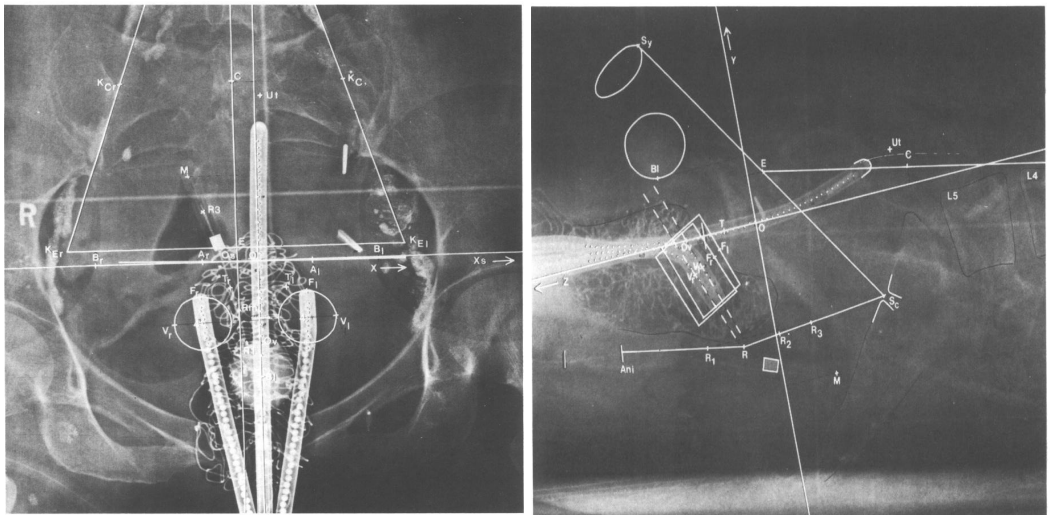

Figure 2-2. Radiographic orthogonal film technique for planning of cervix brachytherapy treatment (from Nucletron product brochure). Left panel: AP view. Right panel: lateral view.

2.2.2 Treatment Planning

Treatment planning based on a pair of radiographic images involved four steps: (i) film mark-up and digitization; (ii) reconstruction of applicator and dose points; (iii) dose specification and source loading; (iv) dose calculation and assessment. In this section the film pair consists of an AP and a lateral radiograph.

2.2.2.1 Film Mark-up and Digitization

Planning began with the identification and marking of applicator and dose points on both the AP and lateral radiographs. The applicator was identified as a series of points for each of its constituent components – tandem, left ovoid, and right ovoid – that started at the tip, spanned a length sufficient to contain the source loading for that component, and were located along its midline. Although it was not required that these points correspond on the two radiographs, dummy source marker positions were usually selected for this purpose (see Figure 2-2). Dose points consisting of Manchester system points A and B (see Section 2.2.2.3

following), and ICRU bladder and rectum points (see ICRU 1985) were then located on each radiograph.

After film marking, all points of interest were entered into the treatment planning system using a film digitizer. The digitizer consisted of a large backlit tablet upon which both radiographs were affixed side-by-side, a manually positioned cursor whose location on the tablet was determined electromagnetically, and an interface to the planning computer. Film digitization involved an initial tablet calibration check followed first by entry of position and orientation points for each radiograph, and then by entry of catheter points and dose points, all under planning system software (originally Nucletron NPS-BPS and later, Nucletron Plato BPS) control. Each individual point was entered by moving the cursor over the point in the AP radiograph, pressing a button on the cursor to transmit its location to the computer, and then repeating for the lateral radiograph. Successful transmission of location data was indicated by an audible beep from the digitizer interface.

2.2.2.2 Reconstruction of Applicator and Dose Points

Reconstruction of the applicator in 3D space from the series of points representing each of its components obtained by digitization was performed by the treatment planning system using a proprietary algorithm. Reconstruction of the dose points was also performed by the planning system, using the orthogonal films method [Khan 2003].

2.2.2.3 Dose Specification and Source Loading

Dose specification and source loading at the CCI were performed according to the Manchester system for cervix brachytherapy [Khan 2003]. The basic features and some of the limitations of this system are described in this section.

2.2.2.3.1 Manchester System Dose Specification

When intracavitary therapy, specified in units of mg•h (where mg represents the mass of ^{226}Ra), was originally used in conjunction with external beam therapy specified in terms of absorbed dose, overall radiation treatment could not be adequately characterized. Also, the dose prescription in terms of mg•h ignored anatomical targets and tolerance organs. The Manchester approach [Tod and Meredith 1938, 1953] was introduced in 1938 to define treatment in terms of dose to a point representative of the target, i.e., uterus, which was a dose limiting point, more or less reproducible from patient to patient. This prescription dose point is known as point A. Additional dose points were also defined initially, and later on as well, for the purpose of monitoring dose in tissues at risk adjacent to the target volume.

Note that in the summary description of the Manchester system following, reference is made to ^{226}Ra tube sources as these were commonly used when the system was first developed and for many decades afterwards. A correspondence between ^{226}Ra tube sources and modern sources of different design containing other "radium equivalent" radionuclides is readily made using the concept of milligram-radium-equivalent (mg-Ra-eq) source strength [Khan 2003]. In this scheme, source strength is specified in terms of the mass of ^{226}Ra that would produce an equivalent exposure rate at a distance of 1 m on the transverse axis of the source. One mg-Ra-eq of a ^{226}Ra substitute yields an exposure rate at 1 m of 0.825 mR/h. Using this concept, the Manchester system originally designed for ^{226}Ra tubes has continued to be used with contemporary sources of different design and radionuclide content right up to the present time.

Point A

Point A is defined to be 2 cm along the axis of the central tube from the lower end of the intrauterine sources and 2 cm from it perpendicularly (Figure 2-3). Hence in those cases when the uterus does not lie in the midline of the body and

symmetric to the ovoids due to anatomical distortions due to disease or otherwise, point A is carried with the uterus.

Point B

The lateral fall-off of the dose is defined by point B which lies 5 cm from the mid-line and 2 cm up from the lower end of the intrauterine sources (Figure 2-3(B)). This point gives the dose in the vicinity of the pelvic sidewall near the obturator nodes and a measure of the lateral spread of the effective dose. The dose at point B depends entirely on the total amount of the activity used.

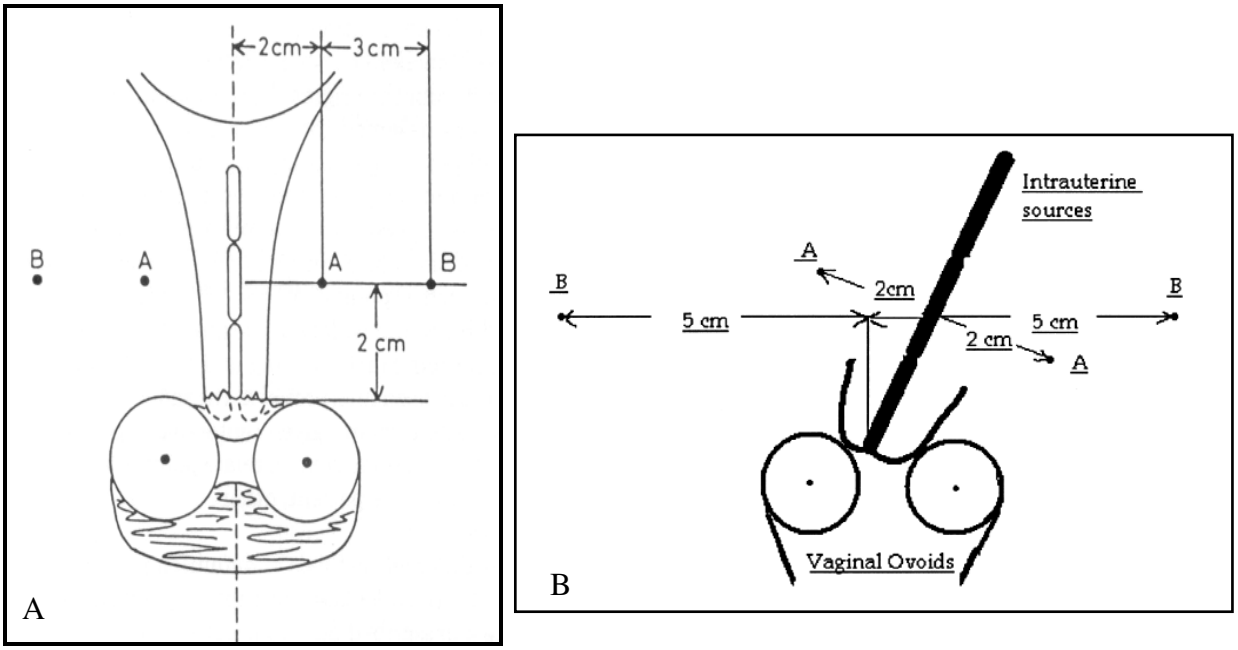

Figure 2-3. (A) Original definition of points A and B for the Manchester system. Point A is 2 cm superior to the vaginal fornix and 2 cm lateral to the uterine canal. Point B is situated 3 cm lateral to point A (from Meredith WJ. Radium dosage: the Manchester system. Edinburgh: Livingstone, 1967). (B) Modified definition of points A and B. Point A is carried with the uterus and it lies 2 cm superiorly from the lower end of the intrauterine sources (along the axis of intrauterine sources) and 2 cm perpendicular to the radium line on either side. Point B, which does not directly depend on the uterus, remains as a fixed point, 5 cm laterally from a point 2 cm up the midline from the end of the radium tube (from Sharma 2005).

Recto-vaginal septum

To limit the dose to surrounding normal tissue, dose to the recto-vaginal septum for any applicator loading is prescribed to be less than 80% of the dose to point A. This can be achieved by carefully packing gauze to a thickness of at least 1.5 cm in the vaginal canal posterior to the ovoids in order to displace the ovoids away from the rectum.

In the original Manchester system, the optimum dose was taken to be 8000 R (roentgen) for brachytherapy treatment alone, delivered to point A in two sessions of about 72 hours each with a 4- to 7-day interval between them, i.e. at a dose rate of 55 R per hour. It was recommended that not more than about one-third of the total dose at point A be delivered from ^{226}Ra in the vaginal ovoids. In modern practice at the CCI, reflecting common practice elsewhere, dose at point A was delivered as a combination of external beam and brachytherapy treatments, typically 45 Gy to the pelvis from the former and 30-35 Gy to the cervix from the latter.

2.2.2.3.2 Manchester System Source Loading

Originally, the distribution of ^{226}Ra in the intrauterine tube and ovoids was specified for applicator insertions having "ideal geometry" insofar as the orientation of the intratuerine tube (lying along patient midline) and ovoids (equidistant from the IU tube and at the same sup-inf level) were concerned. Table 2-1 gives the recommended source loadings for different IU tube lengths and different ovoid sizes for such an ideal geometry.

Table 2-1. Recommended source loadings for different IU tube lengths and different ovoid sizes for an ideal geometry

Intrauterine Tube	mg Ra loaded	Tubes (mg) used for loading	Dose rate to point A (cGy/h)	Dose rate to point B (cGy/h)
Large, 6cm length	35	15-10-10	35	8.8
Medium, 4cm length	25	15-10	35	7.0
Small, 2cm length	20	20	28	5.7
Ovoid	mg Ra loaded	Tubes (mg) used for loading	Dose rate to point A (cGy/h)	Dose rate to point B (cGy/h)
Large	2x22.5	20/25*	19	9.0
Medium	2x20	20	19	8.2
Small	2x17.5	20/15**	19	7.4

** 20 mg tube loaded in 1st application and 25 mg in the 2nd giving a total of 45 mg which is equivalent to 2 applications of 22.5 mg.*
*** 20 mg tube inserted in 1st application followed by 15 mg tube in the 2nd which gives a total of 35 mg (again equivalent to two sessions of 17.5 mg)*

Later, when computer-based planning became available, these loadings were commonly used as a starting point for film-based dose calculation for individual patients, and modified if the dose distribution was found not to be clinically acceptable. This approach to source loading was followed at the CCI for all film-based planning, and continues to be followed today for CT- and MRI-based planning. In modern practice, initial applicator loadings for ^{137}Cs (LDR) and ^{192}Ir (PDR) sources used at the CCI were or are obtained from Table 2-1 by converting mg-Ra-eq to relative source strength (with respect to that of an individual ^{137}Cs pellet or ^{192}Ir stepping source) and accounting for differences in the geometry of the sources (2 cm long ^{226}Ra tubes vs. effectively point ^{137}Cs and ^{192}Ir sources).
At the CCI, applicator reconstruction and source localization in preparation for source loading were based upon x-ray markers visible on the radiographs (see Figure 2-2).

2.2.2.4 Dose Calculation and Assessment

A commercial treatment planning system (in the 1980's Nucletron NPS-BPS and more recently, Nucletron Plato) was used to calculate a 3D isodose distribution relative to the treatment applicator for each patient individually. Dose calculation was based on source locations and dose points reconstructed from AP and lateral radiographic films, and was done for standard Manchester source configurations as described above. The isodose distribution in para-AP and para-lateral planes ("para" indicating planes tilted with respect to the patient) defined with respect to the applicator, and a summary report indicating planned doses to all points of interest, were made available to the attending radiation oncologist for review and approval. If any dosimetric issues of concern were identified, the source configuration was modified appropriately until a clinically acceptable treatment plan was achieved.

2.2.3 Treatment Delivery

The Nucletron Selectron LDR (SLDR) afterloader (Figure 2-4) was used at the CCI from 1982 to 2009 with 20 mCi (nominal) ^{137}Cs pellet sources. This afterloader was originally developed to avoid radiation exposure to hospital personal and to achieve a general overall improvement of dose distribution and accuracy of source positioning compared with ^{226}Ra, manual afterloading and mechanical afterloading techniques used prior to its introduction.

The most important feature of the SLDR afterloading technique was the applicator used. The Manchester-style tandem and ovoid applicator (Figure 2-5) was manufactured of lightweight stainless steel. It consisted of an intrauterine tube (tandem) and ovoids in a range of shapes/sizes to accommodate variations in patient anatomy. The applicator set included three tandems with different curvatures (15°, 30°, and 45°) whose IU length was varied by placement of a cervical stopper. Ovoids had outer diameters of 20, 25 and 30 mm corresponding exactly to the small, medium, and large ovoid dimensions in the classical

Manchester system. Each applicator tube had a special small and lightweight coupling device fitting only the appropriate treatment tube that connected it with the afterloader.

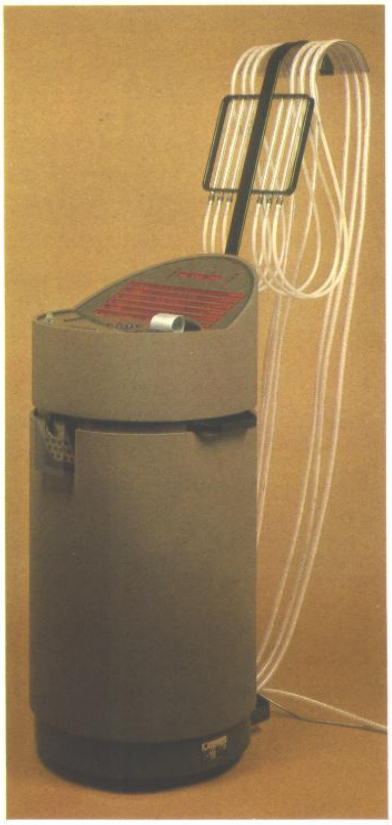

Figure 2-4. Nucletron Selectron LDR afterloader.

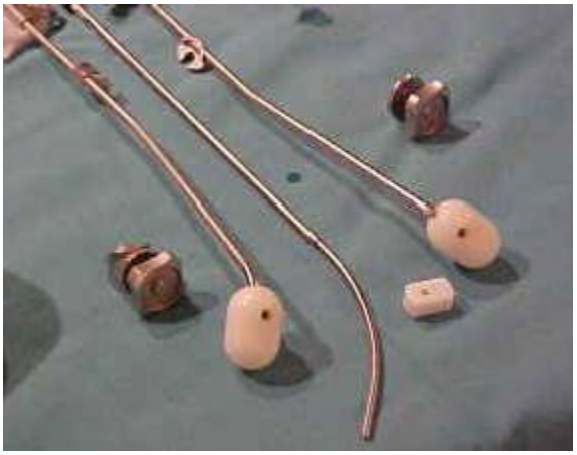

Figure 2-5. Manchester-style T&O applicator for use with the SLDR.

Using the Nucletron SLDR afterloader, brachytherapy treatment was delivered as follows. The patient was brought to the treatment room after the position of the applicators had been radiographically checked using dummy sources (see Section 2.2.1). The dummy source trains were removed and the Selectron treatment tubes connected to the applicator. A universal bed bracket was used to secure the treatment tubes at the foot of the bed and conduct them gradually to the applicator. The configuration of active and inactive pellets in each applicator channel (tandem, left ovoid and right ovoid) specified by the treatment plan was manually

programmed into the Selectron using an integral keypad and channel loading display system located on the top of the afterloader. The Selectron key was then turned on to the treatment mode, following which a hard copy of the treatment data was automatically produced and control of the Selectron functions was transferred to a remote control box mounted on the wall outside the treatment room. The treatment was initiated from the remote control box after all personnel left the treatment room and the door was closed, thereby transferring the programmed source configurations into the applicator from the afterloader.

2.3 CT-based Treatment Planning and Delivery (2007 – 2010)

2.3.1 General Considerations

With the use of modern commercial treatment planning software, applicators can be accurately reconstructed from a CT data set. In image-based brachytherapy, where dose prescription is done according to a 3D contoured target volume, dose prescription to point A may no longer be relevant, but for intercomparison purposes many institutions still report point A dose. Although image-guided brachytherapy using volume optimization is now replacing the point A method, at the CCI, dose prescription has, until very recently, been based on point A. Even though CT-based computerized dosimetry helps in reducing reliance on the Manchester system source loading guidelines, the error associated with using point A dose prescription for all patients may still lead to dose delivery issues for some patients (see Section 1.3.1). Using the combination of computers and PDR or HDR remote afterloading systems, source dwell times can be optimized to deliver dose to either prescription points or to a target volume, thereby facilitating the transition from dose points-based planning to anatomical structures-based planning. In intracavitary applications, with just three catheters and a limited number of allowable dwell positions, dwell time optimization may not be used to

its full advantage. Nevertheless, doses to critical organs like bladder and rectum can be reduced in some situations.

2.3.2 Imaging

Compared to film, CT offers improved accuracy for localization of "dummy" sources and applicators, and, in addition, can show the 3D relationship of the applicators to neighboring anatomical structures. At the CCI, a Philips Brilliance Big Bore CT scanner (Philips Healthcare, Andover, MA) is presently being used for brachytherapy planning using a pelvic helical scan protocol. The CT scan is performed on patients with the applicator inserted. Scans of 3 mm slice thickness are performed using 120 kV tube voltage, 400 mA/slice current, 16×1.5 mm collimation, 0.688 pitch, 500 mm FOV, and 512x512 image matrix. The 85cm bore size can accommodate patients in immobilization devices or with bulky patient monitoring devices without compromising image quality or positioning.

2.3.3 Treatment Planning

CT based treatment planning at the CCI is performed using Varian BrachyVision V8.2 software. With this planning system, CT-based planning does not require any mark-up and digitization of film-based data to determine the source position, which saves planning time. After importing the CT image set into BrachyVision and associating it with the patient, the applicators and reference points are manually identified on the CT images (Figure 2-6). To initiate the treatment plan, standard dwell positions with Manchester weighting are programmed. Then the treatment planning system performs a 3D dose calculation, normalizing the prescription dose to point A. The dwell times are manually revised if the calculated doses to the organs at risk exceed clinically acceptable limits.

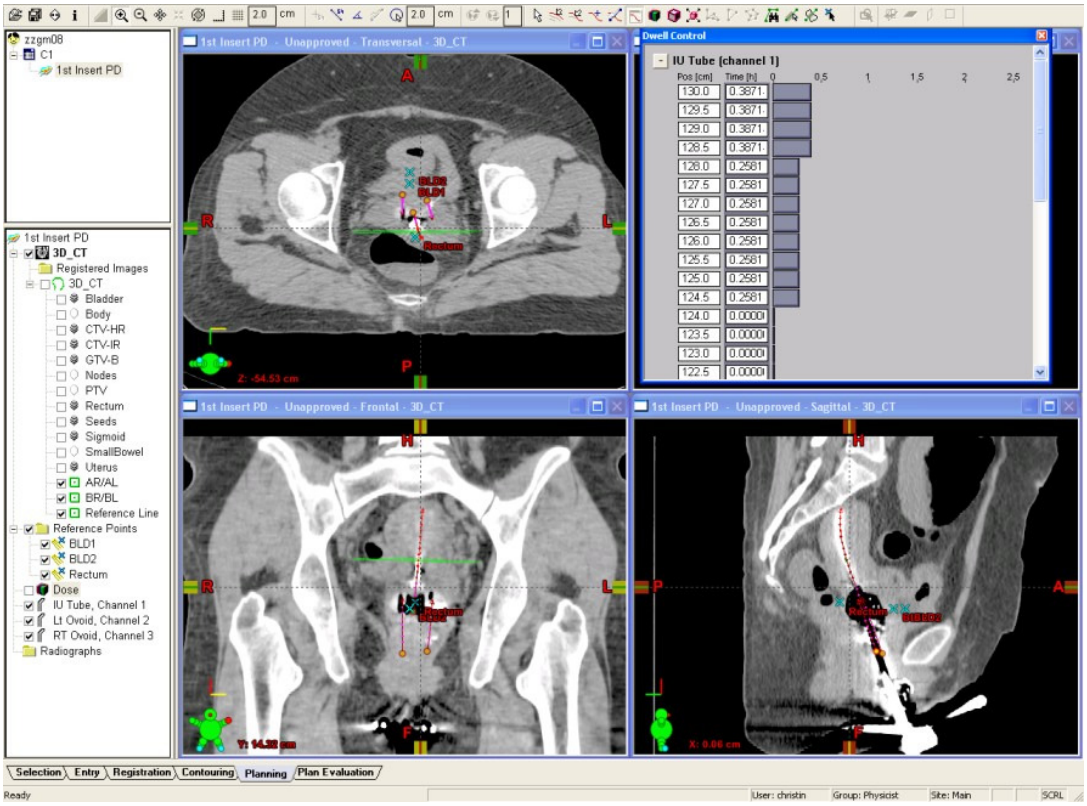

Figure 2-6. Illustration of CT-based treatment planning using the Varian BrachyVision system.

2.3.4 Treatment Delivery

The Varian GammaMed-Plus PDR remote afterloader (Figure 2-7) installed in 2007 at the CCI uses a 0.5 Ci nominal activity ^{192}Ir source. The source can be moved successively into 24 available channels, via the indexer. In each of these channels, 60 dwell positions are available. With the PDR afterloader and the relatively higher activity source, treatment is accomplished by exposing the source from the afterloader for only a fraction of the time, termed the pulse time, during a repeated period, termed the pulse interval. At the CCI, a PDR treatment is designed so that the total elapsed treatment time is equal to that for a corresponding LDR treatment. Compared to SLDR treatment, PDR treatment allows nursing care during the time interval between treatment pulses and also permits visitors without extending the treatment time. Another advantage is the

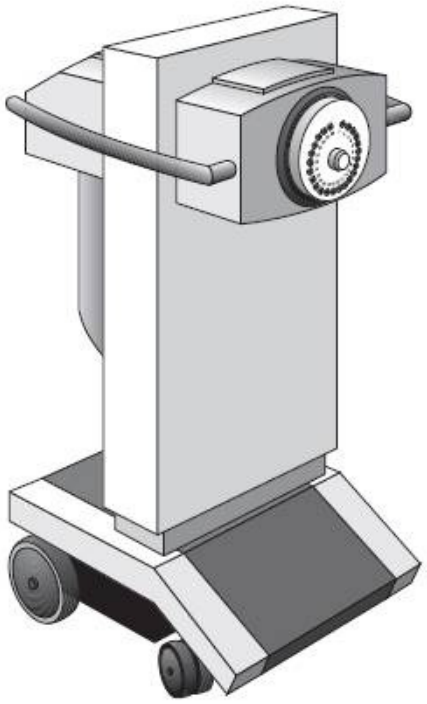

Figure 2-7. Varian GammaMed-Plus PDR afterloader.

ability to achieve greater conformation of the dose to the treatment volume than was possible with the SLDR [Horton *et al.* 2005]; by programming source dwell positions and times, desired isodose distributions can be either fully or partially obtained.

The treatment delivery process is as follows. Before treatment, the Manchester-style tandem and ovoid applicator is inserted into the patient in the operating room, a pelvic CT scan is obtained post insertion, and a treatment plan is generated using the CT images. Following plan approval by a radiation oncologist, source dwell position and dwell time information is transmitted via a local network from the planning computer to the treatment console computer controlling the afterloader operation, and verified for accuracy. Then the applicator is connected to the afterloader via source transfer tubes, and the treatment is initiated. The console computer first sends out a dummy wire to check that applicator connections are satisfactory, and then deploys the PDR source for treatment. The dwell positions and dwell times of the source in the applicator are controlled by the console computer for the duration of the treatment. At the CCI, the prescribed dose is delivered using a pulse interval of one hour at a rate of approximately 55 cGy per pulse, i.e. at a rate numerically equal to the classical low dose rate associated with the Manchester system.

2.4 MRI-Based Treatment Planning and Delivery (2010 & Beyond)

2.4.1 Image-Guided Brachytherapy (IGBT) Guidelines and Dose Reporting Parameters

2.4.1.1 GEC-ESTRO Recommendations for Volume-Based Gynecological Brachytherapy

The ICRU system recommends that reference points like point A not be used because, "such points are located in a region where the dose gradient is high and any inaccuracy in the determination of distance results in large uncertainties in the absorbed doses evaluated at these points." It recommends that doses be reported in terms of total reference air kerma, a description of a reference volume, calculated values of dose to specific normal tissue reference points within the treatment volume, and a system of dose specification that relates the dose distribution to a target volume.

A working group from GEC-ESTRO has published recommendations on contouring of tumor target and organs at risk (OAR) as well as on dose volume parameters to be reported for image-guided BT in definitive radiotherapy for locally advanced cervical cancer. The major advantage of this technique is the possibility to conform the dose given by BT with regard to both volume (3D) and time (4D). By imaging performed before each BT insertion, it is possible to adapt the dose given by BT to the anatomy of each individual patient taking into account not only the position of OARs but also tumor regression which often is obtained by preceding EBRT and chemotherapy [Haie-Meder *et al*. 2005, Potter *et al*. 2006].

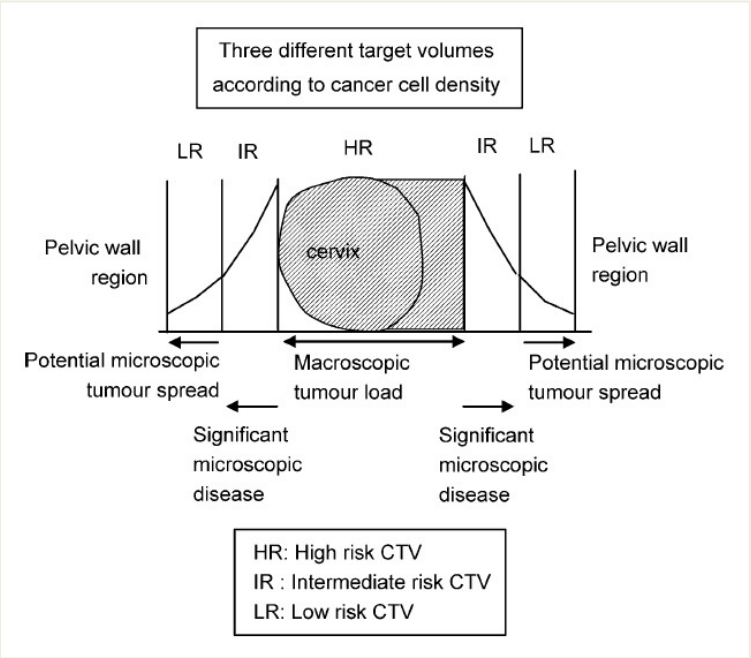

Figure 2-8. Differences in cancer cell density in the three defined target volumes (from Haie-Meder *et al*. Radiotherapy and Oncology, 2005).

2.4.1.2 Dose Parameters to be Used for Reporting

The GEC-ESTRO working group has recommended that the following data be reported for gynecological brachytherapy treatments [Potter *et al.* 2006]:

- Prescribed dose
- Total Reference Air Kerma (TRAK)
- Dose at point A (right, left, mean)
- D100, D90 for GTV and HR-CTV and IR-CTV, respectively (definitions refer to Haie-Meder *et al.* 2005)
  - D90/D100 is the minimum dose delivered to 90%/100% of the volume of interest
  - GTV, gross tumor volume, includes macroscopic tumor extension as detected by clinical examination and as visualized on MRI (see Figure 2-8)
  - HR-CTV, high risk clinical target volume, carries a high tumor load including GTV, the whole cervix and the presumed extracervical tumor extension (see Figure 2-8)

- IR-CTV, intermediate risk CTV, carries a significant microscopic tumor load, encompasses HR-CTV with a safety margin of 5-15 mm (see Figure 2-8)

- Dose to bladder and rectum for ICRU reference points
- $D_{0.1cc}$, D_{1cc}, D_{2cc} for organs at risk (e.g. rectum, sigmoid, bladder)
  - $D_{0.1cc}$ / D_{1cc} / D_{2cc} is the minimum dose in the most irradiated 0.1 / 1 / 2 cm^3 of the tissue volume
- D_{5cc}, D_{10cc} for organs at risk if contouring of organ walls is performed
  - D_{5cc} / D_{10cc} is the minimum dose in the most irradiated 5 / 10 cm^3 of the tissue volume
- Complete description of time–dose pattern: physical and biologically weighted doses (using the standardized radiobiological parameters α/β = 10 Gy for GTV and CTV; α/β = 3 Gy for OAR; $T_{1/2}$ = 1.5 h for GTV, CTV and OAR, see Section 4.2.2 for more about α/β parameters)

2.4.1.3 Dose-Volume Constraints Recommended for Planning

According to previous studies [Lang *et al.* 2007, Lindegaard *et al.* 2008, Trnkova *et al.* 2009], the total biologically effective dose constraints recommended for treatment planning are summarized in Table 2-2.

Table 2-2. Total biologically effective dose constraints.

HR-CTV	D90	≥ 85Gy (α/β = 10 Gy)
Bladder	D_{2cc}	≤ 90 Gy (α/β = 3 Gy)
Rectum	D_{2cc}	≤ 75 Gy (α/β = 3 Gy)
Sigmoid	D_{2cc}	≤ 75 Gy (α/β = 3 Gy)

2.4.2 Imaging

MRI offers superior soft tissue contrast, enables visualization of the cervical tumor size and volume, distinguishes the tumor from normal uterus and cervix, and defines the parametrial and vaginal infiltration of disease [Viswanathan *et al.* 2007]. Clinical MR imaging is presently performed using a Philips 1.5T Gyroscan Interra scanner, although a Philips 3T Interra scanner is also available at the CCI and has previously been used to develop clinical imaging protocols for gynecological brachytherapy. Image acquisition protocols for both MR scanners are described in detail in Appendix A in Chapter 3. A Philips Brilliance Big Bore CT scanner is being used for CT imaging; Section 2.3.2 above describes the technique.

2.4.3 Treatment Planning

The advantage of using anatomical structure-based planning is that the dose prescription is individualized and anatomy-based where the dose is prescribed to volumes rather than to points that may not be correlated with survival, tumor control or even late complications [Datta 2005]. The end goal of this planning technique is to ensure adequate target volume coverage by the prescription dose and the sparing of OARs.

The treatment planning process proceeds as follows:

- The MR and CT image sets are imported into BrachyVision and fused using uterus anatomy guidance as well as matching of the intrauterine tube of the tandem and ovoids applicator.
- Contouring of the GTV, IR-CTV, HR-CTV, and organs at risk (rectum, bladder and sigmoid) is performed by the radiation oncologist on the MR images.

- The planning process starts with the identification of the applicators on CT and locating of the dose reference points. The dwell positions and dwell times are defined as for a standard Manchester loading (see Section 2.2.2.3.2) and the prescribed dose is normalized to point A.
- Guided by isodose curves and DVH parameter constraints (see Table 2-2), the dose distribution is modified as deemed necessary by manually adjusting dwell positions and times to achieve the desired dose coverage of the HR-CTV and sparing of the OARs.

2.4.4 Treatment Delivery

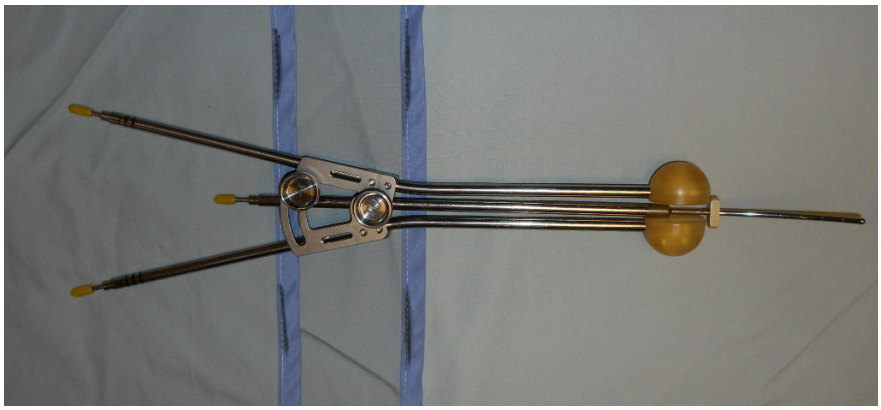

Figure 2-9. MRI-compatible (titanium) Henschke T&O applicator.

The Henschke applicator (Figure 2-9, Mick Radio-Nuclear Instruments, Inc., Mount Vernon, NY) used for image-guided cervix brachytherapy at the CCI consists of an intrauterine tube (tandem) and two hemispherical vaginal ovoids. The applicator tandem length inserted in the uterus is adjustable by placement of a cervical stopper, and three tandems with 0°, 23°, and 45° curvature are available to accommodate variations in patient anatomy. Available ovoid outer diameters of 20 mm, 25 mm, and 30 mm correspond exactly to the small, medium, and large ovoid dimensions in the classical Manchester system. The distance between ovoid

channels is continuously adjustable. The ovoid size, the distance between ovoids and the tandem length are adjusted according to tumor size and topography.

To allow for safe MR imaging, titanium replaces the conventional stainless steel, which would be subject to a strong force from the fixed magnetic field and heating from the RF magnetic field of the MR scanner. Furthermore, the use of a CT/MRI-compatible applicator permits anatomical targets to be delineated with a greater degree of certainty as certain types of image artifacts (e.g. streaking) are minimized, although applicator image distortion is still significant with MRI.

The treatment delivery process is the same as that described in Section 2.3.4. With the stepping source PDR afterloader, source dwell positions can be chosen to match the target shape, and dwell times can be optimized to some extent to adjust the dose distribution to the target volume, and to homogenize the dose inside the target [Hensley 2000].

2.4.5 Physics Issues Associated with MRI-Based Cervix Brachytherapy

1. Because the magnetic susceptibility gradient is so large between the titanium applicator and the soft tissue of the patient, the MR image of the applicator exhibits significant distortions. Accurately locating potential dwell positions in the applicator using exclusively MR-based treatment planning is very difficult. One solution is to perform CT-MRI fusion to transfer the position of applicator on CT to the MR images. Chapter 3 will investigate this issue.

2. There have been a few reports quantifying the anticipated improvements in dosimetry associated with the transition from CT-based planning using Manchester system guidelines to 3D image-based planning according to GEC-ESTRO guidelines [Lindegaard *et al.* 2008, Trnkova *et al.* 2009, Tanderup *et al.* 2010]. Doing this will give us a direct indication of the potential benefits associated with pursuing image-based treatment planning. Accordingly, in

Chapter 4 we will compare traditional Manchester plans and 3D image-based plans obtained using BrachyVision optimization software guided by published DVH parameter constraints.

3. As the generic dose optimization tool in BrachyVision (based on the Nelder-Mead simplex algorithm [Ezzell 2005]) may not be ideal for gynecology brachytherapy applications which involve many variables (e.g. up to 14 dwell times at 14 dwell positions), and as there is a risk of being trapped in local minima so that a global solution is not obtained, an alternative dose optimization method was developed and will be presented in Chapter 4.

References

Datta NR. From 'points' to 'profiles' in intracavitary brachytherapy of cervical cancer. *Curr Opin Obstet Gynecol* 2005; 17(1):35-41.

Ezzell GA. Optimization in Brachytherapy. *Ch22, AAPM Brachytherapy Society Summer School*, July 2005, Seattle WA; 415-34.

Haie-Meder C, Potter R, Van Limbergen E, Briot E, De Brabandere M, Dimopoulos J, Dumas I, Hellebust TP, Kirisits C, Lang S, Muschitz S, Nevinson J, Nulens A, Petrow P, Wachter-Gerstner N. Recommendations from Gynaecological (GYN) GEC-ESTRO Working Group (I): concepts and terms in 3D image based 3D treatment planning in cervix cancer brachytherapy with emphasis on MRI assessment of GTV and CTV. *Radiother Oncol* 2005; 74(3):235-45.

Hensley, F.W., Physics of pulsed dose-rate brachytherapy, *Proc. of the 22nd annual EMBS international conference*, July 2000, Chicago IL.

Horton JL, Lawyer A, Mourtada F, Continuous low dose rate and pulsed dose rate remote afterloader units, *Ch8, AAPM Brachytherapy Society Summer School*, July 2005, Seattle WA; 99-108.

International commission on radiation units and measurements (ICRU). *Dose and volume specification for reporting intracavitary therapy in gynecology*, ICRU report No.38. Bethesda, MD: International Commission on Radiation Units and Measurements. 1985.

Khan, FM. *The physics of radiation therapy*. 3rd ed. 2003: Lippincott Williams & Wilkins. 358-400.

Lang S, Kirisits C, Dimopoulos J, Georg D, Potter R. Treatment planning for MRI assisted brachytherapy of gynecologic malignancies based on total dose constraints. *Int J Radiat Oncol Biol Phys* 2007; 69(2):619-27.

Lindegaard JC, Tanderup K, Nielsen SK, Haack S, Gelineck J. MRI-guided 3D optimization significantly improves DVH parameters of pulsed-dose-rate brachytherapy in locally advanced cervical cancer. *Int J Radiat Oncol Biol Phys* 2008; 71(3):756-64.

Petereit DG, Pearcey R. Literature analysis of high dose rate brachytherapy fractionation schedules in the treatment of cervical cancer: is there an optimal fractionation schedule? *Int J Radiat Oncol Biol Phys* 1999; 43(2):359-66.

Potter R, Van Limbergen E, Gerstner N, Wambersie A. Survey of the use of the ICRU 38 in recording and reporting cervical cancer brachytherapy. *Radiother Oncol* 2001; 58(1):11-8.

Potter R, Haie-Meder C, Van Limbergen E, Barillot I, De Brabandere M, Dimopoulos J, Dumas I, Erickson B, Lang S, Nulens A, Petrow P, Rownd J, Kirisits C. Recommendations from gynaecological (GYN) GEC ESTRO working group (II): concepts and terms in 3D image-based treatment planning in cervix cancer brachytherapy-3D dose volume parameters and aspects of 3D image-based anatomy, radiation physics, radiobiology. *Radiother Oncol* 2006; 78(1):67-77.

Rownd J. Localization II: Volume imaging techniques and accuracy for brachytherapy dosimetry. *Ch13, AAPM Brachytherapy Society Summer School*, July 2005, Seattle WA; 187-200.

Sharma AK. Manchester System for Gynecological Applications. *Ch44, AAPM Brachytherapy Society Summer School*, July 2005, Seattle WA; 805-13.

Tanderup K, Nielsen SK, Nyvang GB, Pedersen EM, Rohl L, Aagaard T, Fokdal L, Lindegaard JC. From point A to the sculpted pear: MR image guidance significantly improves tumour dose and sparing of organs at risk in brachytherapy of cervical cancer. *Radiother Oncol* 2010; 94(2):173-80.

Tod MC, Meredith WJ. A dosage system for use in the treatment of cancer of the uterine cervix. *Br J Radiol* 1938;11:809.

Trnkova P, Potter R, Baltas D, Karabis A, Fidarova E, Dimopoulos J, Georg D, Kirisits C. New inverse planning technology for image-guided cervical cancer brachytherapy: description and evaluation within a clinical frame. *Radiother Oncol* 2009; 93(2):331-40.

Tod MC, Meredith WJ. Treatment of cancer of the cervix uteri – a revised "Manchester method". *Br J Radiol* 1953;26:252.

Viswanathan AN, Dimopoulos J, Kirisits C, Berger D, Potter R. Computed tomography versus magnetic resonance imaging-based contouring in cervical cancer brachytherapy: results of a prospective trial and preliminary guidelines for standardized contours. *Int J Radiat Oncol Biol Phys* 2007; 68(2):491-8.

Williamson JF. Brachytherapy technology and physics practice since 1950: a half-century of progress. *Phys Med Biol* 2006; 51(13):R303-25.

Chapter 3 CT-MRI Fusion

3.1 Introduction

CT has the advantage of accurately localizing intracavitary applicators. The disadvantage is that CT is inferior to MRI with respect to defining target volumes. It was shown that CT contours tended to overestimate the width of the tumor (Viswanathan *et al.* 2007) - the gross tumor volume in cervical cancer derived from CT is larger than that derived from axial MR and sagittal MR or coronal MR, respectively, by a factor of 1.4 and 1.5 [Wachter *et al.* 2001]. MR is known to provide superior image quality especially in soft tissue contrasts. However, applicator localization can be difficult for MRI, since magnetic susceptibility artifacts arising from applicator materials may cause distortion of the imaged applicator [Haack *et al.* 2009]. Special reconstruction techniques may be needed for MR to define the applicator geometry as accurately as with CT. By fusing CT with MR, the position of the applicator can be transferred to MR images, so that one would be able to visualize the applicator position better in relation to the normal surrounding anatomy. It was shown that the use of fused images enables an improved 3D-dose distribution in the target volume and results in a reduced dose to the intestine, the bladder, and the anterior rectal wall [Krempien *et al.* 2003]. However, the application of image fusion should be carefully conducted, because it contains uncertainties due to registration errors and patient motion, which may result in significant uncertainties in DVH parameters.

The geometric distortions of an intracavitary applicator imaged using Cross Cancer Institute MRI facilities were investigated by means of a custom-built phantom. Furthermore, the phantom studies offered the possibility to correct for applicator distortion if necessary. This chapter reports an investigation of how much MRI distortion is present for a titanium tandem and ovoids applicator, and where it is apparent. The CT-MRI registration accuracy and the sources of registration error will also be addressed.

3.2 Methods and Materials

3.2.1 Applicator

A CT/MR compatible titanium Fletcher Suit Delclos (FSD) tandem and ovoids applicator (Varian Brachytherapy, Charlottesville VA) was used. The FSD applicator consists of an intrauterine tube (tandem) and cylindrical vaginal ovoids. To apply to uteri of different sizes, the tandem length is adjustable to a maximum of 90 mm, and the distance between ovoids is also adjustable. The ovoids are tilted, a feature originally designed to take advantage of the anisotropic properties of historically used Cs-137 tube sources in the direction of the two main organs at risk, i.e. the bladder and rectum [Thirion *et al.* 2005]. To facilitate applicator insertion in a patient, the distal part of the tandem is bent at a 45° angle, and a flange is attached near the ovoids to identify the cervical os (against which it rests after applicator insertion) and help prevent uterine perforation. Ovoid caps of diameters 20, 25 and 30 mm are available commercially; the ones used in our work are 25 mm. Clinically, the largest size of cap that fits comfortably into the vaginal fornices is chosen in order to minimize the dose to the vaginal mucosa.

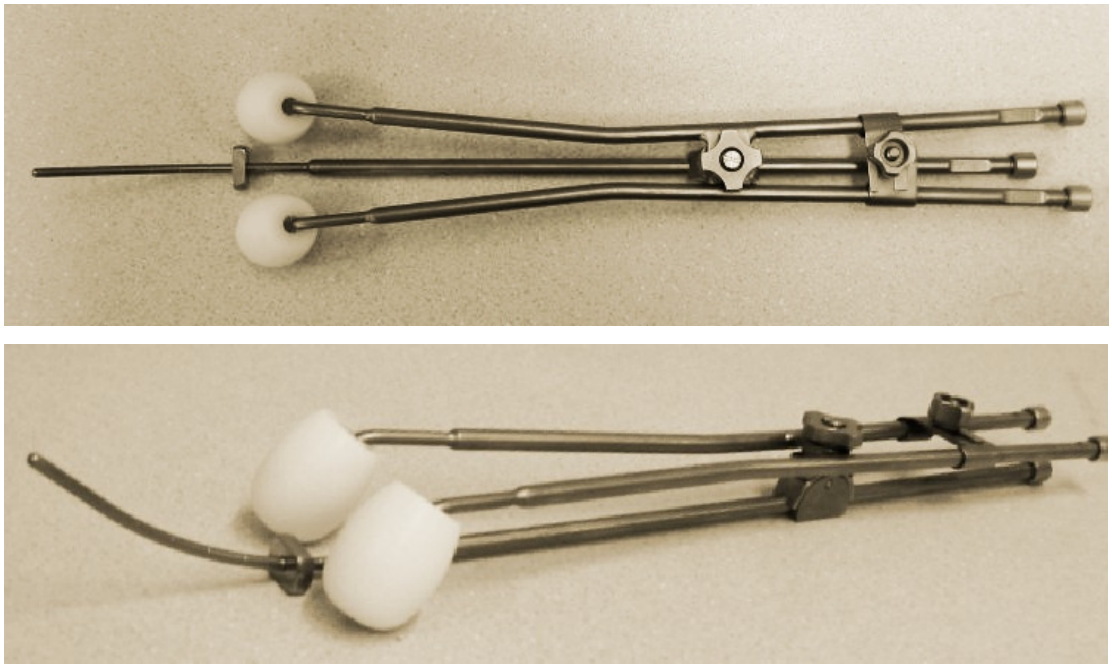

Figure 3-1. CT/MR compatible titanium FSD tandem and ovoids applicator.

3.2.2 Phantom Design and Construction

The design of the phantom was inspired by Haack *et al.*'s research on applicator reconstruction in MRI [Haack *et al.* 2009]. Figure 3-2 is an illustration of the phantom. The key structure in the phantom is a hollow cylinder (7 cm long, 4 cm in diameter, and 0.3 cm in thickness) made of Lucite (PMMA) simulating the uterus wall. The cylinder has a rubber flap at one end so that the tandem can be inserted into it. To rest the applicator and hold gel that simulates human tissue surrounding the uterus, a rectangular plastic frame (PMMA, dimension 15x22x15 cm^3) was constructed. The phantom also includes two parallel plates separated by 7 cm to hold the hollow cylinder in between them. An angled plastic rod located between the two plates allows determination of the longitudinal position of transverse images. Two CT/MRI compatible fiducial markers (5 mm in diameter) were placed at the same locations on the two plates: 2.7 cm from the top edge of the plate. The whole container holds a single gel mixture. The contrast between the cylinder wall and the gel provides visual separation for the gel inside and outside the cylinder on both CT and MR images.

3.2.3 Gel Preparation

Gel was fabricated from a solution of 10% type A porcine skin gelatin powder (Sigma Chemical Co., St. Louis MO) in tap water. A measured amount of gelatin powder was dissolved in ¾ of the total required amount of water at room temperature for 20 minutes until the gelatin was fully wetted. The remaining water was then added and the mixture was heated in a microwave oven with intermittent stirring to form the gel solution. The hot solution was poured into the phantom (cylinder first) and the applicator was inserted into the cylinder with the proximal end resting on the top of the phantom (see Figure 3-2). The gel was then left undisturbed until all visible air bubbles escaped and the gel formed into a semi-solid substance. Because the cylinder is closed only with a flap on one side, the bubbles inside cannot escape after the cylinder is in place (when placed horizontally). Hence attention needs to be given to ensure that the cylinder is full

of gel solution and closed securely before it is placed horizontally. After cooling and solidification of the gel, the applicator becomes fixed firmly. The gel was prepared twice with the applicator positioned slightly differently for imaging. CT and MR scans were obtained of both phantom configurations and recorded as two trials.

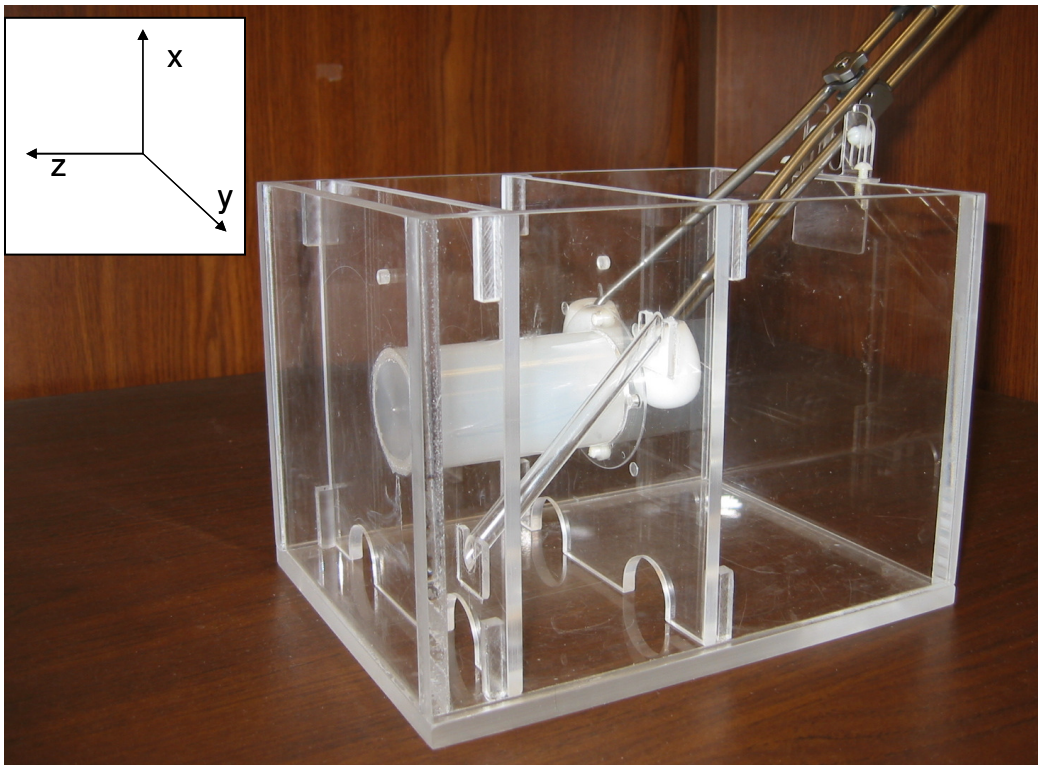

A

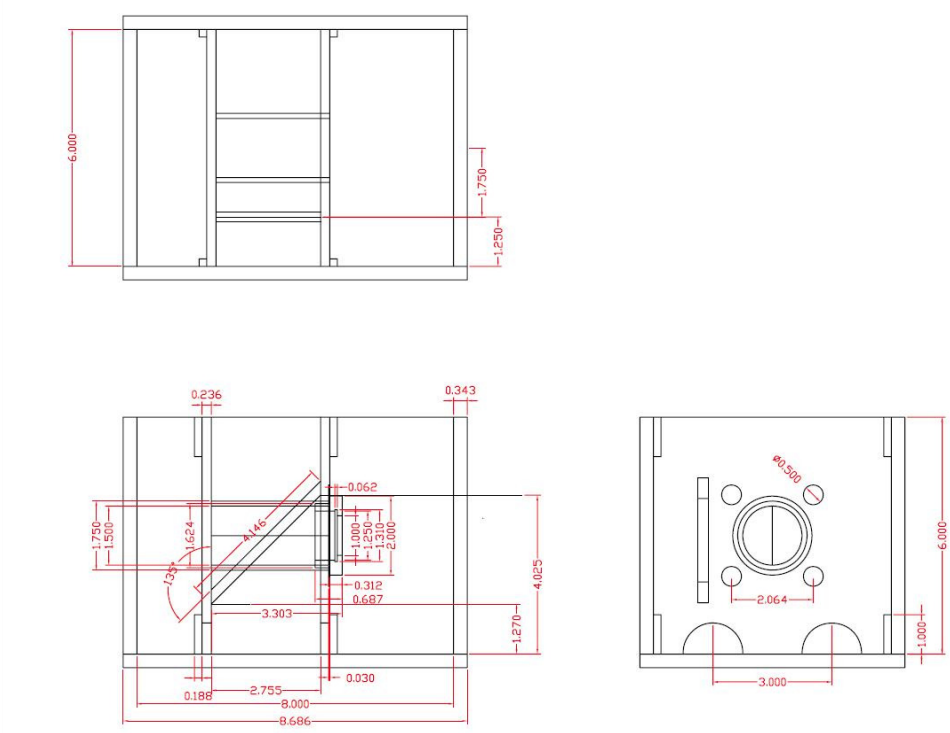

B

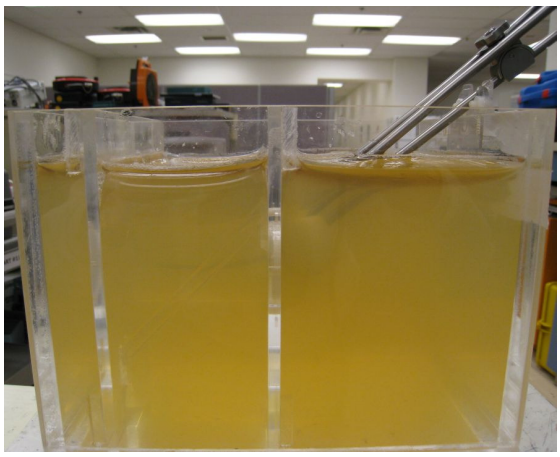

C D

Figure 3-2. Phantom illustration. (A) without gel; (B) three view schematic drawing; (C,D) with gel.

3.2.4 Image Acquisition

MR images were acquired on a Philips Intera 3T MR system (Philips Medical Systems, Cleveland, OH). The phantom was placed on the imaging couch in two orientations for scanning: (i) with the phantom frame and tandem aligned with the scan direction, and (ii) with the phantom rotated in the transversal plane. Image acquisition parameters were: T2 weighted, 1mm 3D isotropic scan sequence, TR/TE 1500/60 ms, FOV 26.6 cm, 1 mm slice thickness (please see Appendix A for a complete description of the protocol). The specific imaging sequence used was optimized for cervix brachytherapy. The average time to complete an MRI scan was 30 min.

CT scans were performed on a Phillips Brilliance Big Bore CT (Philips Medical Systems, Cleveland, OH). As for MR imaging, the phantom was scanned in aligned and rotated orientations with respect to the scan direction. A clinical brain axial scanning protocol was used (see Appendix B for more details), and the image acquisition parameters were: slice thickness 1.5 mm, exposure 500 mAs, and tube voltage 120 kV.

3.2.5 Reference Points

MR and CT images were imported to the Eclipse v.8.6 treatment planning system (Varian Medical Systems, Palo Alto, CA). To enable evaluation of error associated with the subsequent registration of these images, four reference points were marked on both sets of images. The four points were located: at the center of the cylinder bottom, adjacent to the intersection of the axis of the coordinate rod with the central plate, and at the centers of the two CT/MR compatible fiducial markers. Eclipse BrachyVision software was used to locate and mark these points.

3.2.5.1 Locating the Center of the Cylinder Bottom (Point 1)

To locate (x,y) coordinates, the "Circle Cursor" tool was used to approximate the size of the cylinder, and the center coordinates of the cylinder were obtained when the circle cursor was matched with the cylinder circle on the transversal view (Figure 3-3 (A)). The locating error depends on the circle cursor radius (1 mm increments) and how uniformly round the cylinder image is. The maximum locating error is estimated to be about 0.4 mm. Figure 3-3 (B) indicates the longitudinal position where the transversal view is located. The z coordinate of this point was obtained by a voxel-intensity based method: the "Line Profile" tool was used to find the center of the plastic frame of the cylinder bottom in the longitudinal direction (Figure 3-3 (C)). The locating error of z is approximately half the distance of the unit step in voxel intensity in the line profile, i.e., half the slice thickness.

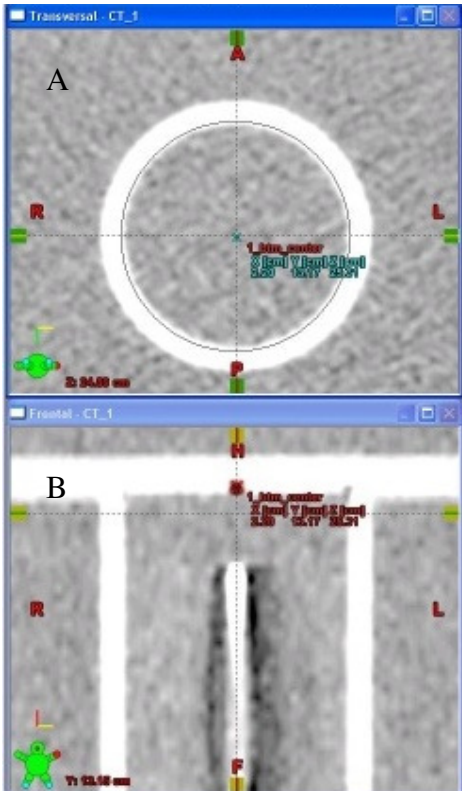

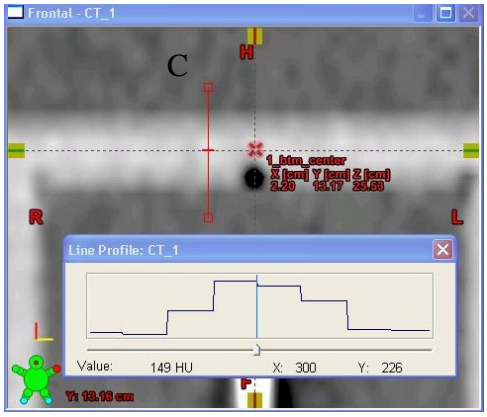

Figure 3-3. Locating the center of the cylinder bottom. (A,B) Locate (x,y) coordinates, (C) locate (z) coordinate.

3.2.5.2 Locating the Point Adjacent to End of the Coordinate Rod (Point 2)

As Figure 3-4 (A) shows, the x coordinate was defined to be the center of the rod in the x direction on the frontal view on the surface of the plastic plate. The y coordinate was defined to be the center of the rod along the y direction on the transversal view (Figure 3-4 (B)). Similar to locating the z coordinate of point 1, the z coordinate of point 2 was located at the center of the plastic plate along the z direction using the "Line Profile" tool (Figure 3-4 (C,D)). Because the line profile was used as before, the locating error was again approximately half of the slice thickness.

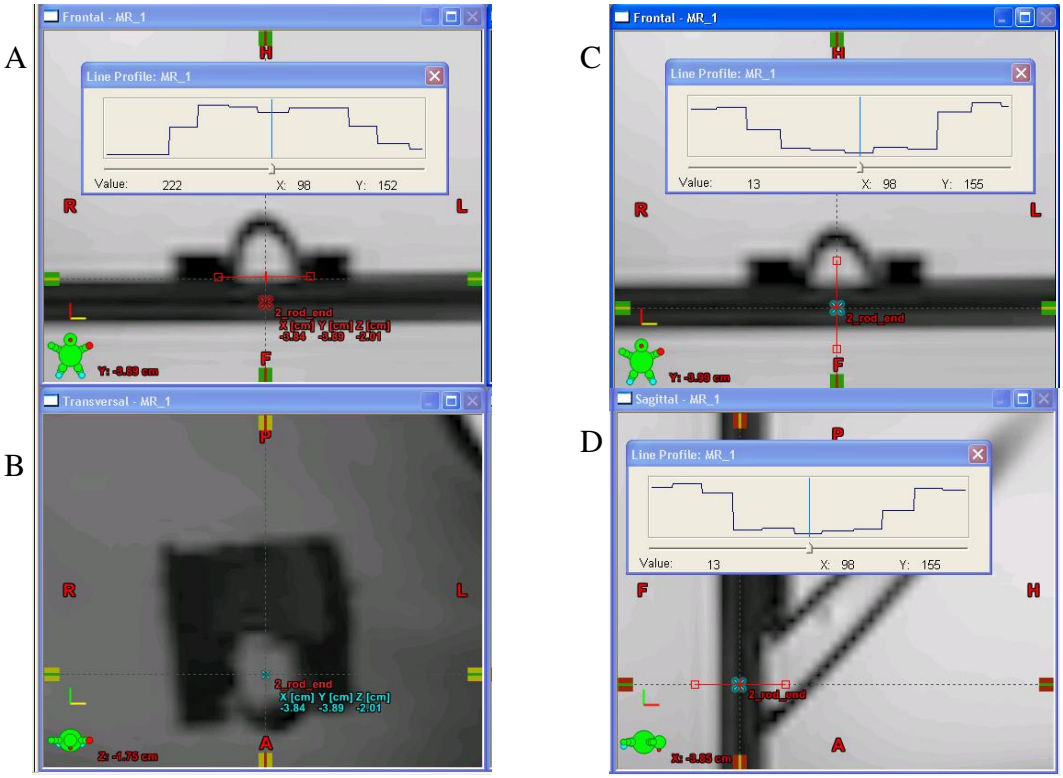

Figure 3-4. Locating the point adjacent to the end of the rod. (A,B) Define (x,y) coordinates, (C,D) define z coordinate.

3.2.5.3 Locating the Two Fiducial Marker Points (Points 3 and 4)

As the fiducial markers are small cylinders having the same orientation as the big hollow cylinder, the (x,y) coordinates were located using the same method for determining the center of the cylinder bottom (point 1): the "Circle Cursor" tool was used to approximate the circumference of the fiducial markers on the transversal view, and the center coordinates of the circle were obtained. The z coordinates were determined using the "Line Profile" tool to find the center positions of the small cylinders in the longitudinal direction.

3.2.6 Registration

Manual registration tools ("Translate" and "Rotate" in the Registration Workspace) in Eclipse v.8.6 were used to register the MR and CT images. The slices containing the cylinder wall and the parallel plates were used to guide the registration because there is visible contrast between plastic and gel. Registered images were evaluated by using "Blending View", "Split View", "Chess View", and "Spy Glass" tools on three image views (Frontal, Sagittal, and Transversal). Registration was performed on four different pairs of acquired images: aligned CT vs. aligned MR, aligned CT vs. rotated MR, rotated CT vs. aligned MR, and rotated CT vs. rotated MR.

3.2.6.1 Registration Error

The coordinates of the reference points on both types of images were obtained from cursor positions on fused images in the Planning Workspace. As there is a coordinate range for the marker remaining highlighted while moving the cursor (indicating the cursor is placed on the marker), the coordinate reading error was estimated as the coordinate range. The registration error (RE) was estimated as the average root mean square distance between MR and CT displayed corresponding reference points on fused images.

$$\mathrm{RE} = 1/4 \sum_{i=1}^{4} \sqrt{(x_{Mi} - x_{Ci})^2 + (y_{Mi} - y_{Ci})^2 + (z_{Mi} - z_{Ci})^2} \quad , \qquad \text{(Eq. 3-1)}$$

where *M* stands for MR, *C* stands for CT, and *i* is the number of reference points.

According to standard error propagation rules, the registration error uncertainty δRE is

$$\delta\mathrm{RE} = \frac{1}{4} \sum_{n=1}^{4} \frac{\sqrt{|x_{Mn} - x_{Cn}|^2 ((\delta x_{Mn})^2 + (\delta x_{Cn})^2) + |y_{Mn} - y_{Cn}|^2 ((\delta y_{Mn})^2 + (\delta y_{Cn})^2) + |z_{Mn} - z_{Cn}|^2 ((\delta z_{Mn})^2 + (\delta z_{Cn})^2)}}{\sqrt{(x_{Mn} - x_{Cn})^2 + (y_{Mn} - y_{Cn})^2 + (z_{Mn} - z_{Cn})^2}}$$

(Eq.3-2)

where δx, δy, δz are the error estimates for reference point definition, contributed by two parts: reference point locating error (δl) and coordinate measurement error (δm). The error propagation is as follows:

$$\delta_j = \sqrt{(\delta l_j)^2 + (\delta m_j)^2} \quad , \qquad \text{(Eq. 3-3)}$$

where *j* could be *x*, *y*, or *z*.

3.2.7 Applicator distortion in MR Images

Inspection of the fused CT-MR images revealed that visible applicator distortion was present in MR, including an extension of the tandem at its tip. To measure the extension of the applicator on MR with respect to CT, the tip of the applicator was marked on both images using the "Line Profile" tool. As Figure 3-5 (A) shows, the point corresponding to the sharp change in "CT value" on the line profile was marked as the applicator tip. For the cases where there is a partial volume effect (Figure 3-5 (B,C)), the point in the middle of the two end-points of the vertical line segment was defined to be the tip. The tip markers on registered CT and MR images were compared and the distance between them (extension) was measured. The error in this distance is estimated from the tip point locating errors for both CT (δ_C) and MR (δ_M) images:

$$\delta = \sqrt{\delta_C{}^2 + \delta_M{}^2} \quad , \qquad \text{(Eq. 3-4)}$$

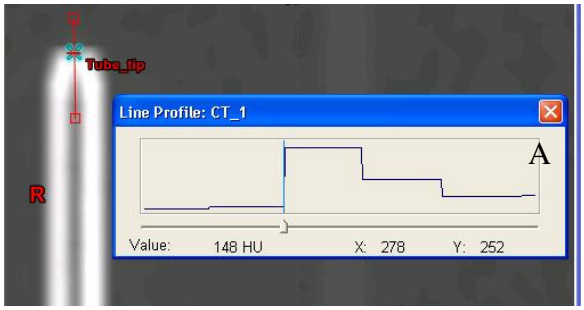

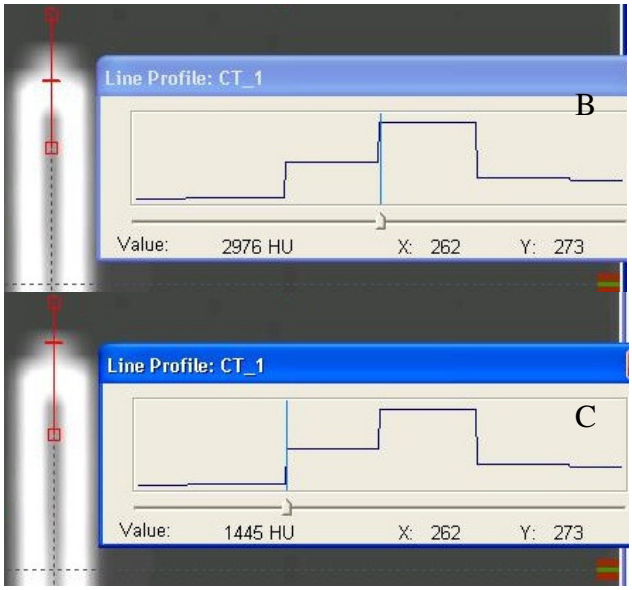

Figure 3-5. Definition of applicator tip position. (A) point corresponding to the sharp change in "CT value" on line profile was marked as the applicator tip; (B,C) two end-points corresponding to the vertical line segment for cases where there is a partial volume effect. The point in the middle of the two points is defined to be the tip.

3.3 Results

Contrast provided by the plastic phantom frame, plastic inserts, and contained gel assisted in distinguishing the phantom structure clearly on all CT and MR images. The applicator with its tandem source channel was clearly visible on all the CT images, while on the MR images the tandem appeared deformed, and its source channel was not visible (Figure 3-6). One can see that the tandem appears to have an expanded middle part and an unexpected neck near the tip. The applicator also looks longer on the MR image than on the CT image, which is illustrated on the fused images (Figure 3-7).

Measurement errors were generated in the process of locating the reference points and the applicator tip, as well as in obtaining the coordinates of reference points from fused images. These error estimates and the sources of error are listed in Table 3-1. For the reference points, the error in obtaining coordinates on fused images was estimated to be 0.25 mm, determined as one-half the observed coordinate range for picking a point using the cursor. Combined with the point

locating uncertainty, estimated to be from 0.4 mm to 0.75 mm depending on the locating tools, the total uncertainty in each coordinate was calculated to range from 0.65 mm to 1 mm.

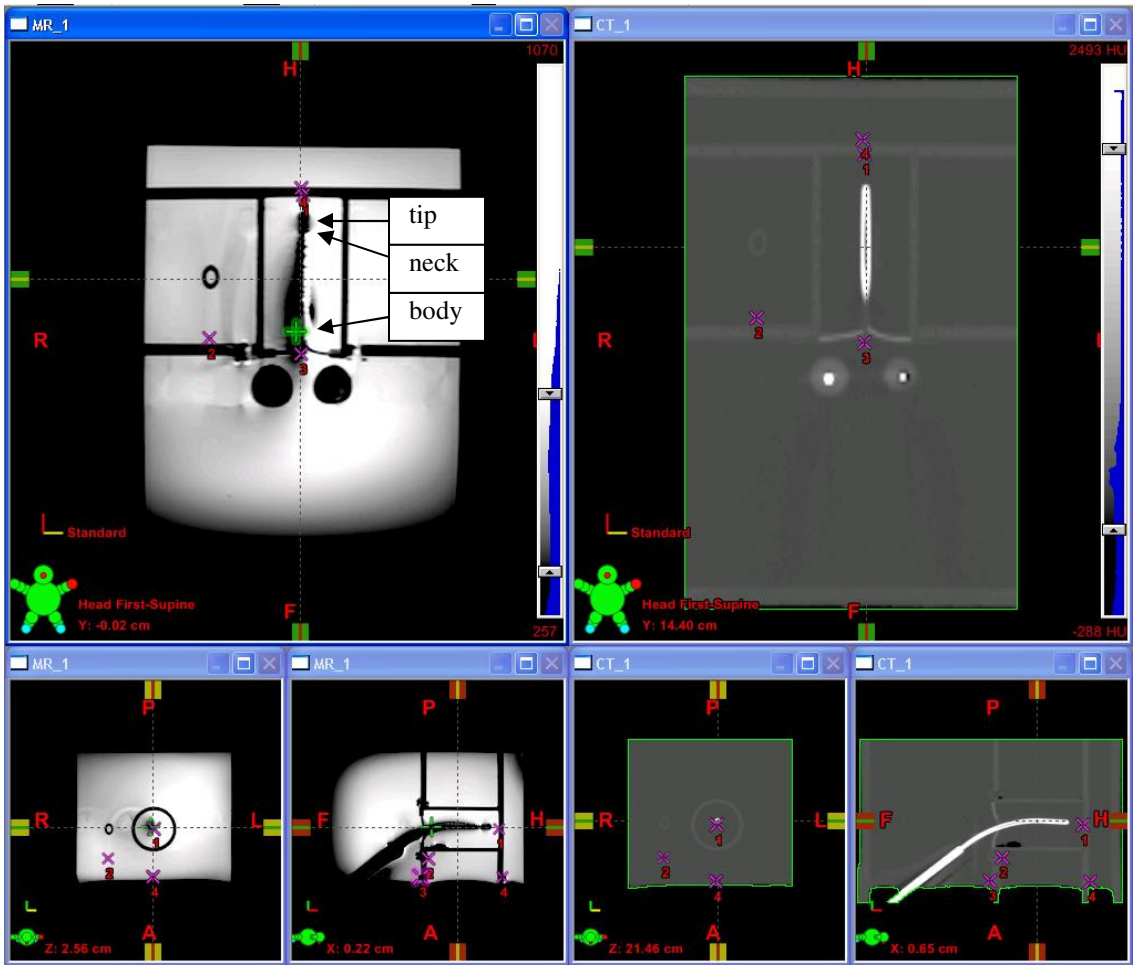

Figure 3-6. MR and CT images of the cervix applicator in the phantom

Table 3-1. Point measurement error estimates

Point #	Coordinate	Error value	Source of error
Locating reference points			
1,3,4	x,y	~ 0.4 mm	depends on the circle cursor radius (1 mm increments) and how uniformly round the cylinder image is.
	z	0.75 mm for CT 0.5 mm for MRI	half of slice thickness
2	x,y,z	0.75 mm for CT 0.5 mm for MRI	half of slice thickness
Reading reference point on fused images			
	x,y,z	~ 0.25 mm	half of coordinate range for highlighted marker (indicating cursor is placed on marker) while moving cursor
Locating tip of applicator			
	z	0.75 mm for CT 0.5 mm for MRI	half of slice thickness

Table 3-2. Registration error estimate and MR image distortion estimate

Trial 1	CT	MR	Registration error (mm) ± 0.9 mm	Extension (mm) of applicator tip on MR with respect to CT ± 0.9 mm
	Straight	Straight	0.7	5.2
	Straight	Rotated	0.6	4.4
	Rotated	Straight	0.7	4.3
	Rotated	Rotated	0.8	3.7
	Average		0.7	4.4
Trial 2	Straight	Straight	0.5	6.0
	Straight	Rotated	0.8	6.3
	Rotated	Straight	0.7	6.7
	Rotated	Rotated	0.7	6.4
	Average		0.7	6.4

The results of registration error calculation (Eq. 3-1) for different pairs of CT and MR images are presented in Table 3-2. Using Eq. 3-2, the uncertainty for the registration error estimate is 0.9 mm. It can be seen that registration errors obtained from different image pairs are close to each other. The registration error is small (less than 0.8±0.9 mm) and within the estimated uncertainty (0.9 mm) for finding it. The mean registration error is 0.67 mm with SD of 0.08 mm. The results indicate that the image registration procedure itself is acceptably accurate and the definition of reference points is reliable.

Figure 3-7 is a fused CT-MR image where the image presentation mode was chosen to display a 50% blend of both modalities. On the fused image, the applicator appears longer on MR than on CT. This length extension provides one measure of the distortion. The extended length on different pairs of registered images was measured and the results are summarized in Table 3-2. The average length extension for trial 1 is 4.4±0.9 mm, while it is 6.4±0.9 mm for trial 2 (The uncertainty of 0.9 mm was calculated from Eq. (3-4)). The difference probably comes from the fact that for trial 1 the CT scan had a partial volume effect at the applicator tip, which led to a relatively less accurate tip location using the voxel intensity based method.

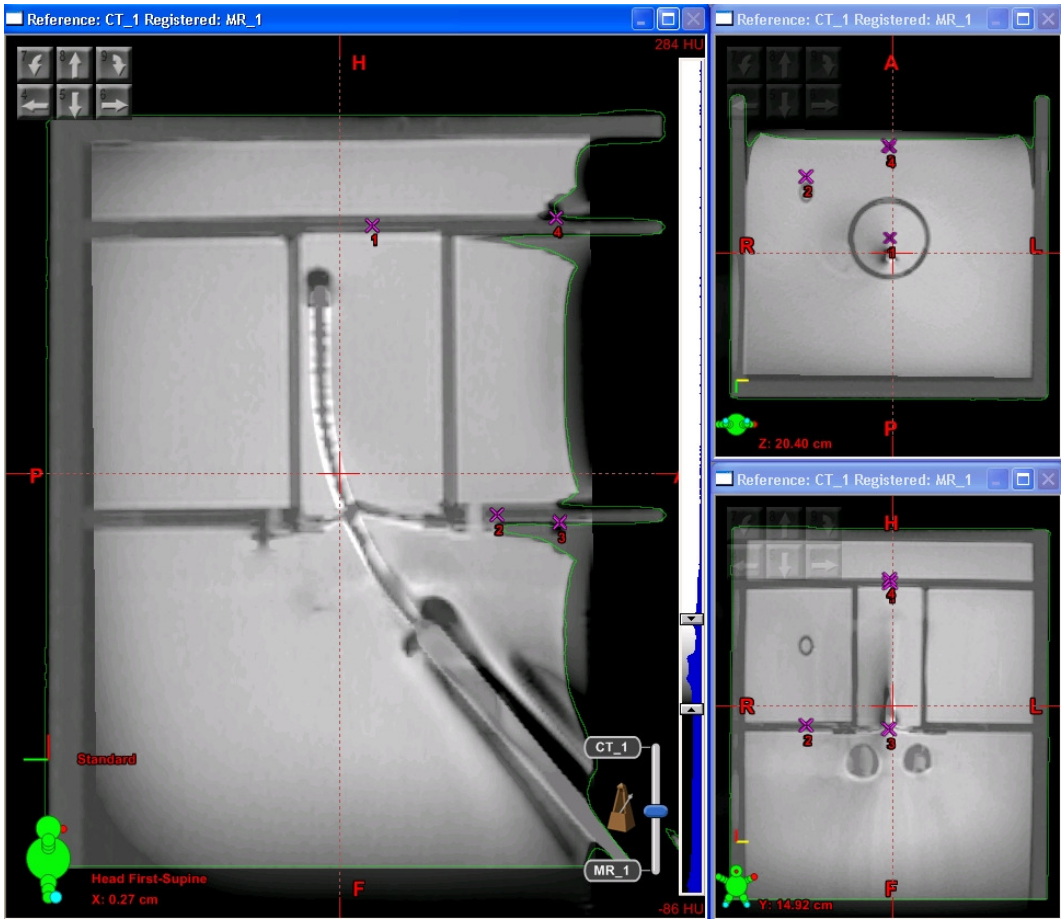

Figure 3-7. Applicator on fused CT-MR image

3.4 Discussion

This study assessed the MR image distortion for a titanium T&O applicator by fusion of CT and MRI phantom scans. The experimental work shows that visible applicator distortion was present in MRI, including an extension of the tandem at its tip. The longitudinal extension of the tandem tip on MRI with respect to CT was measured to be around 5 mm. The other distortions observed in the MR images of the tandem are the narrowed neck and swollen body part in the transverse direction (see Figure 3-6), which does not affect the fixed applicator

geometry defined by the tandem midline. Given the fact that the applicator geometry remains fixed from CT to MR, it is advised to use the tandem midline combined with the external surface of the uterus as guides to clinical CT-MR registration. Using this kind of image registration, the MR distortion in the transverse direction will have very little impact on the clinical objective of identifying the applicator. The use of the external surface of the uterus also ensures that the registration will be best in the volume of greatest clinical interest. Using the central axis of the tandem and the measured extension on MRI enables a final applicator-based refinement to be made to the CT-MR image registration.

An EMBRACE (An **intErnational** study on **MRI**-guided **BRA**chytherapy in locally advanced **CE**rvical cancer) dummy run was conducted at CCI, using the tandem midline combined with the external surface of the uterus for registration. EMBRACE is a multi-center prospective observational study of patients with locally advanced cervical cancer treated using MRI-guided brachytherapy aiming at correlating image-based DVH parameters for the clinical target volume and for organs at risk with outcome analysis [EMBRACE 2008]. The applicator distortion was also observed in the dummy run image. The inspection of registered CT-MR images for a patient performed with 3T MRI shows the tandem tip extension to be ~5 mm (Figure 3-8A), agreeing with our phantom experimental results. This agreement suggests that the evaluation of applicator image distortion with the phantom experiment could be used to guide clinical image registration if the MR image distortion needs to be considered. It was also noted that for another dummy run patient scanned on a 1.5T MR (Philips Achieva 1.5T, software v.2.6.1), the extension is ~3 mm (Figure 3-8 (B)). This is expected since the susceptibility differences at higher magnetic field strengths cause larger field inhomogeneities in the MR images using the titanium applicator [Matsuura *et al.* 2005].

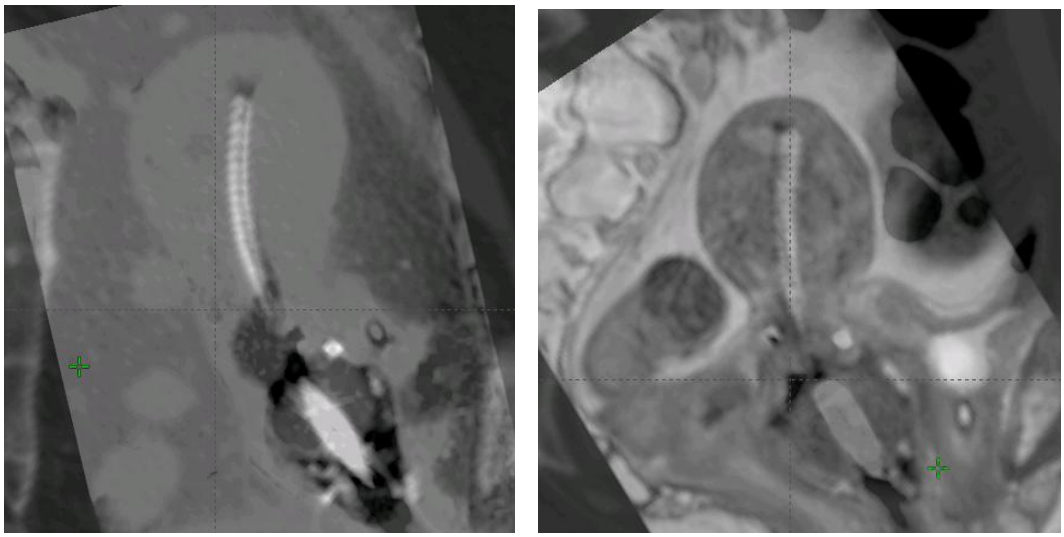

A B

Figure 3-8. Fused CT-MR images of CCI EMBRACE dummy runs. (A) scanned on a 3T MR system, (B) scanned on a 1.5T MR system. Note in panel A the CT image is given higher display weighting, whereas in panel B the MR image is.

The registration error evaluated by reference points in the phantom experiments is small (mean of 0.67 mm and SD of 0.08 mm). This result was obtained in a best case scenario as it was conducted on a rigid phantom and the reference points were well defined; the contrast between gel and plastic plate images was also good enough to permit them to be distinguished. It was noted also that the registration error is related to the author's skill in performing manual registration. As the final registration error obtained is within its estimated uncertainty range, it is unnecessary to pursue a more accurate registration method in this case. The uncertainty in the registration error comes partly from the uncertainty in locating reference points. Because there were no MR compatible markers small enough to act as reference "points", we needed to define reference points at specially selected locations in the phantom. Although it was challenging to define reference points with high precision, the tools in Eclipse BrachyVision software helped to locate the points relatively accurately. With a mean registration error of 0.67 mm (range 0.52-0.76 mm) and SD of 0.08 mm, the definition of reference points proved to be reliable and the image registration procedure proved to be accurate

and acceptable. In the clinical setting, registration error will be greater because of the absence of precisely locatable anatomical fiducial features, and the presence of organ and tissue motion and deformation. Nevertheless, from a visual inspection of the CCI EMBRACE dummy run images (Figure 3-8), using the external surface of the uterus and the tandem midline as guides to CT-MR registration appears to be a feasible approach,

References

An international study on MRI-guided brachytherapy in locally advanced cervical cancer (EMBRACE), 2008, https://www.embracestudy.dk/PublicDocuments/EmbraceProtocol.pdf.

Haack S, Nielsen SK, Lindegaard JC, Gelineck J, Tanderup K. Applicator reconstruction in MRI 3D image-based dose planning of brachytherapy for cervical cancer. *Radiother Oncol* 2009; 91(2):187-93.

Krempien R, Daeuber S, Hensley F, Wannenmacher M, Harms W. Image fusion of CT and MRI data enables improved target volume definition in 3D-brachytherapy treatment planning. *Brachytherapy* 2003; 2(3):164-71.

Matsuura H, Inoue T, Ogasawara K, Sasaki M, Konno H, Kuzu Y, Nishimoto H, Ogawa A. Quantitative analysis of magnetic resonance imaging susceptibility artifacts caused by neurosurgical biomaterials: Comparison of 0.5, 1.5. and 3.0 Tesla magnetic fields. *Neurologia Medico-Chirurgica* 2005; 45(8):395-98.

Thirion P, Kelly C, Salib O, Moriarty M, O'Reilly D, Griffin M, Armstrong J. A randomised comparison of two brachytherapy devices for the treatment of uterine cervical carcinoma. *Radiother Oncol* 2005; 74(3):247-50.

Wachter S, Gerstner N, Lefaza D, Knocke T, Potter R. The impact of MRI on the delineation of gross tumour volume in cervical cancer treatment planning: an interobserver analysis. *Radiother Oncol* 2001; 60:S3.

Viswanathan AN, Dimopoulos J, Kirisits C, Berger D, Potter R. Computed tomography versus magnetic resonance imaging-based contouring in cervical cancer brachytherapy: results of a prospective trial and preliminary guidelines for standardized contours. *Int J Radiat Oncol Biol Phys* 2007; 68(2):491-8.

Appendix A: MR Scan Protocol

A 3D turbo-spin-echo (TSE) sequence was implemented on Philips 1.5 and 3.0 Tesla systems to obtain an image set with 1 mm isotropic resolution over a field-of-view of 266×266×120 mm (foot-head, left-right, and anterior-posterior, respectively). The orientation of the image set was manipulated such that the read-encode dimension (nominally in the foot-head axis) was aligned with the central tandem within the uterus. The TSE turbo factor was implemented in the left-right phase-encode dimension. To prevent fold-over in this left-right direction, bilateral rest slabs, or saturation bands were placed on either side of the imaging volume to prevent tissue signal from outside the FOV from wrapping into the images. In order to recover the remaining transverse signal at the end of each echo train, a Philips DRIVE pulse was appended to the sequence.

As implemented on the 3.0 T system, the TR and TE were set at 1390 and 60 ms, respectively. A 6 element phased-array coil (the Philips SENSE-torso) was used for these scans. Due to the presence of the conductive titanium implant, the specific absorption rate (SAR) from the sequence was manually limited to half that which the scanner would normally allow. Though it may have been safe to operate the scanner under normal conditions, the limited experience that the MR community has with scanning this applicator at 3 Tesla made it prudent to take this precaution and limit potential localized heating. A consequence of this SAR limitation was that the refocusing pulses within the echo train were reduced significantly to 120 degrees. The total sequence duration was 19 minutes.

For the 1.5 T implementation, the TR and TE were set at 1000 and 80 ms, respectively. The coil used for this system was a 5 element phased-array cardiac coil. This coil was similar to the one used on the 3 T both in size and coverage. SAR is less of a concern at the lower field strength, and as a result the refocusing pulses were allowed to remain at an optimal 180 degree flip angle. The SAR from this sequence as implemented was already well below regulatory limits, so no

extra precautions in the form of manual limitations were taken. Also due to reduced heating concerns, the turbo factor on the 1.5 T scanner was increased to 34 to reduce the overall scan time, which in this implementation was 12 minutes.

Appendix B: CT Scan Detail

Because the phantom size is close to that of a human head, a brain axial CT protocol was used. The CT scan was performed with 120 kV tube voltage, 400 mAs exposure, and 16×0.75 mm collimation, using a gantry rotation speed of 1.5 seconds, a standard resolution scanning mode, a scan cycle time of 3 seconds, a brain standard (UB) filter without edge enhancement, and a 512×512 image matrix. Images were reconstructed with a slice thickness of 3 mm and a slice separation of 3 mm.

Chapter 4 Dose Optimization

4.1 Introduction

Traditional Manchester technique prescribes dose to point A which is related to applicator position rather than an anatomy based requirement. With the introduction of 3D image-based treatment planning with emphasis on an MRI assessment of the GTV and CTV, the dose distribution can be conformed to the target volume as visualized on MRI, thereby allowing a higher dose to be delivered to the tumor while sparing dose to the organs at risk, and potentially producing a greater local control and reducing treatment related morbidity. Although 3D image-based dosimetry is extensively used in EBRT and even in prostate brachytherapy [Bortfeld 1999, Yoshioka *et al.* 2005, Potter *et al.* 2008, Lessard and Pouliot 2001], it has not been implemented clinically in cervical brachytherapy in most centers [Potter *et al.* 2008].

4.1.1 Inverse Planning

The implementation of inverse planning integrates the anatomical information of each individual patient with the clinical dosimetric requirement. In contrast to the traditional manual trial-and-error treatment planning known as "forward planning", “inverse planning” utilizes pre-defined target doses, dose–volume constraints, and other importance factors for the target and each organ at risk. An optimization program is then used to determine the treatment plan which best matches all the input criteria.

Inverse planning has been implemented in EBRT for many years [Bortfeld 1999]. With the recent advances in imaging techniques and the identification of dose limits for cervix brachytherapy [Lang *et al.* 2007, Lindegaard *et al.* 2008, Trnkova

et al. 2009], it is logical to use inverse planning for brachytherapy of cervical cancer.

4.1.2 Objective Function

Frequently there are multiple clinical objectives which may compete with each other, like: “maximize the dose to the CTV” and “minimize the dose to the adjacent organs”. There is no guarantee that these multiple objectives can simultaneously be fulfilled, but specific trade-offs between the various objectives may be achieved depending on the judicious choice of importance factors. Commonly, the different clinical objectives (dosimetric constraints for tumor and critical organs) are combined and transformed into a single mathematical function called an “objective function”. The task of the inverse planning algorithm is to find a solution that optimizes the objective function.

4.1.3 Optimization Methods

Anatomy-based dose optimization is the final step in achieving 3D image-based treatment planning. For PDR cervix brachytherapy, given n possible source positions (dwell positions), the problem is to decide which dwell positions and dwell time configurations for the applicator fulfill a set of limits and constraints related to target coverage and OAR sparing to the highest possible degree.

Mathematical optimization is the study of the *extremal* values of a function: finding the extremal values and for what values of the independent variables the function attains its extremes. It is a branch of mathematics which has many topics with a huge literature.

There are many approaches to optimization problems and most of them use iterative numerical techniques. In practice, and without loss of generality, optimization problems are formulated as minimization problems. One major class

of methods for solving these is the "deterministic" methods (e.g., steepest descent, conjugate gradient, Nelder-Mead simplex) [Ezzell 2008]. These approaches find solutions by searching for a result that reduces the value of the objective function in each iteration; because each subsequent solution is obtained by moving "downhill", they are also called "downhill" search methods. These methods attain the extremal values rapidly but may be trapped in a local minimum when the objective function is mathematically nonlinear and presents multiple minima. The volume optimization algorithm in our treatment planning system (BrachyVision V8.2, Varian Brachytherapy, Palo Alto, CA) implements a Nelder-Mead simplex algorithm [Ezzell 2008], which is a relatively simple "downhill" search algorithm. It works well for situations with a limited number of variables.

4.1.4 Simulated Annealing

Another major class of methods introduces an element of randomness into the search process, and is called "stochastic" methods. "Simulated annealing (SA)" class algorithms are typical examples. SA was first introduced by Kirkpatrick et al. in 1983 [Kirkpatrick *et al.* 1983], and later was proved to be very useful in many previously intractable problems [Morrill *et al.* 1995]. SA has been the most widely used algorithm in EBRT in inverse radiotherapy planning [Bortfeld 1999], and has been investigated in a few gynecological cancer brachytherapy studies [Sloboda 1992, Dewitt *et al.* 2005, Chajon *et al.* 2007, Kubicky *et al.* 2008].

An SA algorithm searches for an optimal solution to an objective function in a fashion analogous to the natural process that occurs as a crystal cools from its initially high temperature and settles into its lowest energy state [Metropolis *et al.* 1953]. In SA, an effective temperature is introduced into the system being optimized, to simulate and control the cooling process as in a physical system. SA process starts from a high effective temperature, like one that "melts" the system being optimized, and then slowly lowers the temperature until the system "freezes" such that no further changes occur. At each temperature, the simulation

must proceed long enough for the system to reach a steady state. As is common to optimization problems, an iterative process is used in SA algorithms. If, during each iteration, only those configurations that lower the cost function of the system are accepted (as in "down-hill" methods), it is analogous to extremely rapid quenching from high temperatures to T=0. This is the reason why the resulting solutions of "down-hill" methods can be metastable [Kirkpatrick *et al.* 1983]. In contrast, SA methods do not strictly move downhill. They allow for controlled uphill steps in iterations in order to broaden the search for a better solution. The sequence of temperature reductions and the number of rearrangements of the *n* unknown variables attempting to reach equilibrium at each temperature are considered an annealing schedule [Kirkpatrick *et al.* 1983]. The wider sampling and hill climbing enable the annealing to have the potential of escaping local optima [Morrill *et al.* 1995, Ezzell 2008].

Besides the advantage of a greater likelihood of avoiding local extremum, SA has two more attractive characteristics. The most desirable is its simplicity to code and implement. The other is that SA can be used to optimize complex many-dimensional objective functions, even those without a closed functional form [Morrill *et al.* 1995]. These characteristics are especially suitable for our brachytherapy optimization problem.

Conversely, due to its stochastic nature, SA typically cannot guarantee that the best solution found is at true minimum, either local or global. Successive solutions to the same problem are not necessarily repeatable unless the same set of random numbers is used. The difference between successive solutions varies inversely with the speed of the cooling schedule [Morrill *et al.* 1995]. The computational burden is also very high for large problems so that a long execution time may be required to obtain a solution close to the global minimum. As computing speeds and capability improve, SA is becoming increasingly useful. Also in radiotherapy problems, we are looking for a practical solution that best meets dose volume constraints, but not necessarily at true physical optimum.

The purpose of this chapter is to apply the SA technique to 3D image-based dose optimization to deliver a highly conformal PDR cervix treatment (using tandem and ovoid applicator) with dose-volume constraints. In this chapter we first compare traditional Manchester plans and 3D image-based treatment plans obtained using the commercial BrachyVision software. There have been a few reports quantitatively comparing 3D image-based treatment plans with traditional Manchester plans [Lindegaard *et al.* 2008, Trnkova *et al.* 2009, Tanderup *et al.* 2010], as well as one comparing them with traditional Fletcher system plans [Jamema *et al.* 2010]. An SA method is then introduced and applied to a clinical-data-based computer simulation model. Effects on the results of optimization due to variations in structure sizes and distances between the structures were investigated using the model. DVH parameters (D90 of HR-CTV and D_{2cc} of OARs) and a conformal index (COIN) [van't Riet *et al.* 1997, Baltas *et al.* 1998] were used to evaluate the 3D dose distribution. The effect of the number of dwell positions on the dose distribution was also investigated.

4.2 Methods and Materials

4.2.1 Patients and Treatment

For this study 14 cervical cancer patients were randomly selected. All patients initially received whole pelvic EBRT of 36 - 45 Gy in 20 - 25 fractions prior to brachytherapy.

A CT/MRI compatible titanium Henschke-style tandem and ovoids applicator (Mick Radio-Nuclear Instruments, Inc., Mount Vernon, NY) was used for the brachytherapy treatments (see Section 2.4.4 for description of the applicator).

CT and 3T MRI scans were made after insertion of the applicator. The image acquisition protocol for MR scanning was the same as described in Chapter 3. The CT scan was obtained on a Philips Brilliance Big Bore Scanner (Philips

Healthcare, Andover MA). Special procedures including the use of under-knee supports were followed to minimize patient movement. The image data sets were exported from the scanners to a DICOM server and then imported into the BrachyVision planning system. Image fusion of CT and MRI was performed manually with the help of a mutual information metric. Applicator reconstruction was based on visualization of the applicator components in the CT images. Target and OAR volumes were defined according to GEC-ESTRO Working Group recommendations [Haie-Meder *et al.* 2005, Potter *et al.* 2006]. For each patient, the GTV and the HR-CTV were delineated by the radiation oncologist, incorporating information from T2-weighted MR images. OARs included the bladder, rectum, and sigmoid. ICRU rectum and bladder points were also determined.

This was followed by the planning of a PDR ^{192}Ir intracavitary brachytherapy treatment.

4.2.2 Dose Constraints and Conversion of EQD_2 to Physical Dose

To compare the effects of different dose rates and fraction sizes, the linear-quadratic (LQ) model for incomplete mono-exponential sublethal damage repair is commonly applied and recommended for clinical practice [Potter *et al.* 2006]. The recommended model parameters are α/β = 10 Gy for the target volumes (squamous cell cancer) and α/β = 3 Gy for the involved OARs [Potter *et al.* 2006], where α, β are tissue specific LQ parameters and the ratio (α/β) is a measure of a tissue's sensitivity to fractionation, that is, the size of dose given on each treatment.

Based on previous research [Lang *et al.* 2007, Lindegaard *et al.* 2008, Trnkova *et al.* 2009] and DVH parameters reported from our center for traditional treatment, the total biologically weighted dose constraints (the equivalent dose in 2 Gy fractions, EQD_2, was used) for radiotherapy were set to: minimum dose to 90% of

the HR-CTV (D90) ≥ 85Gy ($\alpha/\beta = 10$ Gy), minimum dose to the 2 cm^3 receiving the highest dose (D_{2cc}) of the bladder ≤ 90Gy ($\alpha/\beta = 3$ Gy), and D_{2cc} of rectum/sigmoid ≤ 75Gy ($\alpha/\beta = 3$ Gy), respectively. As both EBRT and brachytherapy contribute to the effects incurred by the tumor and OARs, the physical dose constraints for the PDR brachytherapy portion of the treatment were calculated from the total biologically weighted dose constraints and the time-dose pattern of external beam radiotherapy. The steps are detailed below:

First, convert known physical EBRT doses to EQD_2:

The biologically effective dose (BED) according to the LQ model is given by [Potter *et al.* 2006]

$$BED = Nd(1 + g\frac{d}{\alpha/\beta}), \qquad \text{(Eq. 4-1)}$$

where N indicates the number of fractions for EBRT or number of pulses for PDR radiotherapy, d is the dose per fraction and g is the incomplete repair function which for conventional fractionated EBRT equals 1.

The biologically weighted dose normalized to 2 Gy fractionation (EQD_2) is calculated as

$$EQD_2 = \frac{BED}{1 + 2/(\alpha/\beta)}. \qquad \text{(Eq. 4-2)}$$

Next, assuming that the volumes and points of dosimetric interest for brachytherapy receive the full EBRT dose, *obtain EQD_2 for the PDR portion as*:

$$EQD_2(PDR) = EQD_2(total) - EQD_2(EBRT), \qquad \text{(Eq. 4-3)}$$

Finally, convert EQD_2 for PDR portion to physical dose:

By reversing Eq. 4-2, one has

$$BED = EQD_2(1 + \frac{2}{\alpha/\beta}). \qquad \text{(Eq. 4-4)}$$

From Eq. 4-1, one obtains the physical dose for PDR, *D*, as

$$D = Nd = N\frac{-N + \sqrt{N^2 + 4Ng \bullet BED/(\alpha/\beta)}}{2g/(\alpha/\beta)}. \qquad \text{(Eq. 4-5)}$$

In Eq. 4-5, *N* indicates the number of pulses. For PDR the incomplete repair function, *g(PDR)*, is given by

$$g(PDR) = \frac{2}{\mu t}\left(1 - \frac{NY - SY^2}{N\mu t}\right), \qquad \text{(Eq. 4-6)}$$

where $\mu = \frac{\ln 2}{T_{1/2}}$, $Y = 1 - e^{-\mu t}$, $K = e^{-\mu x}$ and $S = \frac{NK - K - NK^2 e^{-\mu t} + K^{N+1} e^{-\mu N t}}{(1 - Ke^{-\mu t})^2}$

with *t* being the time for each pulse, *x* the time between pulses without irradiation, μ the repair rate constant, $T_{1/2}$ the half time for sublethal damage repair and N the total number of pulses.

Values for some of the parameters used in this work are as follows. The number of pulses (*N*) is either 50 or 58 for the patients investigated. The approximate time for each pulse (*t*) is 20 minutes for the average source strength used at the CCI, and the time between pulses without irradiation (*x*) is approximately 40 minutes.

As the value of half-time for repair for different tissues is not well established (most have been estimated experimentally but little data exist at dose rates lower than 1 Gy/h), a value of $T_{1/2}$ of 1.5 h is recommended for all tissues involved [Potter *et al.* 2006]. According to Potter *et al.*, treatment schedules with pulse sizes of 0.5 to 1.5 Gy repeated every 1 to 3 hours, would reproduce the effects of a low dose rate irradiation with a decrease in therapeutic ratio not greater than 10%, unless there are very short values of $T_{1/2}$ in late reacting normal tissues.

4.2.3 Computer Simulation Model

To test the SA method for cervix brachytherapy, a computer simulation model was constructed including a HR-CTV, organs at risk (bladder, rectum, and sigmoid), and tandem and ovoid PDR source positions. The number of tandem

source positions was generated according to the size of the HR-CTV – to make sure the tandem sources cover the HR-CTV from top to bottom. If the HR-CTV bottom is below the tandem flange, the lowest tandem source position is at the level just above flange. The distance between two adjacent tandem dwell positions is 5 mm. With reference to the actual shape of each structure (e.g., as Figure 4-1(A) shows), regular shapes of spheres and cylinders were used in the model to simulate the structures: HR-CTV and rectum are modeled as cylinders, and bladder and sigmoid as spheres. As the sigmoid shape had large variability among the patients considered, it was difficult to simulate it with one fixed shape. Hence that part (a balloon) of the sigmoid that was closest to the treatment applicator was considered in this model and simulated by a sphere. The actual relation of these structures is presented in Figure 4-1(B). The structure size, relative position of each structure, structure importance factors and dose constraints are variable and controlled by the user.

The model parameters include flange position (acting as coordinate system origin in the model), a point on the approximately straight portion of the tandem (to define the z axis of the model together with flange), center positions of all structures, diameters of bladder and involved sigmoid balloons, diameters and lengths of the cylinders simulating HR-CTV and rectum, angle of rectum with respect to tandem line in sagittal view, distance between the flange and the ovoid center line, and distance between the two ovoids.

A clinically relevant set of model parameters was created by making measurements on patient images displayed in BrachyVision. The structure center positions were obtained directly from the image coordinates for each patient as reported by the BrachyVision software. During the measurement process, the images on coronal and sagittal views were rotated so that the part of the tandem in the HR-CTV was straight and in line with the vertical slider bar on the treatment planning system. The measurements were performed on either the sagittal or coronal slices of the patient's fused MR-CT images, depending on the location of

the larger dimension of the structures. For rectum, the angle it made with the tandem line was recorded on the sagittal view.

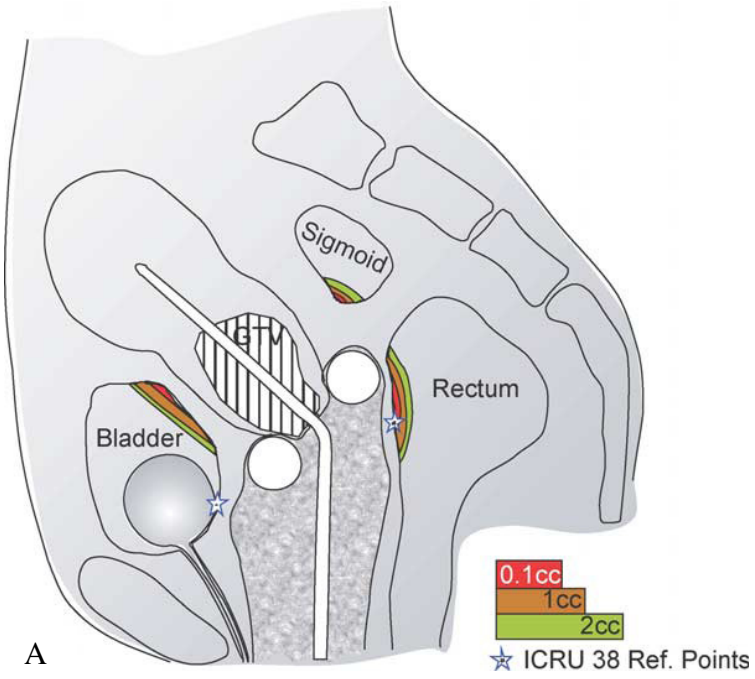

A

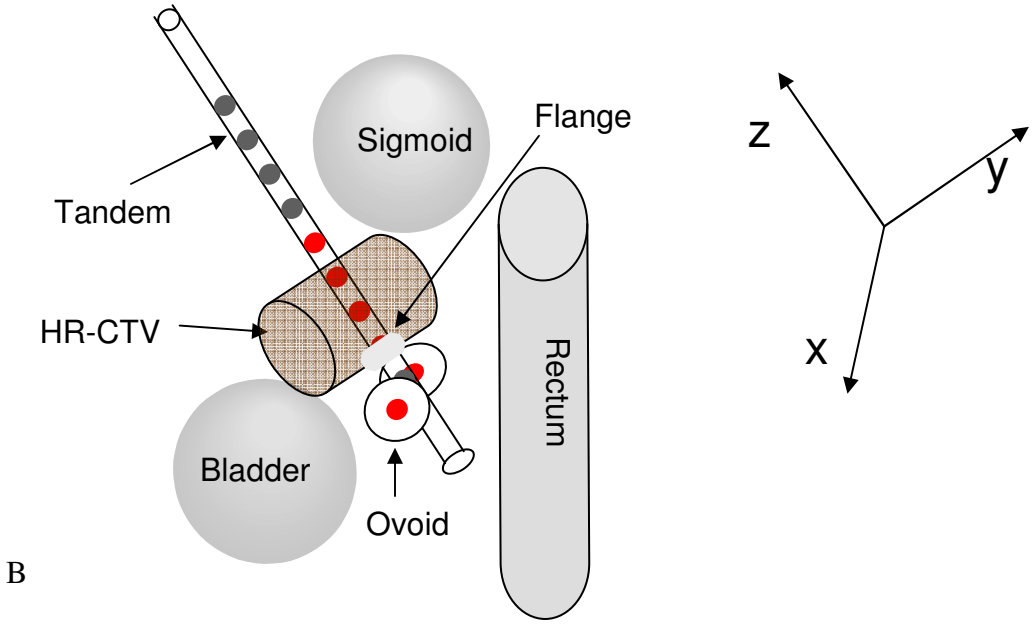

B

Figure 4-1. (A) Schematic anatomical diagram (sagittal view) indicating the relation between the structures and the most irradiated tissue volumes for rectum, sigmoid and bladder, from Potter et al. 2006; (B) computer simulation model. Red dots indicate activated dwell positions, and grey dots indicate inactivated dwell positions.

For the purpose of testing the SA software, one set of model parameters was roughly obtained from a patient's image data as described above, and seven more sets were subsequently generated by changing the sizes of and the distances between the structures. Effects of structure size and distance between structures were investigated.

For the purposes of clinical investigation using the SA software, sets of structure parameters were carefully defined by making measurements for five patients on the fused MR-CT images used for clinical treatment.

4.2.4 Treatment Planning and Optimization

To begin, we generated both the Manchester plan and an optimized plan for all 13 patients using our BrachyVision treatment planning system. The Manchester plan was practically a clinical plan, with a standard loading pattern and prescription to point A according to the ICRU guidelines [ICRU 1985]. The standard loading pattern was designed to simulate the historical radium loading (see Appendix). The dose to point A was normalized to 30 or 35 Gy in 50 or 58 pulses. For some patients, the relative dwell times in the ovoids were adjusted from their standard Manchester loading values to reduce dose to the rectum.

The optimized plan was produced using the built-in volume optimization software in the BrachyVision treatment planning system. The radiation source dwell times were adjusted by the software to meet the CTV and OAR constraints for the 3D image-based treatment planning study. To use the clinical experience collected over many decades in cervix cancer brachytherapy, the optimization started from the standard loading pattern. The dose distribution was continuously checked, and the optimization was stopped when the dose constraints were met, or further improvement was not feasible.

4.2.4.1 Objective Function

For our own optimization methods, constructing an objective function is required. An objective function is the mathematical form transformed from clinical objectives and will be optimized by the optimization technique. The objective function of our method is based on the dose prescription constraints on the target and each organ at risk (mainly consists of D90 to HR-CTV and D_{2cc} to bladder, rectum and sigmoid). It is constructed as follows.

For the i^{th} structure, a penalty value E_i over the structure is given by

$$E_i = I(V_{Li} - PV_{Li}) \bullet \lambda_{Li} + I(V_{Ui} - PV_{Ui}) \bullet \lambda_{Ui}, \qquad \text{(Eq. 4-7)}$$

where $I()$ is a function: $I(x) = \begin{cases} x, & x > 0 \\ 0, & x \le 0 \end{cases}$. V_{Li} is the actual volume in the structure receiving dose lower than the lower dose constraint, and PV_{Li} the maximally allowed volume in the structure receiving dose lower than the lower dose constraint (e.g., the maximally allowed volume lower than the lower dose constraint to HR-CTV, D90, is $V_{HR\text{-}CTV} \times 10\%$). V_{Ui} is the actual volume of the structure receiving dose greater than the upper dose constraint, and PV_{Ui} the maximally allowed volume in the structure receiving dose greater than the upper dose constraint (e.g., the maximally allowed volume greater than the upper dose constraint to bladder, D_{2cc}, is 2000 mm^3). λ_{Li} and λ_{Ui} are importance or weighting factors applied to each structure. Those structures or dose constraints with more importance are usually given higher weighting factors.

The objective function E of the dwell time distribution is given by the sum of penalty values of all structures:

$$E = \sum_i F_i \bullet E_i, \qquad \text{(Eq. 4-8)}$$

where $F_i = C/(PV_{Li} + PV_{Ui})$, which is a normalization factor to make the penalty value of each structure comparable. C is an arbitrary constant and is set to 2000 in this implementation.

4.2.4.2 Dose Calculation

According to TG43 [Nath *et al.* 1995], the dose rate at a dose calculation point i, from a dwell position j occupied by a point-like source, is given by the following equation:

$$\dot{D}_{ij} = (S_k \Lambda / r_{ij}^2)\, g(r_{ij}) \Phi_{an}(r_{ij}) \quad , \qquad \text{(Eq. 4-9)}$$

where S_k is the air kerma strength of the source, Λ is the dose rate constant, r_{ij} is the distance between the dwell position j and the dose calculation point i, $g(r_{ij})$ the radial dose function, and $\Phi_{an}(r_{ij})$ the anisotropy factor. This expression yields accurate dose rate calculations for our GammaMed plus PDR source, whose active volume is a cylinder, 0.6 mm in diameter and 0.5 mm long (Figure 4-2). Since for distances within 6 cm from this source, $g(r_{ij}) \approx 1$ with a variation < 1%, and for distances within 10 cm the variation is < 5%, $g(r_{ij})$ was set to unity for simplification. For the same reason, $\Phi_{an}(r_{ij})$ was also set to unity.

The dose D_i at each dose calculation point i is given by the sum of the dose rate contributions from all dwell positions j with respective dwell times t_j:

$$D_i = \sum_j \dot{D}_{ij} t_j \, . \qquad \text{(Eq. 4-10)}$$

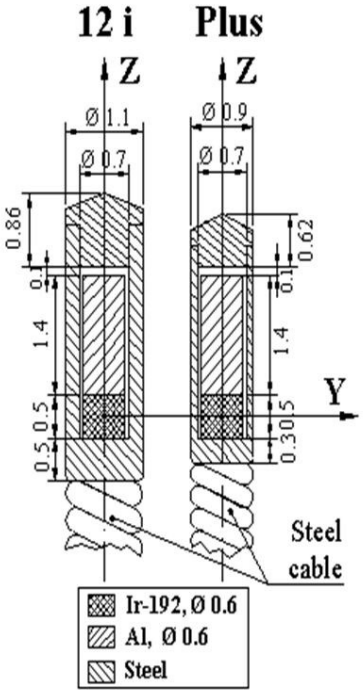

Figure 4-2. The GammaMed 12i and Plus PDR sources (Perez-Calatayud et al.). Dimensions are in mm. This 0.9 mm external diameter, 2.92 mm long ^{192}Ir source is used in the GammaMed Plus PDR system. The source design incorporates an active core of length 0.5 mm and diameter 0.6 mm, whose center is located 2.37 mm from the source tip. A 1.4 mm long, 0.6 mm diameter aluminum plug is also located within the source capsule, distal to the active core. The encapsulating material is stainless steel having a sidewall thickness of 0.1 mm.

4.2.4.3 SA Algorithm

a. Simulated annealing

The simulated annealing algorithm is an anatomy-based inverse planning optimization algorithm. After the volumes of interest are contoured, dose constraints are applied to dose calculation within each volume. The algorithm identifies the combination of dwell times that best conforms to the dose constraints of the target volumes and critical organs, in order to achieve the purposes of penalizing over/under doses in target(s) while protecting OARs from overdoses.

Starting with an initial dwell time distribution, the SA algorithm generates a small random displacement to the dwell times and calculates the resulting objective function value (called "energy" hereafter) at each step k. By evaluating the energy difference between new energy and old energy, $\Delta E=E(k+1)-E(k)$, the transition is either accepted or rejected. If $\Delta E<0$, the transition is always accepted. If $\Delta E>0$, the transition becomes the new state with probability determined by an acceptance function. The probability of accepting the transition is

$$P(\Delta E) = \exp[-\Delta E / \kappa_B T(k)], \qquad \text{(Eq. 4-11)}$$

simulating the Boltzmann probability factor, where κ_B is the Boltzmann constant, and T is the effective-temperature parameter. If $P(\Delta E)$ is greater than a random number selected in the interval (0,1), the new transition is used to start the next step, otherwise the old state is retained. The unique characteristic of annealing distinguishing it from downhill iterative methods is that it does not easily get stuck in a local minimum because transitions out of a local minimum are always possible at nonzero temperature. It can be inferred from Eq. 4-11 that at lower temperature the new configuration is accepted with reduced probability. The temperature parameter decreases according to the cooling schedule, and when the temperature is sufficiently low, the algorithm will not evolve further.

b. Cooling schedule:

Simulated annealing achieves the optimization by finding the low-temperature state of a system when an objective function is given. At each temperature, the simulation must proceed long enough for the system to reach a steady state [Kirkpatrick *et al.* 1983].

Geman and Geman [Geman and Geman 1984] have proven that if the cooling schedule is constructed as follows (a necessary and sufficient condition), i.e. the effective temperature at iteration k, T(k), is inversely proportional to a logarithmic function of time given a sufficiently high initial temperature T_0,:

$$T(k) /T_0 = 1/\log(1+k), \qquad \text{(Eq. 4-12)}$$

then the convergence of the classical SA algorithm to the global minimum can be achieved.

However the above schedule is too slow in actual implementation. A fast cooling schedule was chosen to cool exponentially:

$$T(k)=(T_1/T_0)^k T_0, \qquad \text{(Eq. 4-13)}$$

which was used by [Kirkpatrick *et al.* 1983], with the ratio $T_1/T_0=0.8$. The initial temperature and the ratio are chosen empirically.

c. Relevant technical issues:

Random displacement generation

In this application to tandem-ovoid cervix brachytherapy, with the dwell time at each source position on the order of 1000 seconds, the random transition of dwell times at each step was chosen to be 20 seconds times normally distributed random numbers (with mean 0 and standard deviation 1). Larger displacements are more efficient in keeping the solutions off local extrema, but may result in metastable solutions because the transitions at each step are too wide. To mitigate this effect, a smaller random displacement is applied generally, but increased when the resultant new energies equal the old energies for three consequent times, which indicate the current configuration may be too far away from the objective solution.

When a new configuration is accepted, the random displacement is dropped to the original smaller range.

Stopping criteria

At each temperature, the simulation needs to proceed long enough for the system to reach a steady state. For the cooling schedule of Eq. 4-13, at each temperature, sufficient dwell time rearrangements are attempted such that either there are 20 accepted rearrangements, or the number of attempts exceeds 300. If the new dwell time rearrangements have been rejected a large number of times (2000-4000), the system is considered "frozen" and annealing stops. Annealing also ceases if the energy equals zero.

Initial temperature

Empirically we chose to start at a high effective temperature, T_0=5-10, to "melt" the system. At this temperature, most solutions are accepted even if they increase the energy from the last iteration.

Weighting factors

Controlling the balance between normal tissue sparing and the delivery of sufficient dose to the target volume is a major issue of dose distribution optimization. Weighting factors are not in percentile format as often seen in some commercial software. Currently weighting factors to all structures in the range of 8 – 10 will result in reasonable computation time for a general model test. Lower weights, e.g. 1 for all computation targets, will result in slower convergence of the algorithm.

However a strict fulfillment of dose constraints is sometimes too restrictive, especially when the OAR is in the immediate neighborhood of the HR-CTV. The problem can be reduced to some degree by applying different weighting factors for different structures and by slightly relaxing dose constraints on OARs. The weighting factors determine the relative importance of fulfilling the respective

constraint. A small weighting factor allows for some overdose beyond the barrier and may be used if this consequence is only a relatively mild complication. A large weighting factor must be used if any overdose may cause severe complications and has to be prevented by all means.

Number of dwell positions

One might be tempted to start from the maximum number of possible dwell positions and let the computer determine the number required (it is intuitive to think that a non-necessary dwell position will have zero dwell time if the computer finally finds that there is no need to include this dwell position). However, due to the large search space and the presence of non-unique solutions, this approach is generally impractical. In this study, different numbers of dwell positions were attempted for optimization. The maximum number is the one transferred from the Manchester plan and the minimum number is obtained for each patient by removing distal dwell positions in the tandem so that the superior aspect of the HR-CTV is covered. Results were evaluated by comparing DVH parameters.

Initial dwell times

To make sure the optimization algorithm is not unduly influenced by the initial choice of dwell times (in other words, to verify that the method does not get stuck in some local minimum), different initial dwell times were also investigated for optimization.

Computation resolution

A dose calculation grid having a spatial resolution of 1 mm in each Cartesian direction was used for all computation.

A flow chart of the SA algorithm follows.

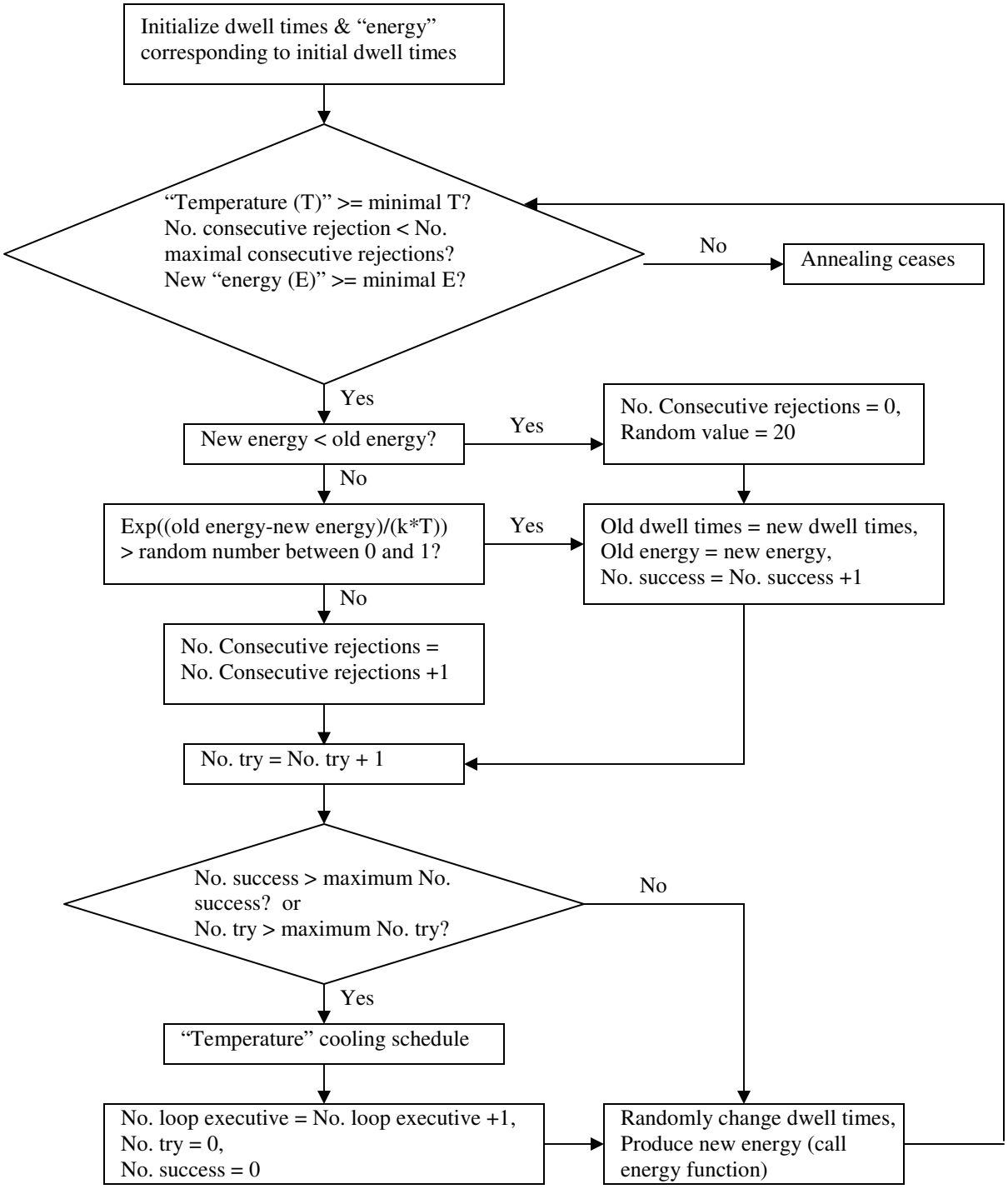

Figure 4-3. Flow chart of Simulated Annealing algorithm.

4.2.5 Evaluation

So far, in gynecologic brachytherapy in our center, the correlations between radiation dose and normal tissue effects have been assessed using point doses, standardized and proposed by the ICRU report 38 [ICRU 1985]. As it is generally agreed that dose-volume histogram relations are superior to point doses in assessing dose volume effects, dose-volume parameters have been proposed by the GEC-ESTRO GYN group [Potter *et al.* 2006]. The following parameters have been used in this study to assess plan quality: D90 and V100 for HR-CTV; D_{2cc} for organs at risk.

D90/D100 is the minimum dose delivered to 90%/100% of the volume of interest. Because D100 is extremely dependent on target delineation − small variations in the contour can cause large deviations due to steep dose gradients − D100 is not recommended as a reporting value due to its limited accuracy. D90 is less sensitive to these influences and is therefore considered to be a more 'stable' parameter [Potter *et al.* 2006]. D90 is also proposed as the prescription dose.

V100 is the volume (with regard to the GTV or CTV) receiving at least 100% of the prescribed physical dose. It describes how closely the intended treatment could be achieved in terms of target coverage, providing information indirectly on the proportion of underdosed area. Because V100 is based on the prescribed physical dose, it is only relevant within a specific dose rate and fractionation schedule. It can only be used for intra-patient plan comparison or comparison of patients treated with the same dose (rate) and fractionation [Potter *et al.* 2006].

When assessing late effects from brachytherapy, small organ volumes irradiated to a high dose are of major interest. As the dose distribution is inhomogeneous and because there is rapid dose fall-off especially in the organ volumes near the sources, dose assessment is recommended in reference to clearly defined dose values in these limited volumes [Potter *et al.* 2006]. D_{2cc} is thus recommended for

recording and reporting. D_{2cc} is the minimum dose in the most irradiated 2 cm^3 tissue volume, which is usually located adjacent to the applicator (Figure 4-1 (A)). These dose volume parameters can easily be calculated from a DVH and converted to biologically weighted EQD_2 doses, which makes them suitable for comparing plans that use different dose rate techniques such as PDR and HDR.

With intracavitary brachytherapy, there is an inhomogeneous dose distribution, which is more prominent in the tissues adjacent to the dwell positions. Therefore, in this study, a conformation index is used to compare different treatment plans. The COIN was introduced by Baltas *et al.* [Baltas *et al.* 1998] to quantitatively assess the degree of conformality, and has been applied in several studies [Brooks *et al.* 2005, Chajon *et al.* 2007]. This index defines the treatment quality by incorporating anatomic information and the radiation to the tumor, noncritical healthy issues, and organs at risk as follows:

$$COIN = CN \times \prod_{i=1}^{N} (1 - \frac{V_{OARref,i}}{V_{OAR,i}}), \qquad \text{(Eq. 4-13)}$$

where N is the number of OARs, $V_{OARref,i}$ is the i-th OAR volume receiving at least the reference dose, $V_{OAR,i}$ is the i-th OAR volume, and CN the conformation number defined by van't Riet *et al.* [van't Riet *et al.* 1997]:

$$CN = \frac{CTV_{ref}}{CTV} \times \frac{CTV_{ref}}{V_{ref}}, \qquad \text{(Eq. 4-14)}$$

where CTV_{ref} is the target volume receiving at least the reference dose D_{ref}, CTV is the target volume, and V_{ref} the volume covered by the reference dose in the whole body. CN takes into account not only the coverage of CTV by the reference dose, but also the excess radiation to normal tissue outside the CTV. The ideal situation is shown by CN=1, where the CTV is totally covered by a reference dose and no dose is given to the surrounding normal tissues outside the CTV. The latter part of Eq. 4-13 takes into account the unwanted radiation to the critical OARs. The ideal situation exists when no OAR receives any dose higher than the reference dose, so that this part also equals unity.

ICRU point A is also adopted for evaluation and comparison with the traditional Manchester plan.

4.3 Results

4.3.1 Comparison of Manchester Plan and BrachyVision Optimized Plan

Table 4-1. Total biologically effective dose constraints (summarized from previous research [Lang et al. 2007, Lindegaard et al. 2008, Trnkova et al. 2009]).

HR-CTV	D90	≥ 85Gy (α/β = 10 Gy)
Bladder	D_{2cc}	≤ 90 Gy (α/β = 3 Gy)
Rectum	D_{2cc}	≤ 75 Gy (α/β = 3 Gy)
Sigmoid	D_{2cc}	≤ 75 Gy (α/β = 3 Gy)

Table 4-2. Physical dose constraints for brachytherapy treatment, calculated according to Section 4.2.2.

Patient No.	1	2	3	4	5	6	7	8	9	10	11	12	13
EBRT prescription dose (Gy)	45	40	45	39.6	45	36	45	45	45	36	36	36	36
EBRT fractions	25	22	25	22	25	20	25	25	25	20	20	20	20
HR-CTV D90 (Gy) ≥	38.24	42.63	38.24	42.33	38.24	44.9	38.24	38.24	38.24	44.9	44.9	44.9	44.9
Bladder D_{2cc} (Gy) ≤	39.15	42.4	39.15	42.18	39.15	44.1	39.15	39.15	39.15	44.1	44.1	44.1	44.1
Rectum D_{2cc} (Gy) ≤	29.76	33.58	29.76	33.33	29.76	35.52	29.76	29.76	29.76	35.52	35.52	35.5	35.52
Sigmoid D_{2cc} (Gy) ≤	29.76	33.58	29.76	33.33	29.76	35.52	29.76	29.76	29.76	35.52	35.52	35.5	35.52

Table 4-3. Dose volume parameters (Gy) for the Manchester plan and the BrachyVision optimized plan, using the dose constraints in Table 4-2.

Patient No.	1	2	3	4	5	6	7	8	9	10	11	12	13
	Manchester plan												
HR-CTV D90	37.23	**32.77**	**31.92**	**30.77**	41.34	**31.15**	**35.67**	35.94	**35.1**	50.09	**16.2**	**41.19**	**34.29**
Bladder D_{2cc}	**42.78**	40.90	**48.00**	**53.42**	40.93	25.8	36.23	**47.16**	37.67	56.17	34.94	NA	28.76
Rectum D_{2cc}	16.96	22.95	24.46	27.99	**40.05**	**45.79**	**34.6**	24.88	29.04	21.94	28.67	24.82	33.44
Sigmoid D_{2cc}	27.90	24.01	20.05	**40.03**	30.30	27.17	**34.4**	27.37	22.63	27.01	NA	**36.57**	26.43
	Optimized plan with dose constraints in Table 4-2												
HR-CTV D90	39.13	47.12	43.55	**40.77**	37.15	**39.47**	37.11	38.36	38.25	60.80	46.00	45.61	48.70
Bladder D_{2cc}	38.01	42.27	37.45	**45.14**	32.84	21.19	33.10	38.04	39.18	43.40	42.64	NA	31.80
Rectum D_{2cc}	14.81	18.19	17.39	20.60	**31.41**	**49.02**	**31.23**	20.96	29.47	20.70	26.15	26.36	34.60
Sigmoid D_{2cc}	29.16	32.63	29.24	**42.78**	15.68	**41.58**	28.32	29.03	27.49	28.10	NA	30.59	33.70

Note: bold values indicate that the corresponding dose constraints are not satisfied.

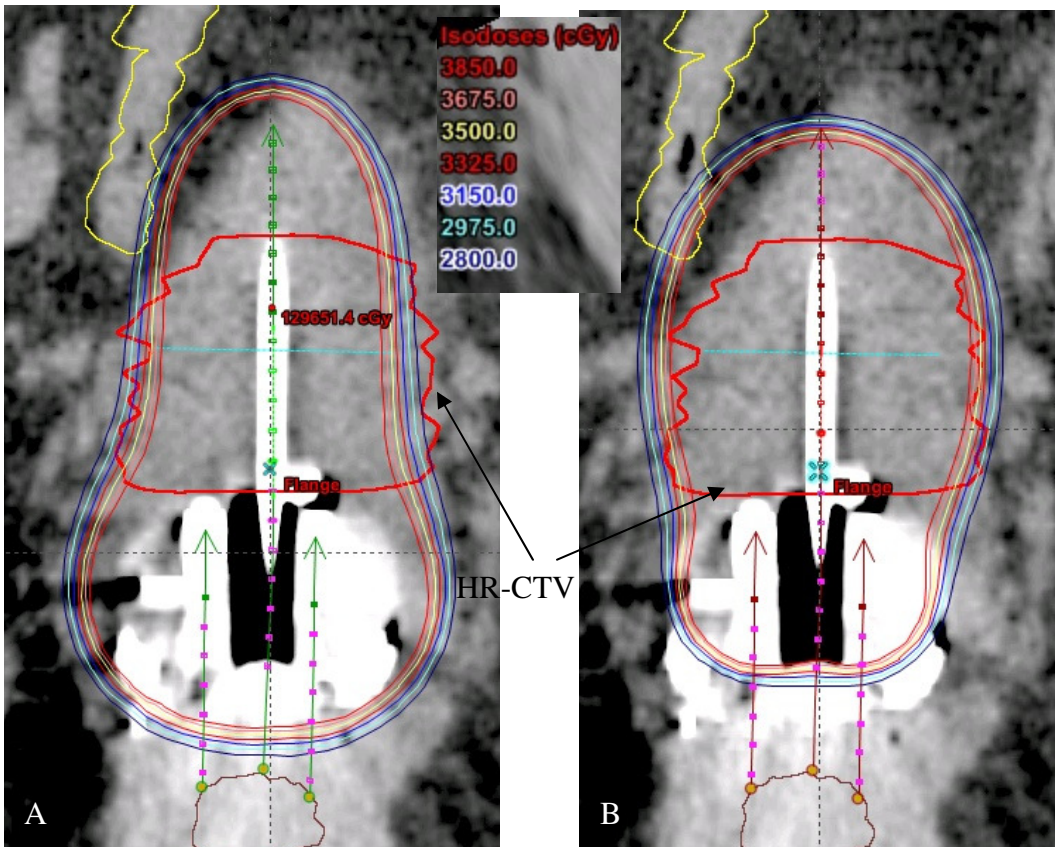

Figure 4-4. An example of the dose distribution in a para-coronal plane containing prescription points A (one at each end of the light blue line) for (A) a Manchester plan and (B) an optimized plan for the same patient, using BrachyVision software. The HR-CTV contour appears in red. The prescription dose is 3500 cGy.

Table 4-2 summarizes the physical dose constraints for brachytherapy treatment planning optimization, which were calculated from the total biologically effective dose constraints (Table 4-1) and actual EBRT treatment plans. A typical pear-shaped dose distribution was obtained for the Manchester plan as shown in Figure 4-4 (A). On the optimized plan (Figure 4-4 (B)), the isodose distribution is much more conformal to the HR-CTV contour and there is significantly less dose outside the HR-CTV.

Dose volume parameters for both plans were extracted from the respective DVHs and are summarized in Table 4-3. One can see that the optimized plans are

generally superior to the Manchester plans as, for a significant number of patients, the doses to the OARs are reduced: e.g., all three OAR D_{2cc}'s for patients 5, 7; bladder and rectum D_{2cc} for patients 1, 3, 4, and 8 (even with higher HR-CTV D90); bladder D_{2cc} for patient 10 (with much higher HR-CTV D90); sigmoid D_{2cc} for patient 12. For some patients although there is no improvement in dose sparing to OARs, HR-CTV D90 is remarkably higher: e.g., patients 2, 11, and 13. The dose constraints were fully met for most patients by the optimization technique, for example patients 1, 2, 3, 8, 9, 10, 11, 12, and 13. For patients 4, 5, 7 there is one OAR whose D_{2cc} is a little bit higher than the corresponding constraint. Only for patient 6 do OARs receive doses far beyond the specified dose constraints.

We hypothesize that some factors may be responsible for the lack of complete success: the contoured OARs are possibly too big or too close to the HR-CTV, or the optimization technique itself is not entirely suitable for this type of problem. With our simulation model and our own optimization technique, these factors are investigated in the next section. For simplification, the dose constraints for optimization in the following sections all use HR-CTV D90 $\geq$ 35 Gy, bladder D_{2cc} $\leq$ 40 Gy, and rectum/sigmoid $D_{2cc} \leq$ 30 Gy, which were generalized from Table 4-2.

4.3.2 Influence of OAR Size and Distance from HR-CTV on SA Optimization Using Our Simulation Model

Table 4-4 and Figure 4-5 summarize our investigation of 4 sigmoid radii (18, 22, 24 and 26 mm) and 2 distances between the sigmoid and the HR-CTV (34.1 and 30.6 mm). The values in bold indicate that the dose constraint was not satisfied for the corresponding case. The table shows that when the OAR sizes and distances from the HR-CTV are in a reasonable range, the SA method can effectively optimize dwell times. See cases 1, 2, 3, and 5 for instances where the dose constraints are all met.

Table 4-4. Dose volume parameters for investigation of the influence of sigmoid size and distance from the HR-CTV on SA optimization, using our simulation model. Basic physical conditions: radius and length of HR-CTV is 10 mm and 30 mm respectively; radius and length of rectum is 10 mm and 100 mm respectively; radius of bladder is 28 mm; center distance between HR-CTV and bladder is 37.7 mm; center distance between HR-CTV and rectum is 55.6 mm.

Case index	Sigmoid parameters		HR-CTV D90 (Gy)	Bladder D_{2cc} (Gy)	Sigmoid D_{2cc} (Gy)	Rectum D_{2cc} (Gy)	Energy (E) value
	Radius (mm)	Center distance to HR-CTV (mm)					
1	18	34.1	35	35.8	17.5	8.1	0
2	22	34.1	35	36.8	24.8	8.3	0
3	24	34.1	34.9	36.1	17.3	8.2	160
4	26	34.1	35	34.4	**37.1**	7.8	9848
5	18	30.6	35	36.3	21.7	8.2	0
6	22	30.6	35	34	**31.3**	7.8	1928
7	24	30.6	34.9	33.5	**38.2**	7.6	12352
8	26	30.6	**29.7**	27.3	**40.4**	6.3	30551
Dose constraints			≥35	≤40	≤30	≤30	

Note: bold values indicate that the corresponding dose constraints are not satisfied.

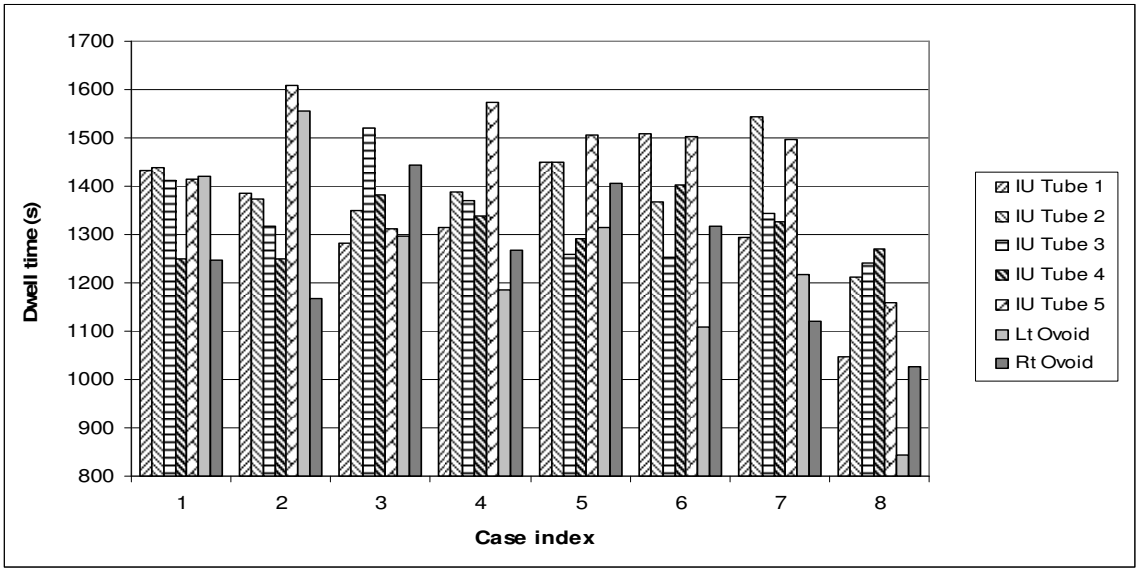

Figure 4-5. Dwell times obtained for 8 cases in Table 4-4. Importance factors (weights) to HR-CTV and OARs all set to 8. For each case, a total of 5 IU tube dwell positions and 2 ovoid dwell positions were used (1 left and 1 right ovoid position).

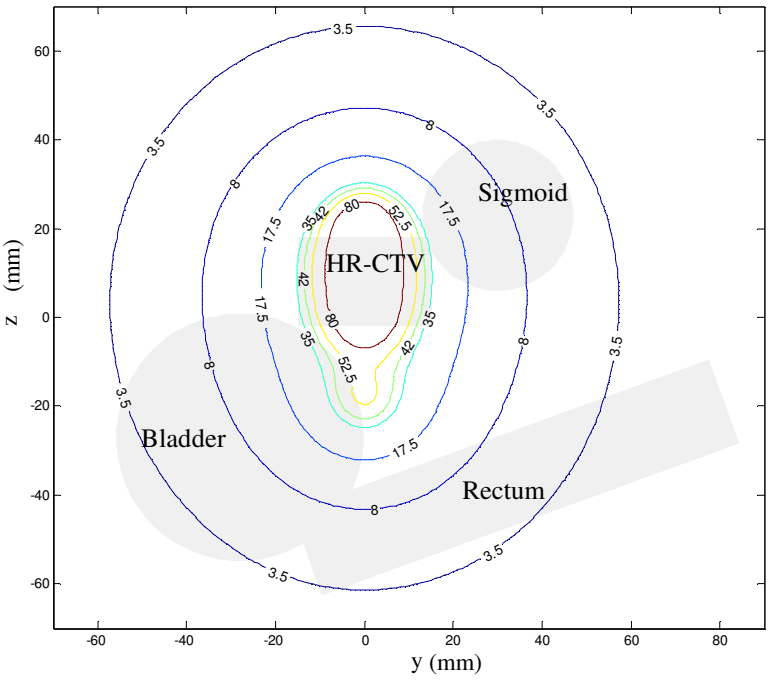
Sigmoid
HR-CTV
Bladder
Rectum
z (mm)
y (mm)

A

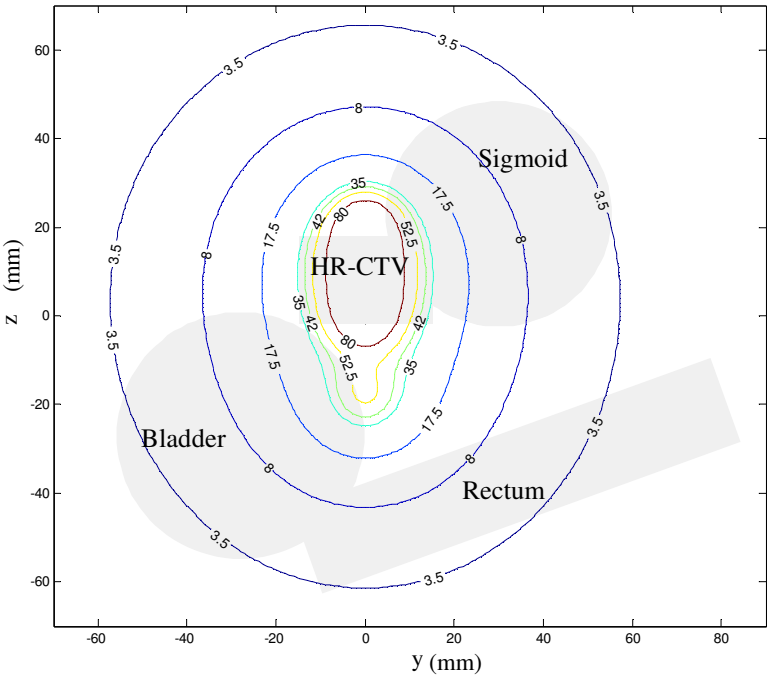
Sigmoid
HR-CTV
Bladder
Rectum
z (mm)
y (mm)

B

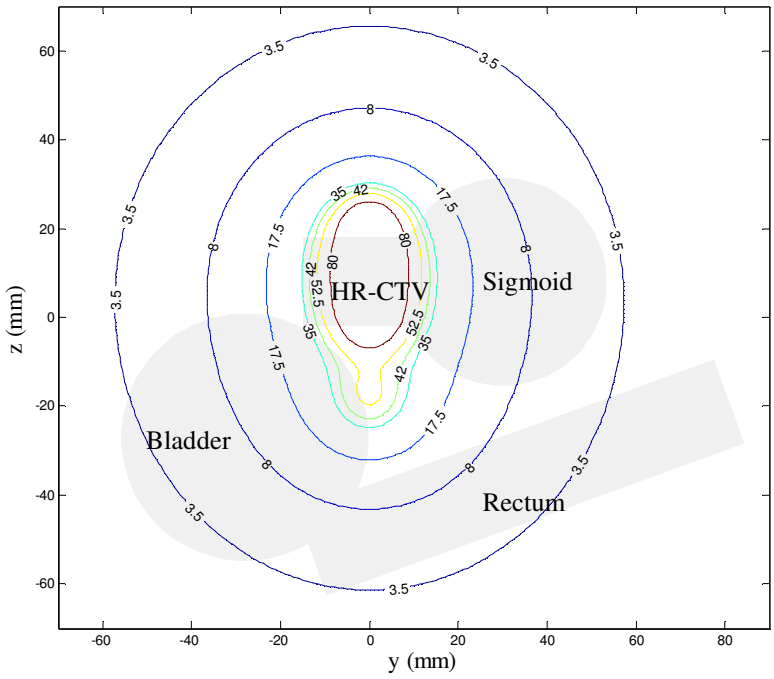

C

Figure 4-6. Isodose distributions (Gy) in the x=0 plane (sagittal view) of selected case plans. (A) Case 1: sigmoid radius = 18mm, center distance between sigmoid and HR-CTV = 34.1 mm. (B) Case 4: sigmoid radius = 26 mm, center distance between sigmoid and HR-CTV = 34.1 mm. (C) Case 7: sigmoid radius = 24mm, center distance between sigmoid and HR-CTV = 30.6 mm. HR-CTV and OAR cross-sections in the x=0 plane are displayed.

When the size of an OAR is increased (the center position fixed), or the distance between the OAR and the HR-CTV is shortened, there can be overlap between the OAR and the HR-CTV (see Figure 4-6), in which case it is more difficult for the SA method to optimize the dwell times to meet the prescription criteria of delivering high dose to the HR-CTV while sparing dose to OARs. The results shown in Table 4-4 are as expected: increasing the sigmoid radius to 26 mm (Case 4) results in a larger energy value compared to the smaller sigmoid radius and the dose to sigmoid (37.1 Gy) exceeding the upper bound of 30 Gy. When the distance between the sigmoid and the HR-CTV is shorter (30.6 mm), only for the case of sigmoid radius = 18 mm (case 5) are the dose constraints all met. The shortest distance combined with the largest sigmoid (Case 8) has the greatest

energy value of 30551 (suggesting the system is not stable) and neither the HR-CTV D90 nor the sigmoid dose constraint is met.

In clinical practice there will be little if any overlap between the HR-CTV and OARs delineated by the radiation oncologist, as these are distinct structures from an anatomical viewpoint. Hence the above test cases for which such overlap is present to a considerable extent, i.e. cases 4, 7, 8, should be regarded as extreme cases for the SA method that are highly unlikely to be encountered in cervix brachytherapy clinical practice. Nevertheless, this is an instructive exercise which aids in the understanding of the manner in which the SA algorithm functions.

4.3.3 Application of SA to Clinically Measured Data

4.3.3.1 Optimization Starting from Three Different Initial Dwell Times

Five patients were selected for making measurements on the fused MR-CT images to define structure parameters. Four of them (patients 1-4) have been investigated in Section 4.3.1, and one patient (patient 14) was newly added. For each patient, the optimization began from three different initial dwell times: 1) 1000 s for all dwell positions, 2) 5000 s for all dwell positions, and 3) standard Manchester loading. The standard loading is specified as relative dwell-time weights of 1.5 for the 4 distal tandem dwell positions beginning at the start position nearest the tip specified by the radiation oncologist, 1.0 for all remaining tandem dwell positions above the cervical stop, and 9 for the ovoid dwell positions. Absolute dwell times are thus 1000 s × [1.5, 1.5, 1.5, 1.5, 1, 1… 9, 9] for IU tube and ovoids, sequentially. Three plans were generated for each patient using the DVH constraints given in the dosimetric parameter tables which follow. For comparison, the relevant parameters for the corresponding Manchester plan are also listed.

Table 4-5. Dosimetric parameters of four plans for patient 1.

Plan index	Initial dwell times (s)	HR-CTV D90 (Gy)	Bladder D_{2cc} (Gy)	Rectum D_{2cc} (Gy)	Sigmoid D_{2cc} (Gy)	V100 (%)	Point A Dose (Gy)	COIN
1	1000	35.1	14.1	7.4	17.6	90	40.0	0.2163
2	5000	57.9	24.1	12.5	29.4	100	64.5	0.1057
3	Standard loading	35.0	28.5	17.3	21.5	90	36.8	0.1117
M.		**33.4**	28.1	17.2	20.7	86	35.0	0.1134
Dose constraint		≥35	≤40	≤30	≤30			

Note: bold value indicates that the corresponding dose constraint is not satisfied.
M. stands for Manchester plan.

Table 4-6. COIN calculation for Table 4-5, volume in mm^3.

Plan index	CTV	CTV_{ref}	V_{ref}-organ	CN	V_{ref}-rectum	V-rectum	V_{ref}-bladder	V-bladder	V_{ref}-sigmoid	V-sigmoid
1	29171	25033	98362	0.2184	0	8339	0	14423	0	3145
2	29171	29171	207889	0.1403	0	8339	17	14423	773	3145
3	29171	26143	174955	0.1339	0	8339	644	14423	399	3145
M.	29171	25427	168342	0.1317	0	8339	589	14423	321	3145

Note: CTV is the target volume, CTV_{ref} is the target volume receiving at least the reference dose of 35 Gy, V_{ref}-organ is the volume covered by the reference dose in whole body, and CN the conformation number. V_{ref}-OAR is the OAR volume receiving at least the reference dose of 35 Gy, and V-OAR is the OAR volume. M. stands for Manchester plan.

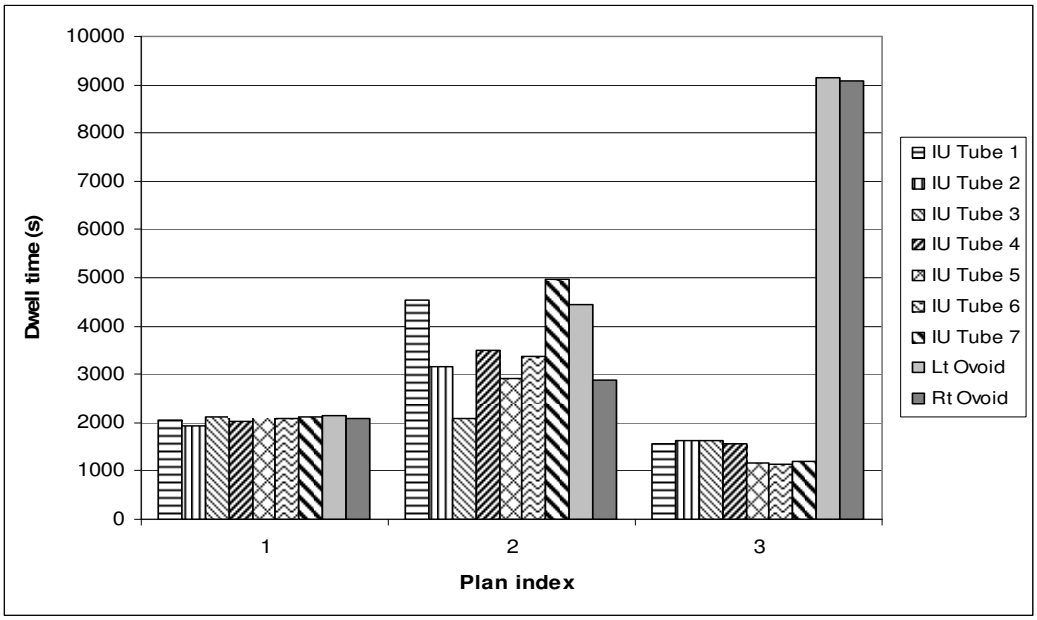

Figure 4-7. Optimized dwell times obtained for patient 1 by SA method. A total of 7 IU tube dwell positions and 2 ovoid positions (one in each ovoid) were used.

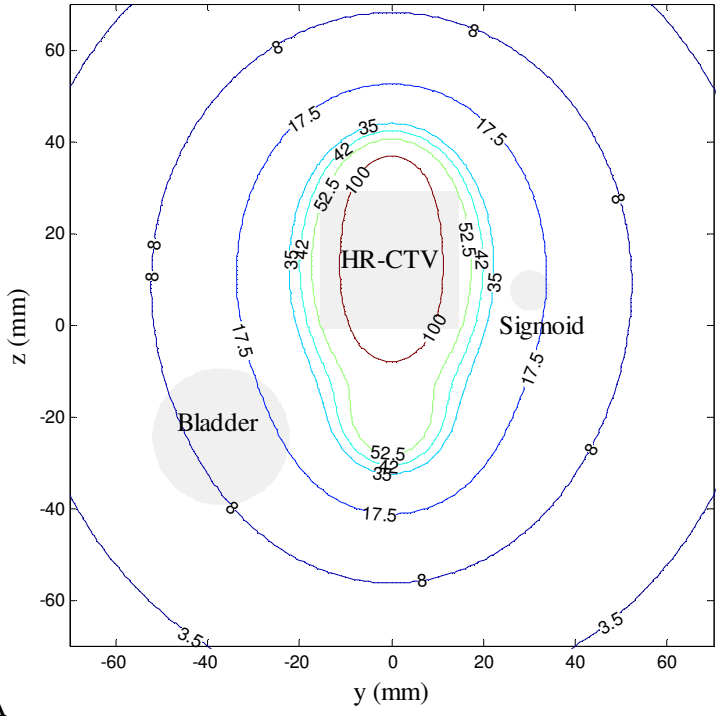

A

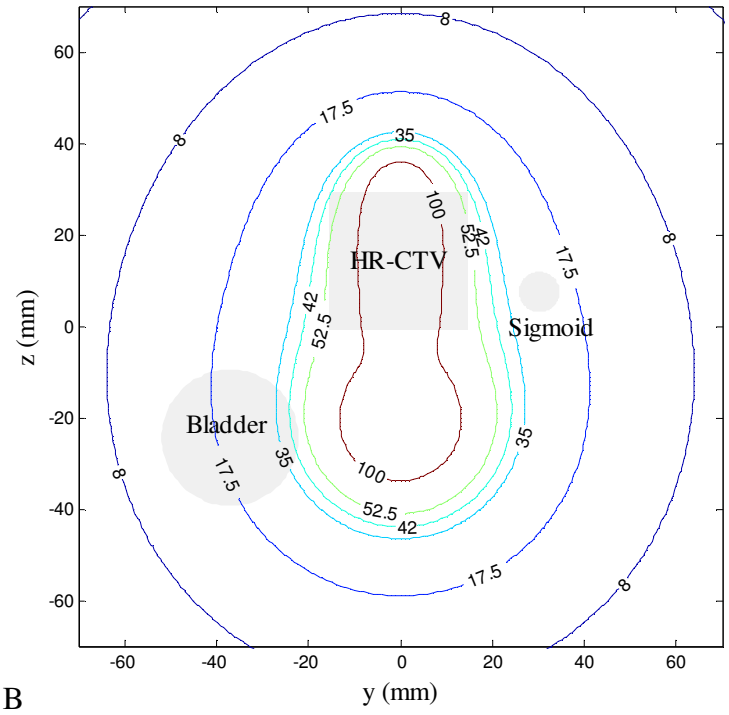

B

Figure 4-8. Isodose distributions (Gy) of (A) Plan 1 and (B) Plan 3 for patient 1 in the x=0 plane (sagittal view).

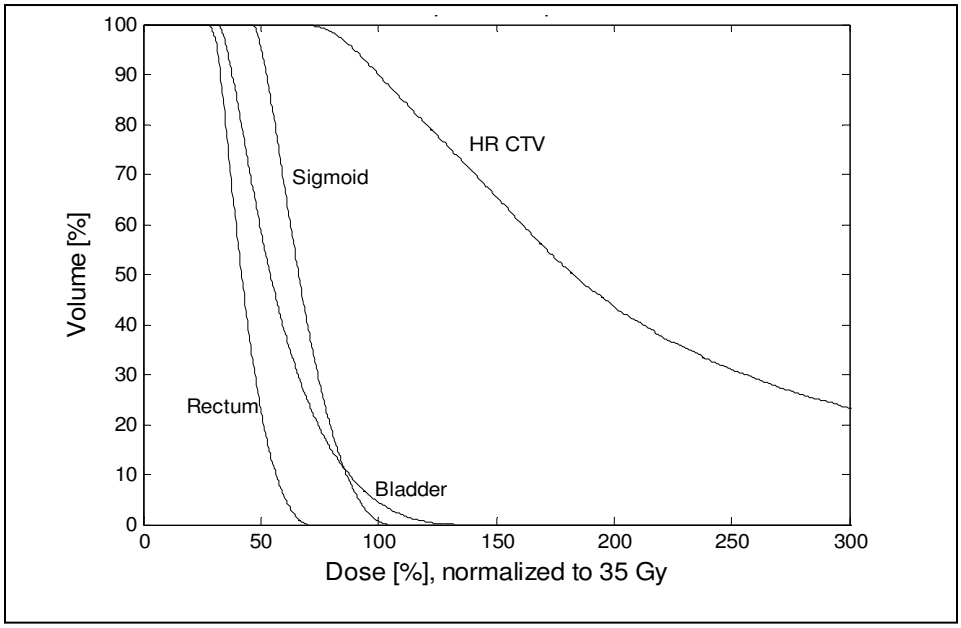

Figure 4-9. DVHs of Plan 3 for patient 1.

As shown in Figure 4-7, the optimized dwell times are quite different for the three plans using the SA method, and they are relatively close to their initial dwell times (e.g., long ovoid dwell times were obtained for the standard loading). All three optimized plans have the dose constraints satisfied on HR-CTV and OARs (Table 4-5), though relatively higher doses to HR-CTV and OARs were obtained when the initial dwell times are longer. This indicates that the specified dose constraints are quite loose for the patient 1 data and there exist multiple solutions to achieve the prescribed dose.

The COIN value helps to determine the best plan. As Tables 4-5 and 4-6 illustrate, the shortest initial dwell times resulted in an optimized plan with the greatest COIN value (plan 1 in Table 4-5). The COIN details in Table 4-6 show that plan 1 differs from the other two mainly in V_{ref}-organ, the volume covered by the reference dose in the whole body. The relatively shorter dwell times in plan 1 lead to the least volume in the body receiving the reference dose (35 Gy in this study); thus the highest conformation index is obtained.

Plan 3 starts from the standard loading, and the optimized dwell times are close to the original dwell times. Although the resulting dose distribution meets the dose constraints, the associated COIN value is much lower than that of plan 1, suggesting that there could be other better plans with respect to the standard loading that could be generated for a patient.

Using the SA method, the final energy values for patients 2, 3, and 4 are all close to 0, and the dosimetric parameters of the optimized plans for patients 2, 3 and 4 all meet the dose constraints (Tables 4-7, 9, 11).

It is noted that for patient 2, the COIN values (less than 0.08) are much lower than those for other patients (0.1- 0.3). By looking into the COIN details in Table 4-8, one can see that the sigmoid volume of patient 2 (V-sigmoid, 2638 mm^3) is smaller than that of other patients (3145 - 20913 mm^3). Moreover, the sigmoid volume receiving at least the reference dose of 35 Gy (V_{ref}-sigmoid, 1916 – 2212 mm^3) is comparable to the entire sigmoid volume, which decreases the COIN value significantly. Nevertheless, considering the fact that the sigmoid shape has large variability among the patients considered, and that only the part of the sigmoid that was closest to the treatment applicator was measured and simulated by a sphere in this study, the actual sigmoid volume should be much larger than the recorded size for patient 2. Hence this COIN value is not accurate; it can only be used for intra-patient comparison rather than inter-patient comparison.

Table 4-7. Dosimetric parameters of four plans for patient 2.

Plan index	Initial dwell times (s)	HR-CTV D90 (Gy)	Bladder D_{2cc} (Gy)	Rectum D_{2cc} (Gy)	Sigmoid D_{2cc} (Gy)	V100 (%)	Point A Dose (Gy)	COIN
1	1000	34.9	40.0	18.9	24.3	90	55.0	0.0767
2	5000	34.9	40.4	19.9	24.8	90	53.9	0.0751
3	Standard loading	35.0	39.1	30.1	29.3	90	55.2	0.0379
M.		**25.7**	**42.4**	**39.0**	16.4	65.6	35.0	0.1214
Dose constraint		≥35	≤40	≤30	≤30			

Note: bold values indicate that the corresponding dose constraints are not satisfied.

Table 4-8. COIN calculation for Table 4-7, volume in mm^3.

Plan index	CTV	CTV_{ref}	V_{ref}-organ	CN	V_{ref}-rectum	V-rectum	V_{ref}-bladder	V-bladder	V_{ref}-sigmoid	V-sigmoid
1	75480	67838	201240	0.303	0	27563	3474	48412	1919	2638
2	75480	67826	205384	0.2968	0	27563	3653	48412	1916	2638
3	75480	67960	240627	0.2543	0	27563	3768	48412	2212	2638
M.	75480	49262	193343	0.1663	0	27563	4539	48412	512	2638

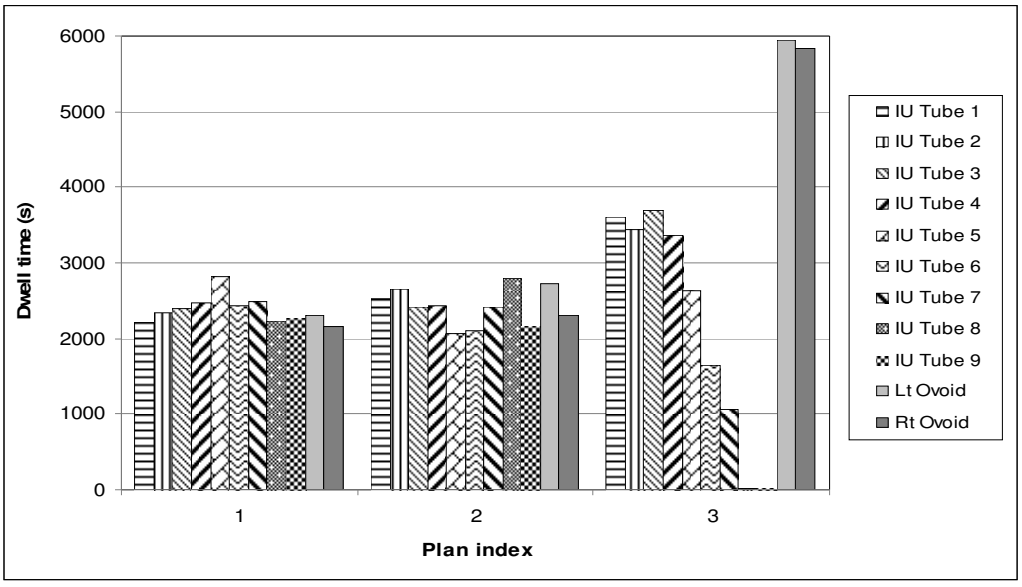

Figure 4-10. Optimized dwell times obtained for patient 2 by SA method. In total 9 IU tube dwell positions and 2 ovoid positions (one in each ovoid) were used.

Table 4-9. Dosimetric parameters of four plans for patient 3.

Plan index	Initial dwell times (s)	HR-CTV D90 (Gy)	Bladder D_{2cc} (Gy)	Rectum D_{2cc} (Gy)	Sigmoid D_{2cc} (Gy)	V100 (%)	Point A Dose (Gy)	COIN
1	1000	35.0	39.9	16	17.0	90	66.8	0.2755
2	5000	35.0	40.0	16.2	17.2	90	67.0	0.2683
3	Standard loading	34.9	40.0	17.8	18.0	90	76.8	0.2332
M.		**25.3**	**69.6**	30.6	16.5	64.3	35.0	0.1568
Dose constraint		≥35	≤40	≤30	≤30			

Note: bold values indicate that the corresponding dose constraints are not satisfied.

Table 4-10. COIN calculation for Table 4-9, volume in mm^3.

Plan index	CTV	CTV_{ref}	V_{ref}-organ	CN	V_{ref}-rectum	V-rectum	V_{ref}-bladder	V-bladder	V_{ref}-sigmoid	V-sigmoid
1	93555	84284	261435	0.2904	0	27522	3611	70326	0	5729
2	93555	84239	267949	0.2381	0	27522	3671	70326	0	5729
3	93555	84344	308270	0.2467	0	27522	3833	70326	0	5729
M.	93555	59940	206288	0.1862	0	27522	11093	70326	0	5729

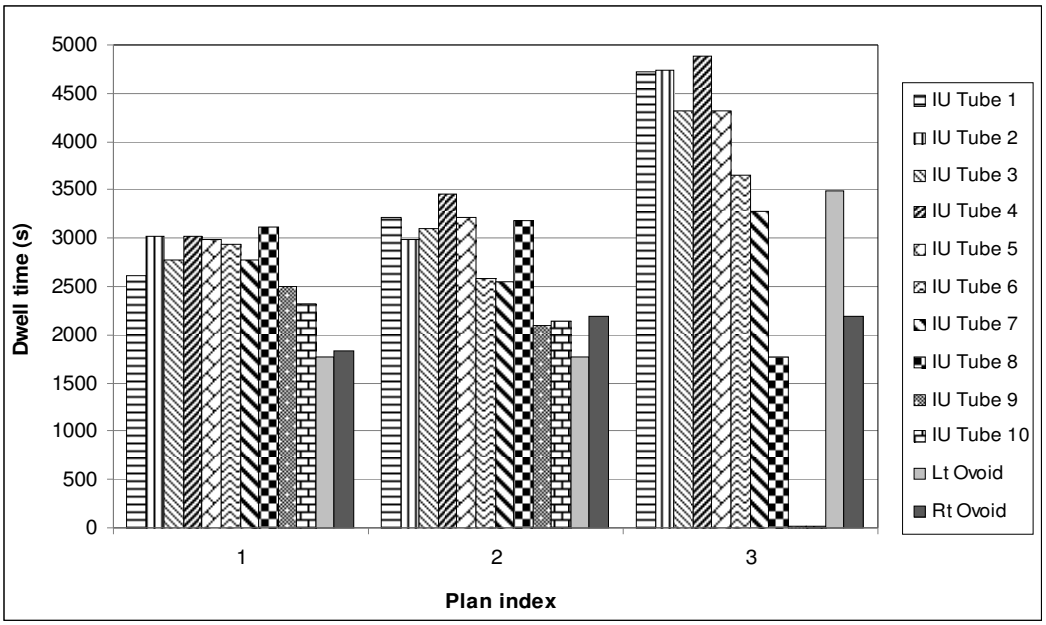

Figure 4-11. Optimized dwell times obtained for patient 3 by SA method. In total 10 IU tube dwell positions and 2 ovoid positions (one in each ovoid) were used.

Table 4-11. Dosimetric parameters of four plans for patient 4.

Plan index	Initial dwell times (s)	HR-CTV D90 (Gy)	Bladder D_{2cc} (Gy)	Rectum D_{2cc} (Gy)	Sigmoid D_{2cc} (Gy)	V100 (%)	Point A Dose (Gy)	COIN
1	1000	35.0	29.8	29.8	11.5	90	42.7	0.3177
2	5000	35.7	29.8	30.1	11.8	91	44.6	0.3149
3	Standard loading	35.0	30.0	30.2	12.6	90	54.0	0.2768
M.		35.3	**72.8**	**84.7**	15.9	90.6	35.0	0.1837
Dose constraint		≥35	≤40	≤30	≤30			

Note: bold values indicate that the corresponding dose constraints are not satisfied.

Table 4-12. COIN calculation for Table 4-11, volume in mm^3.

Plan index	CTV	CTV_{ref}	V_{ref}-organ	CN	V_{ref}-rectum	V-rectum	V_{ref}-bladder	V-bladder	V_{ref}-sigmoid	V-sigmoid
1	56448	50844	142683	0.321	33	95221	853	88068	0	7813
2	56448	51582	148239	0.318	47	95221	817	88068	0	7813
3	56448	50921	164098	0.2799	67	95221	817	88068	0	7813
M.	56448	51014	196663	0.2344	8989	95221	11879	88068	0	7813

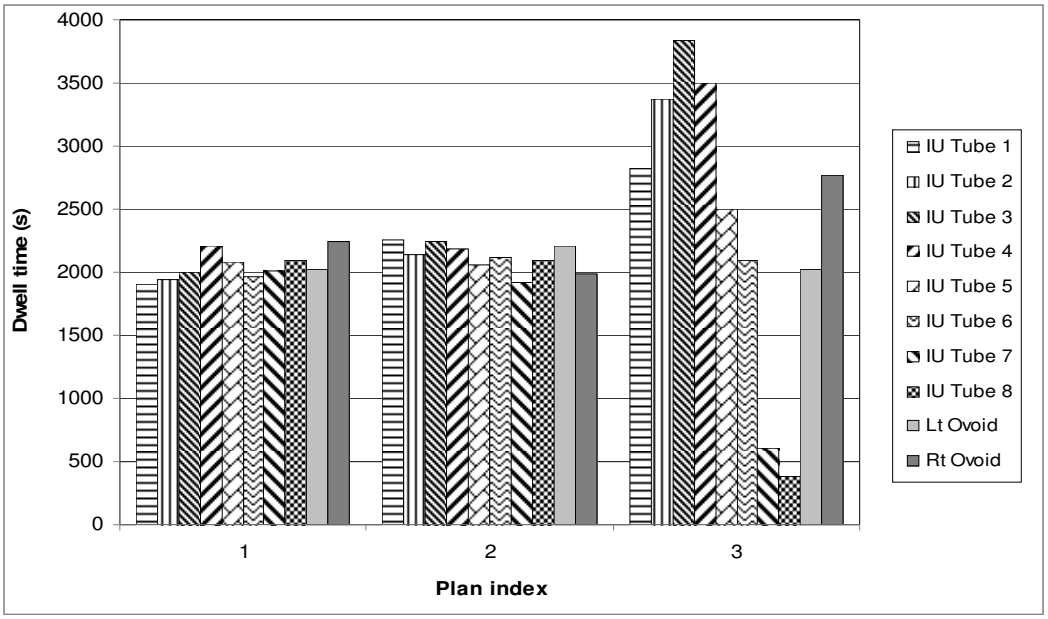

Figure 4-12. Optimized dwell times obtained for patient 4 by SA method. In total 8 IU tube dwell positions and 2 ovoid positions (one in each ovoid) were used.

For patient 14, the physical relationship between the HR-CTV and OARs in the x=0 plane (Figure 4-15) shows that the HR-CTV and the rectum are quite big, and the rectum and the sigmoid are immediately adjacent to the HR-CTV. Therefore it is not unexpected that none of the three plans in Figure 4-13 meets the prescription dose (Table 4-13).

Unlike patients 1 and 2, where the optimized dwell times are quite different for the three plans, the three optimized plans for patient 14 have dwell times relatively close to each other (Figure 4-13). This is also expected because the optimization process was looking for a solution to a more challenging problem with partially conflicting constraints for HR-CTV and rectum and sigmoid. Though the method did not ultimately find a perfect solution, the obtained dwell times represent a compromise between the conflicting dose constraints.

On the other hand, all three optimized plans have a relatively shorter left ovoid dwell time (Figure 4-13), indicating that perhaps the ovoid dwell times should not always be as long as those used in a standard Manchester loading.

Table 4-13. Dosimetric parameters of four plans for patient 14.

Plan index	Initial dwell times (s)	HR-CTV D90 (Gy)	Bladder D_{2cc} (Gy)	Rectum D_{2cc} (Gy)	Sigmoid D_{2cc} (Gy)	V100 (%)	Point A Dose (Gy)	COIN
1	1000	**31.8**	13.8	30.2	**31.0**	85.7	48.8	0.3086
2	5000	**33.0**	14.2	30.2	**32.4**	87.5	51.0	0.3100
3	Standard loading	**32.5**	13.8	30.2	**32.7**	86.2	52.5	0.3020
M.		**29.9**	19.9	**75.1**	25.1	82.1	35.0	0.2222
Dose constraint		≥35	≤40	≤30	≤30			

Note: bold values indicate that the corresponding dose constraints are not satisfied; M. stands for Manchester plan.

Table 4-14. COIN calculation for Table 4-13, volume in mm^3.

Plan index	CTV	CTV_{ref}	V_{ref}-organ	CN	V_{ref}-rectum	V-rectum	V_{ref}-bladder	V-bladder	V_{ref}-sigmoid	V-sigmoid
1	68170	58434	160682	0.3117	0	67136	0	14423	143	14423
2	68170	59625	165265	0.3156	0	67136	0	14423	255	14423
3	68170	59049	167062	0.3062	0	67136	0	14423	198	14423
M.	68170	55785	192680	0.2369	4160	67136	0	14423	198	14423

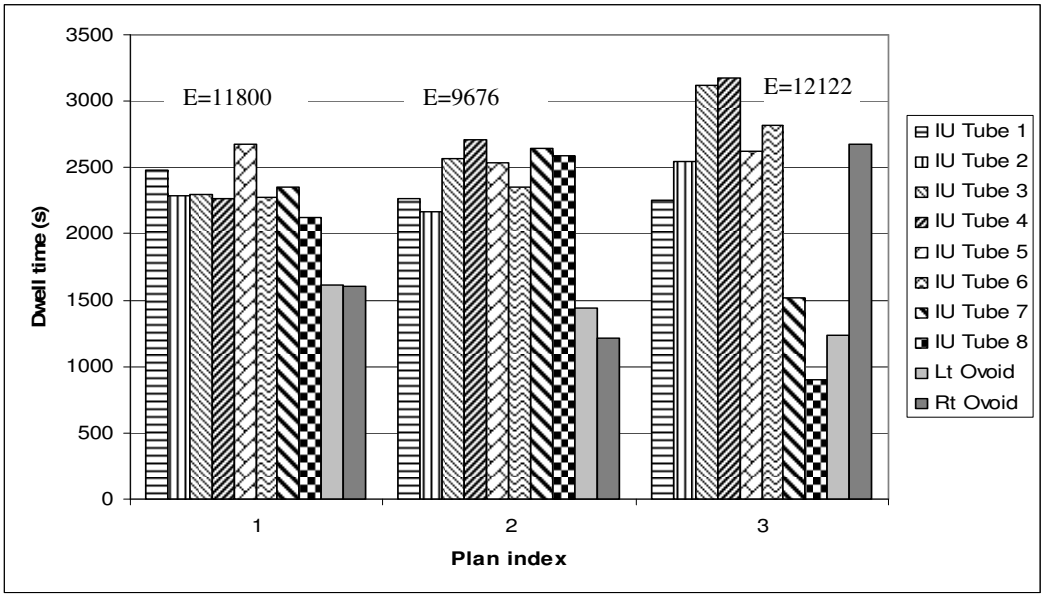

Figure 4-13. Optimized dwell times obtained for patient 14 by SA method. Importance factors (weights) to HR-CTV and OARs all set to 8. A total of 8 IU tube dwell positions and 2 ovoid positions (one in each ovoid) were used.

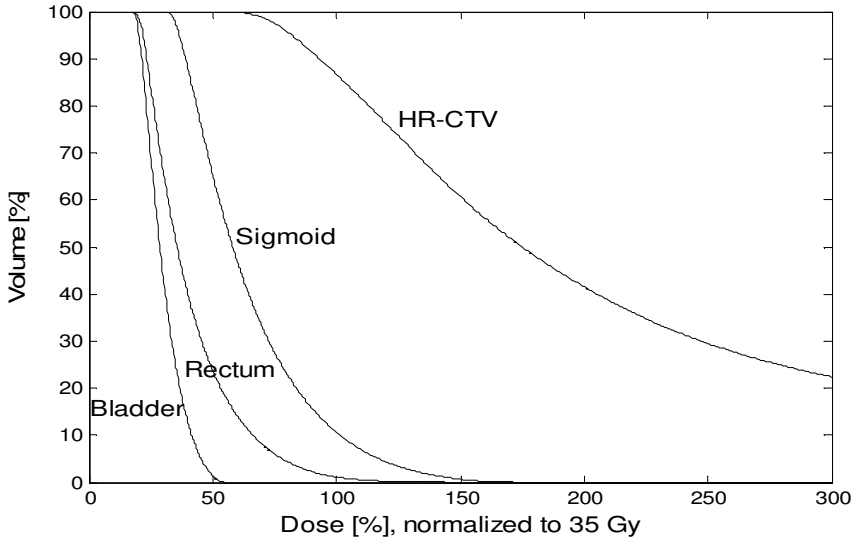

Figure 4-14. DVHs of plan 3 for patient 14.

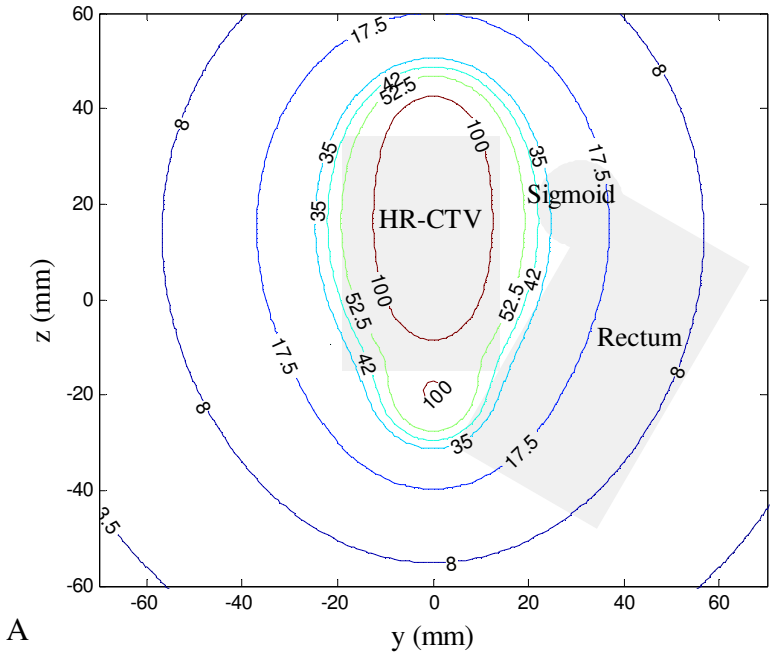

A

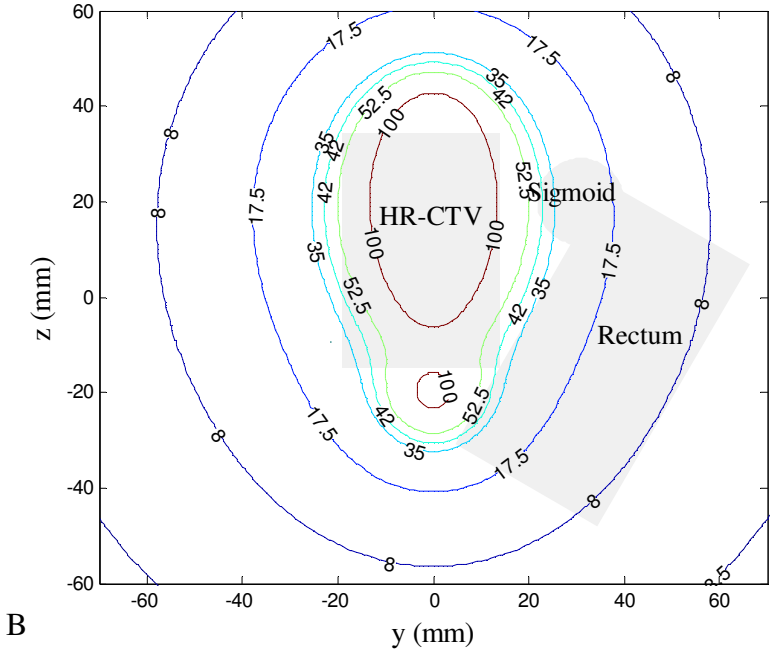

B

Figure 4-15. Isodose distributions (Gy) of (A) plan 1 and (B) plan 3 for patient 14 in the x=0 plane (sagittal view).

4.3.3.2 Comparison of Plans with Different Number of Dwell Positions

For patients 1, 2, 3, and 4, the number of dwell positions is changed from the minimum number, for which the top of the HR-CTV is covered, to the maximum number, which is used clinically. Patient 14 is not included in this part of the study as no completely satisfactory plans could be obtained. The optimization starts by assigning 1000 s to all dwell positions. The dosimetric parameters of the optimized plans for these patients are shown in Table 4-15 to Table 4-22.

Table 4-15. Dosimetric parameters of five plans for patient 1, each differing in the number of dwell positions.

Plan index	Number of dwell positions	HR-CTV D90 (Gy)	Bladder D_{2CC} (Gy)	Rectum D_{2CC} (Gy)	Sigmoid D_{2CC} (Gy)	Point A Dose (Gy)	COIN	Sum of dwell times (m)
1	9	35.1	14.1	7.4	17.6	40.0	0.2184	316.2
2	10	34.8	13.1	6.8	17.3	40.6	0.2142	319.1
3	11	34.9	13.1	6.8	17.4	41.1	0.2044	332.9
4	12	35.0	13.3	7.0	17.6	41.4	0.1917	352.8
5	13	35.0	12.8	6.7	17.6	41.6	0.1857	362.2
Dose constraint		≥35	≤40	≤30	≤30			

Table 4-16. COIN calculation for Table 4-15. Volume in mm^3.

Plan index	CTV	CTV_{ref}	V_{ref}-organ	CN	V_{ref}-rectum	V-rectum	V_{ref}-bladder	V-bladder	V_{ref}-sigmoid	V-sigmoid
1	29171	25033	98362	0.2184	0	8339	0	14423	0	3145
2	29171	26210	109965	0.2142	0	8339	0	14423	0	3145
3	29171	26224	115339	0.2044	0	8339	0	14423	0	3145
4	29171	26257	123294	0.1917	0	8339	0	14423	0	3145
5	29171	26244	127141	0.1857	0	8339	0	14423	0	3145

Table 4-17. Dosimetric parameters of five plans for patient 2, each differing in the number of dwell positions.

Plan index	Number of dwell positions	HR-CTV D90 (Gy)	Bladder D_{2CC} (Gy)	Rectum D_{2CC} (Gy)	Sigmoid D_{2CC} (Gy)	Point A Dose (Gy)	COIN	Sum of dwell times (min)
1	10	34.8	40.0	22.6	17.5	56.0	0.0818	371.5
2	11	34.9	40.0	18.9	24.3	55.0	0.0767	435.0
3	12	34.9	39.6	19.1	26.7	53.7	0.0689	450.7
4	13	35.0	38.3	18.5	29.9	53.6	0.0581	474.4
5	14	35.0	37.7	18.4	32.5	52.9	0.0507	475.7
Dose constraint		≥35	≤40	≤30	≤30			

Table 4-18. COIN calculation for Table 4-17. Volume in mm^3.

Plan index	CTV	CTV_{ref}	V_{ref}-organ	CN	V_{ref}-rectum	V-rectum	V_{ref}-bladder	V-bladder	V_{ref}-sigmoid	V-sigmoid
1	75480	67780	193073	0.3125	0	27563	3404	48412	1902	2638
2	75480	67838	201240	0.303	0	27563	3474	48412	1919	2638
3	75480	67922	208903	0.2926	0	27563	3379	48412	1970	2638
4	75480	67942	216539	0.2824	0	27563	2982	48412	2060	2638
5	75480	67974	226458	0.2703	0	27563	2838	48412	2112	2638

Table 4-19. Dosimetric parameters of three plans for patient 3, each differing in the number of dwell positions.

Plan index	Number of dwell positions	HR-CTV D90 (Gy)	Bladder D_{2CC} (Gy)	Rectum D_{2CC} (Gy)	Sigmoid D_{2CC} (Gy)	Point A Dose (Gy)	COIN	Sum of dwell times (min)
1	10	35	39.9	15.7	16.8	67.5	0.3000	486.5
2	11	35	40.0	15.6	16.9	66.5	0.2898	503.2
3	12	35	39.9	16.0	17.0	66.8	0.2755	528.2
Dose constraint		≥35	≤40	≤30	≤30			

Table 4-20. COIN calculation for Table 4-19. Volume in mm^3.

Plan index	CTV	CTV_{ref}	V_{ref}-organ	CN	V_{ref}-rectum	V-rectum	V_{ref}-bladder	V-bladder	V_{ref}-sigmoid	V-sigmoid
1	93555	84284	239818	0.3163	0	27522	3629	70326	0	5729
2	93555	84284	248574	0.3055	0	27522	3608	70326	0	5729
3	93555	84284	261435	0.2904	0	27522	3611	70326	0	5729

Table 4-21. Dosimetric parameters of four plans for patient 4, each differing in the number of dwell positions.

Plan index	Number of dwell positions	HR-CTV D90 (Gy)	Bladder D_{2CC} (Gy)	Rectum D_{2CC} (Gy)	Sigmoid D_{2CC} (Gy)	Point A Dose (Gy)	COIN	Sum of dwell times (min)
1	8	35.0	30.0	30.2	11.1	39.1	0.3459	310.8
2	9	35.0	29.8	30.1	11.3	41.4	0.3318	326.3
3	10	35.0	29.8	29.8	11.5	42.7	0.3177	341.3
4	11	35.1	29.9	29.9	11.8	44.1	0.3010	361.5
Dose constraint		≥35	≤40	≤30	≤30			

Table 4-22. COIN calculation for Table 4-21. Volume in mm^3.

Plan index	CTV	CTV_{ref}	V_{ref}-organ	CN	V_{ref}-rectum	V-rectum	V_{ref}-bladder	V-bladder	V_{ref}-sigmoid	V-sigmoid
1	56448	50759	130595	0.3495	44	95221	876	88068	0	7813
2	56448	50856	136741	0.3351	46	95221	827	88068	0	7813
3	56448	50844	142683	0.321	33	95221	853	88068	0	7813
4	56448	50893	150894	0.304	35	95221	869	88068	0	7813

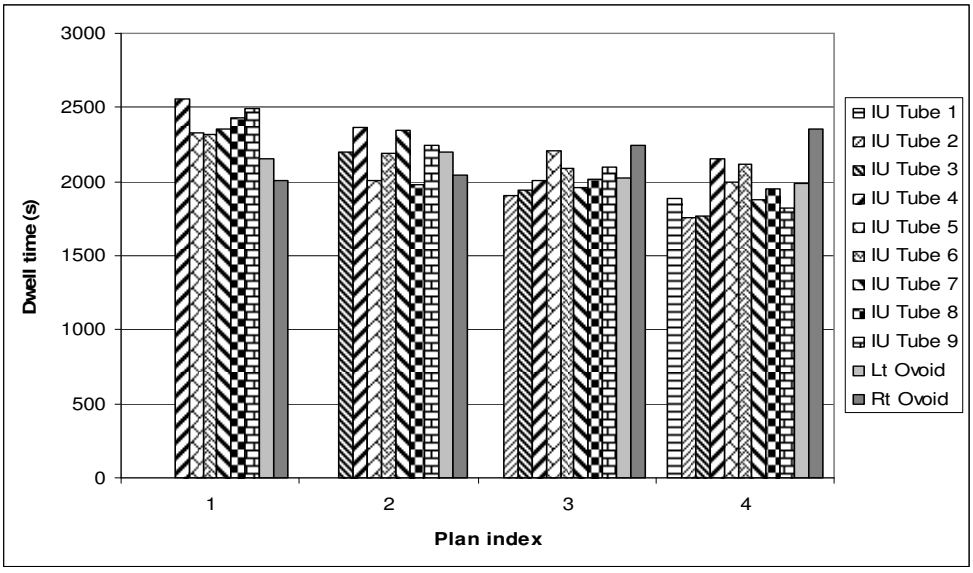

Figure 4-16. Optimized dwell times obtained for patient 4, by SA method. Weights to HR-CTV and OARs were all set to 8. In total, 6, 7, 8, and 9 IU tube dwell positions for plans 1, 2, 3, and 4 respectively, and 2 ovoid positions (one position in each ovoid) for all plans, were used.

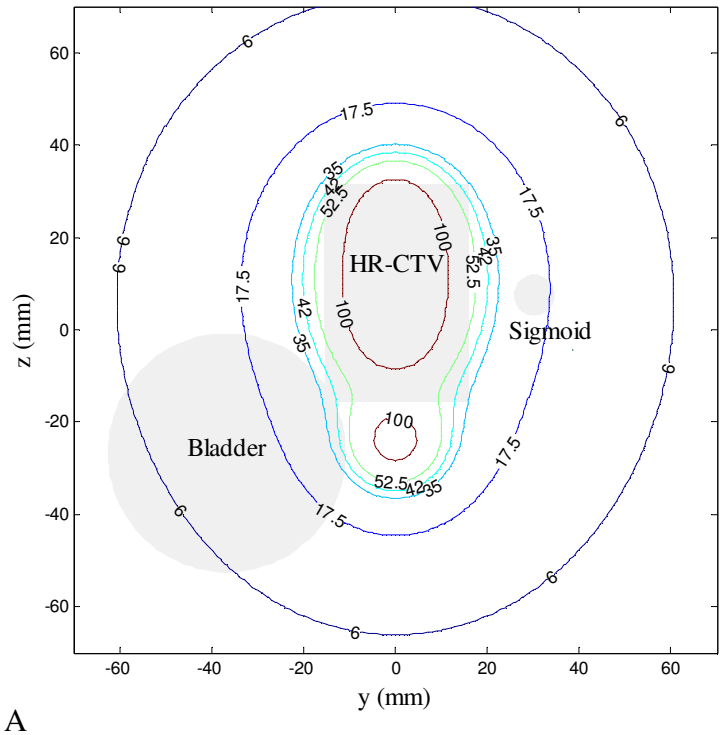
HR-CTV
Sigmoid
Bladder
z (mm)
y (mm)
6
17.5
35
42
52.5
100

A

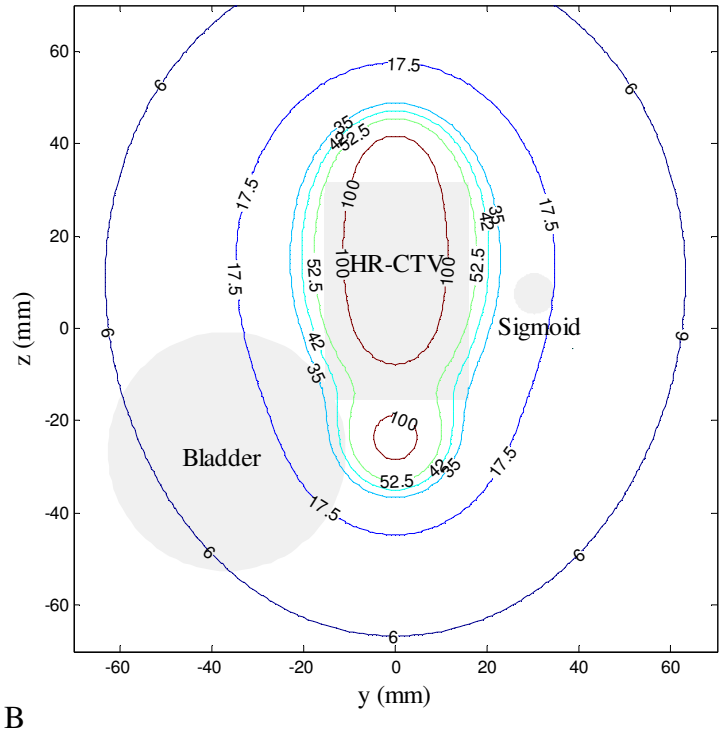
HR-CTV
Sigmoid
Bladder
z (mm)
y (mm)
6
17.5
35
42
52.5
100

B

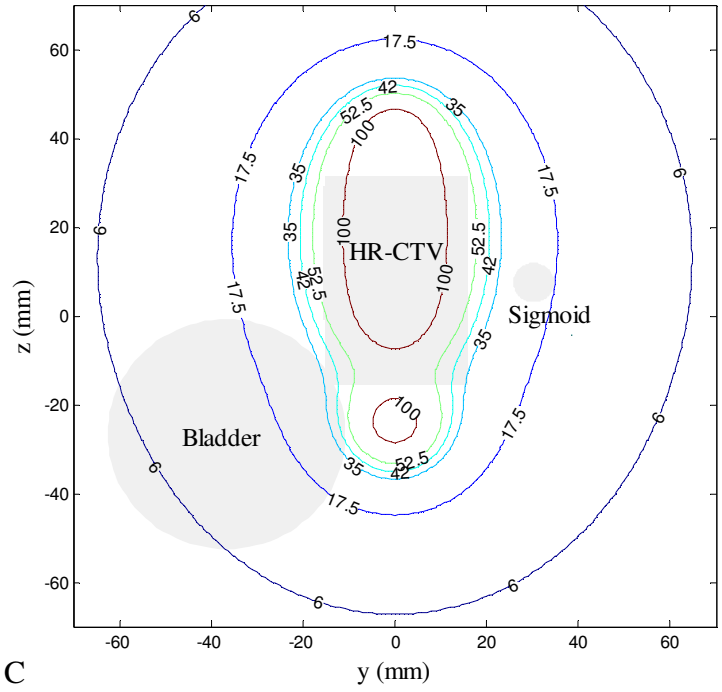

Figure 4-17. Isodose distributions (Gy) of (A) plan 1, (B) plan 3, and (C) plan 4 for patient 4 in the x=0 plane (sagittal view).

Although the number of dwell positions is changed, the SA algorithm generated plans that still satisfied the dose constraints for all patients. The results are shown in Tables 4-15, 17, 19, and 21.

It is interesting to note that for all four patients, COIN values decrease with increasing number of dwell positions. From the associated COIN tables, it can be seen that this is due to the decreased conformation number (CN). When the number of dwell positions is increased, a greater volume of normal tissue outside of the HR-CTV is irradiated such that V_{ref}-organ is greater. Although the target volume receiving the reference dose (CTV_{ref}) could also be increased and the OAR volume receiving the reference dose could be (although not always) decreased, these changes are not as remarkable as the increase in V_{ref}-organ, thus the resulting lower COIN is expected. This conclusion is also supported by the corresponding isodose distributions (e.g., Figure 4-17 for patient 4). These plots

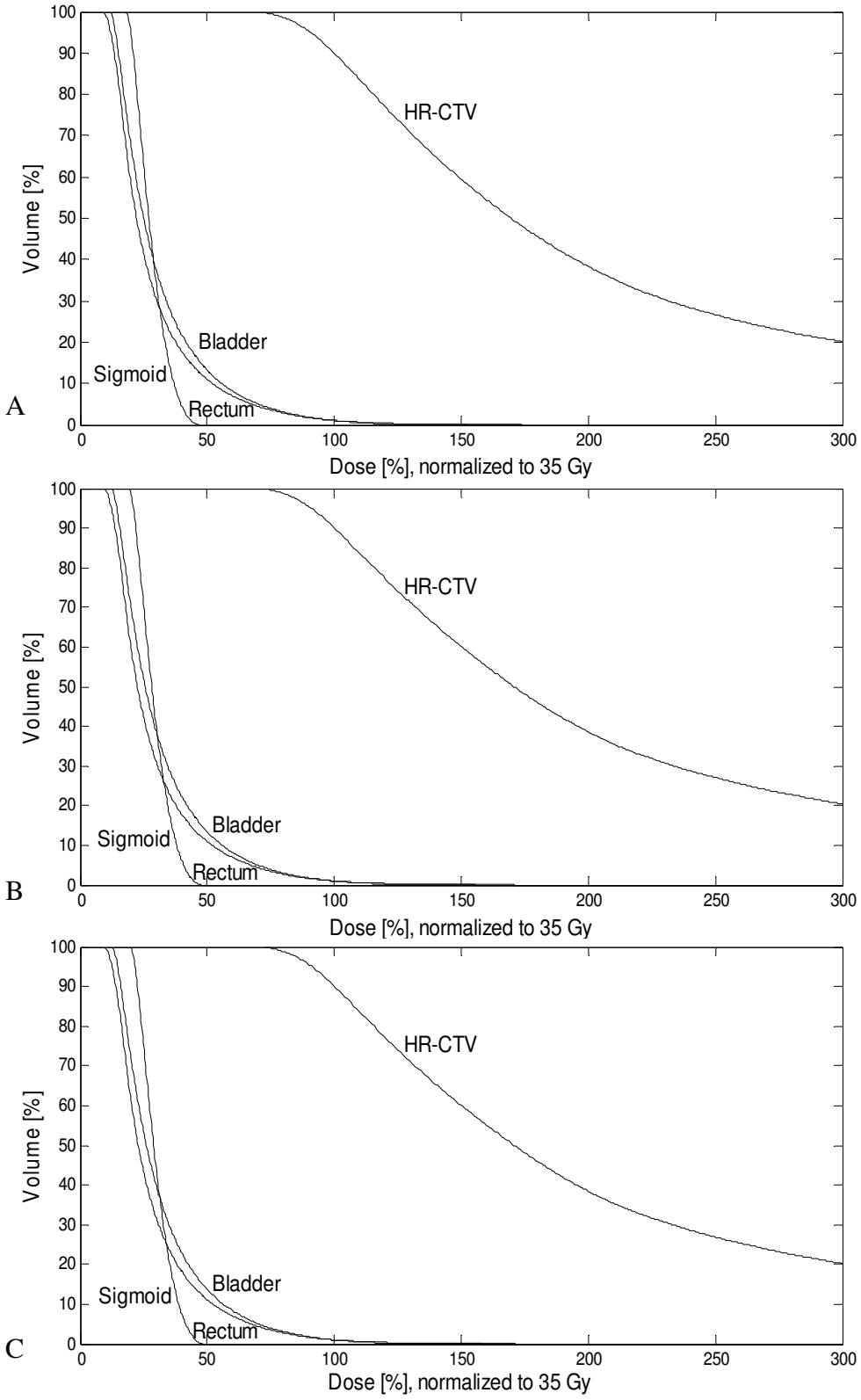

Figure 4-18. DVHs of (A) plan 1, (B) plan 3, and (C) plan 4 for patient 4.

illustrate that, the greater the number of dwell positions, the higher the dose delivered to normal tissue outside the HR-CTV. Furthermore, the total dwell times provided in Tables 4-15, 17, 19, and 21 demonstrate that, to meet the dose constraints, a plan having a greater number of dwell positions also tends to have a greater total dwell time. This trend is not detectable by examining HR-CTV and OAR DVHs (Figure 4-18) as the optimization process is directly based on DVH parameter constraints for these structures alone, and does not incorporate a normal tissue dose-volume constraint.

4.4 Discussion

The simulated annealing algorithm combined with an objective function incorporating constraints on the dose volume parameters D90 for HR-CTV and D_{2cc} for OARs (bladder, rectum, and sigmoid) is effective in optimizing tandem and ovoid cervix brachytherapy treatment plans. It can produce plans which largely satisfy clinically recommended dose volume constraints and validates the target concepts introduced by GEC ESTRO in 2006 [Potter *et al.* 2006].

Compared to traditional Manchester system plans, these optimized plans exhibited some distinctive characteristics as follows:

1. In general, optimization led to a reduction in the dose to normal tissue around the target while providing adequate coverage of the HR-CTV by the prescribed dose. The reduction was primarily due to the smaller number of dwell positions needed to achieve the prescribed dose coverage for an optimized plan. When dwell positions for an optimized plan were identical to those for the standard plan, normal tissue dose reduction was less pronounced. This suggests that the introduction of a dose constraint for normal tissue outside of the HR-CTV and OARs may be helpful in conforming the prescription dose more tightly to the HR-CTV.

2. Point A doses in optimized plans were generally higher than the prescription dose (to point A) of 35 Gy in the corresponding Manchester plan. For some cases, the dose to point A was as high as 70 Gy while OAR D_{2cc}'s remained under the specified dose limits. On the other hand, most Manchester plans delivering 35 Gy to point A did not meet the dose volume constraints.

3. Most of the optimized plans had prominently reduced ovoid dwell times compared to standard loadings, resulting in lower ovoid surface doses. The clinical implications of these lower surface doses are not known.

Given that the dose volume constraints used in this work are clinically applicable (according to published clinical experience), our results support the hypothesis that 3D image-based treatment planning using dose prescription to a target volume for an individual patient is superior to planning using dose prescription to point A combined with standard loading.

As applied to cervix brachytherapy, dose optimization using simulated annealing has its own distinctive features, as follows:

1. For easy cases, i.e. smaller HR-CTV volumes with good separation from adjoining OARs, there were multiple solutions which differed markedly from each other. Since, for this kind of situation, the dose volume constraints were readily satisfied, many different dwell time configurations led to dose distributions satisfying the constraints. On the other hand, for difficult cases, i.e. larger HR-CTV volumes immediately adjacent to one or more OARs, there was usually only one solution (true minimum of the objective function) to the problem. For this situation, the different solutions obtained by SA tended to approach the true minimum, and the DVH parameters of the slightly different plans were close to each other.

2. For the easy cases, choosing longer initial dwell times often led to relatively longer optimized dwell times which resulted in relatively higher doses to the

HR-CTV and OARs. This occurred because our SA process progressively shortens dwell times that are initially too long only until all dose constraints are met, which for the easy cases tended to be at higher dose levels. One way to avoid this tendency would be to make the selection of initial dwell times dependent on a clinical evaluation of the relative importance of OAR complications and tumor eradication. An alternative would be to add a normal tissue dose constraint to the objective function, in order to minimize overall HR-CTV and OAR dose levels while still meeting the other dose constraints. COIN is also recommended for evaluation and comparison of different treatment plans. It should be noted that use of an upper limit for target dose was not introduced in this study. Consequently, in some cases (e.g. patient 1, initial dwell times set to 5000 s) D90 was as high as 58 Gy. For such cases, it might be appropriate to consider introducing an upper limit for HR-CTV D90 having a high importance factor.

3. When different numbers of dwell positions were considered for optimization, treatment plans using all available dwell positions were produced by our SA method. The difference between these plans is not detectable by inspecting the DVH parameters reported, but directly affects the isodose distribution in the irradiated area. Generally, although plans with a greater number of dwell positions tended to have shorter individual dwell times, they had larger total dwell times and unnecessarily greater reference volumes. Considering the individual dwell times do not differ much, a plan with fewer dwell positions is preferable, since it has a smaller reference volume and is usually associated with a higher COIN value.

For the cases investigated, the HR-CTV D90 and OAR D2cc's were not sufficient to decide whether one optimized plan was better than another or not. Hence the COIN calculation provided a useful tool for numerically comparing conformity between plans.

COIN takes into account not only the coverage of the HR-CTV by the reference dose, but also the excess radiation of normal tissue outside the HR-CTV and especially unwanted radiation to the critical OARs. An ideal situation occurs when the HR-CTV is totally covered by the reference dose while no dose above the reference dose is given to surrounding normal tissues. A limitation of using COIN for evaluation is that the HR-CTV and critical organs are equally weighted [Brooks *et al.* 2005], hence the index cannot identify the difference between good CTV coverage with high dose to OARs, and poor CTV coverage with low dose to OARs. The individual parameters that make up the COIN need to be provided to assess each situation, as has been done here by way of the COIN-associated tables appearing in Sections 4.3.3 and 4.3.4.

References

Baltas D, Kolotas C, Geramani K, Mould RF, Ioannidis G, Kekchidi M, Zamboglou N. A conformal index (COIN) to evaluate implant quality and dose specification in brachytherapy. *Int J Radiat Oncol Biol Phys* 1998; 40(2):515-24.

Bortfeld T. Optimized planning using physical objectives and constraints. *Seminars in Radiation Oncology* 1999; 9(1):20-34.

Brooks S, Bownes P, Lowe G, Bryant L, Hoskin PJ. Cervical brachytherapy utilizing ring applicator: comparison of standard and conformal loading. *Int J Radiat Oncol Biol Phys* 2005; 63(3):934-9.

Chajon E, Dumas I, Touleimat M, Magne N, Coulot J, Verstraet R, Lefkopoulos D, Haie-Meder C. Inverse planning approach for 3-D MRI-based pulsed-dose rate intracavitary brachytherapy in cervix cancer. *Int J Radiat Oncol Biol Phys* 2007; 69(3):955-61.

Dewitt KD, Hsu IC, Speight J, Weinberg VK, Lessard E, Pouliot J. 3D inverse treatment planning for the tandem and ovoid applicator in cervical cancer. *Int J Radiat Oncol Biol Phys* 2005; 63(4):1270-4.

Ezzell GA. Optimization in Brachytherapy. *Ch22, AAPM Brachytherapy Society Summer School*, July 2005, Seattle WA; 415-34.

Geman S, Geman D. Stochastic Relaxation, Gibbs Distributions, and the Bayesian Restoration of Images. *Ieee Transactions on Pattern Analysis and Machine Intelligence* 1984; 6(6):721-41.

Haie-Meder C, Potter R, Van Limbergen E, Briot E, De Brabandere M, Dimopoulos J, Dumas I, Hellebust TP, Kirisits C, Lang S, Muschitz S, Nevinson J, Nulens A, Petrow P, Wachter-Gerstner N. Recommendations from Gynaecological (GYN) GEC-ESTRO Working Group (I): concepts and terms in 3D image based 3D treatment planning in cervix cancer brachytherapy with emphasis on MRI assessment of GTV and CTV. *Radiother Oncol* 2005; 74(3):235-45.

International commission on radiation units and measurements (ICRU). Dose and volume specifiation for reporting intracavitary therapy in gynecology, *ICRU report* No.38. Bethesda, MD: International Commission on Radiation Units and Measurements. 1985.

Jamema SV, Kirisits C, Mahantshetty U, Trnkova P, Deshpande DD, Shrivastava SK, Potter R. Comparison of DVH parameters and loading patterns of standard loading, manual and inverse optimization for intracavitary brachytherapy on a subset of tandem/ovoid cases. *Radiother Oncol* 2010; 97(3):501-6.

Kirkpatrick S, Gelatt CD, Vecchi MP. Optimization by Simulated Annealing. *Science* 1983; 220(4598):671-80.

Kubicky CD, Yeh BM, Lessard E, Joe BN, Speight JL, Pouliot J, Hsu IC. Inverse planning simulated annealing for magnetic resonance imaging-based intracavitary high-dose-rate brachytherapy for cervical cancer. *Brachytherapy* 2008; 7(3):242-7.

Lang S, Kirisits C, Dimopoulos J, Georg D, Potter R. Treatment planning for MRI assisted brachytherapy of gynecologic malignancies based on total dose constraints. *Int J Radiat Oncol Biol Phys* 2007; 69(2):619-27.

Lessard E, Pouliot J. Inverse planning anatomy-based dose optimization for HDR-brachytherapy of the prostate using fast simulated annealing algorithm and dedicated objective function. *Med Phys* 2001; 28(5):773-9.

Lindegaard JC, Tanderup K, Nielsen SK, Haack S, Gelineck J. MRI-guided 3D optimization significantly improves DVH parameters of pulsed-dose-rate brachytherapy in locally advanced cervical cancer. . *Int J Radiat Oncol Biol Phys* 2008; 71(3):756-64.

Metropolis N, Rosenbluth AW, Rosenbluth MN, Teller AH, Teller E. Equation of State Calculations by Fast Computing Machines. *Journal of Chemical Physics* 1953; 21(6):1087-92.

Morrill SM, Lam KS, Lane RG, Langer M, Rosen, II. Very Fast Simulated Reannealing in Radiation-Therapy Treatment Plan Optimization. . *Int J Radiat Oncol Biol Phys* 1995; 31(1):179-88.

Nath R, Anderson LL, Luxton G, Weaver KA, Williamson JF, Meigooni AS. Dosimetry of interstitial brachytherapy sources: recommendations of the AAPM Radiation Therapy Committee Task Group No. 43. American Association of Physicists in Medicine. *Med Phys* 1995; 22(2):209-34.

Perez-Calatayud J, Ballester F, Serrano-Andres MA, Puchades V, Lluch JL, Limami Y, Casal F. Dosimetry characteristics of the Plus and 12i Gammamed PDR 192Ir sources. *Med Phys* 2001; 28(12):2576-85.

Potter R, Haie-Meder C, Van Limbergen E, Barillot I, De Brabandere M, Dimopoulos J, Dumas I, Erickson B, Lang S, Nulens A, Petrow P, Rownd J, Kirisits C. Recommendations from gynaecological (GYN) GEC ESTRO working group (II): concepts and terms in 3D image-based treatment planning in cervix cancer brachytherapy-3D dose volume parameters and aspects of 3D image-based anatomy, radiation physics, radiobiology. *Radiother Oncol* 2006; 78(1):67-77.

Potter R, Fidarova E, Kirisits C, Dimopoulos J. Image-guided adaptive brachytherapy for cervix carcinoma. *Clin Oncol (R Coll Radiol)* 2008; 20(6):426-32.

Sloboda RS. Optimization of brachytherapy dose distributions by simulated annealing. *Med Phys* 1992; 19(4):955-64.

Trnkova P, Potter R, Baltas D, Karabis A, Fidarova E, Dimopoulos J, Georg D, Kirisits C. New inverse planning technology for image-guided cervical cancer brachytherapy: description and evaluation within a clinical frame. *Radiother Oncol* 2009; 93(2):331-40.

Tanderup K, Nielsen SK, Nyvang GB, Pedersen EM, Rohl L, Aagaard T, Fokdal L, Lindegaard JC. From point A to the sculpted pear: MR image guidance significantly improves tumour dose and sparing of organs at risk in brachytherapy of cervical cancer. *Radiother Oncol* 2010; 94(2):173-80.

Trnkova P, Potter R, Baltas D, Karabis A, Fidarova E, Dimopoulos J, Georg D, Kirisits C. New inverse planning technology for image-guided cervical cancer brachytherapy: description and evaluation within a clinical frame. *Radiother Oncol* 2009; 93(2):331-40.

van't Riet A, Mak AC, Moerland MA, Elders LH, van der Zee W. A conformation number to quantify the degree of conformality in brachytherapy and external beam irradiation: application to the prostate. *Int J Radiat Oncol Biol Phys* 1997; 37(3):731-6.

Yoshioka Y, Nishimura T, Kamata M, Harada H, Kanazawa K, Fuji H, Murayama S. Evaluation of anatomy-based dwell position and inverse optimization in high-dose-rate brachytherapy of prostate cancer: a dosimetric comparison to a conventional cylindrical dwell position, geometric optimization, and dose-point optimization. *Radiother Oncol* 2005; 75(3):311-7.

Appendix Planning Guidelines for GammaMedplus Manchester-Style T&O Applicator and Henschke MRI-Compatible T&O Applicator

Applicator descriptions

These flexible-geometry applicators can be used for both PDR and HDR treatments. They consist of an intra-uterine tube (tandem) and ovoids in a range of shapes/sizes to accommodate variations in patient anatomy. Both applicator sets include three tandems with different curvatures whose IU length is varied by placement of a cervical stopper. For the Manchester-style set, tandems have 15°, 30°, and 45° curvature; for the Henschke set, 0°, 23°, and 45° curvature. For both applicator sets, ovoids have outer diameters of 20, 25, and 30 mm corresponding exactly to the small, medium, and large ovoid dimensions in the classical Manchester system.

Imaging

A CT scan of the pelvis with 2mm slice thickness is recommended for treatment planning with BrachyVision. Markers are not required as the planning system is able to locate dwell positions accurately within each applicator channel with respect to the channel tip, once the applicators have been defined.

Applicator definition

The CT volume image display should be manipulated (translate, rotate, adjust display window) so that the tip one of the applicator channels is fully visualized in an image view (typically the para-sagittal). A lower display window setting of 600HU works well. The applicator can then be entered from that view, placing the tip at the outer end of the catheter, ie. the point of the arrow marking the applicator channel tip should coincide with the catheter outer end. The other two applicator channels are entered in the same way.

Defining a new applicator in BrachyVision causes the applicator properties window to be opened for data entry. The value to enter for the applicator property "First Source Position [cm]:" depends upon which applicator is being used (Manchester-style or Henschke), and which applicator channel is being entered (IU tube or ovoid). The following table summarizes the required values for each applicator and channel:

Applicator	Channel	First Source Position [cm]
Manchester-style	IU tube	0.2
	Rt ovoid	0.2
	Lt ovoid	0.2
Henschke	IU tube	0.1
	Rt ovoid	1.0
	Lt ovoid	1.0

The values for all channels of the Manchester-style applicator and the IU tube channel of the Henschke applicator reflect the catheter thicknesses at the tips. The first source position for the Henschke ovoids must be pulled back 1.0cm to place the source at the geometrical center of the ovoids (value applies to all ovoid sizes). Note that the planning system adds a fixed offset of 3.5mm (distance from the inner end of the channel to the center of the first source position) to the First Source Position value to obtain the actual first dwell position. After the first source positions have been specified, dwell-time weighting is done in exactly the same way for both applicators.

Dwell-time weighting

In the classical Manchester system originally designed for use with Ra-226 tube sources of 20mm total length, and in the ideal geometrical arrangement of applicator components, component loadings and dose rates are as follows:

Applicator component	Loading [mg Ra]	Point A dose rate [cGy/h]	Point B dose rate [cGy/h]
Tandem, 6cm length	15-10-10	35.0	8.8
Tandem, 4cm length	15-10	35.0	7.0
Ovoids, small	2×17.5	19.0	7.4
Ovoids, medium	2×20.0	19.0	8.2
Ovoids, large	2×22.5	19.0	9.0

The GammaMed Plus afterloader has a default source step size of 5mm, so the useful working correspondence "4 dwell positions" = "1 Ra-226 tube" can be made in the tandem. In each ovoid, only the single dwell position at the ovoid center is used (to provide the best possible dose uniformity on the ovoid surface.) With these correspondences, relative dwell-time weights for PDR can be inferred from classical Manchester system loadings, as follows:

Applicator component	Relative dwell weights
Tandem, 3-8cm length	1.50, 4 dwell positions beginning at start position
	1.00, remaining dwell positions above stopper
Ovoid, small	$1.75 \times 4 = 7.0$, first dwell position (ovoid center)
Ovoid, medium	$2.00 \times 4 = 8.0$, first dwell position (ovoid center)
Ovoid, large	$2.25 \times 4 = 9.0$, first dwell position (ovoid center)

The relative contributions of GammaMed Plus applicator components to the dose at Point A will then follow closely those in the classical Manchester system. Absolute dose contributions are of course determined by normalization to the prescribed Point A dose per pulse (e.g. 60cGy per hour). Note that a clinical directive to use a starting dwell position in the tandem other than the first dwell position is equivalent to using a shorter tandem, and so is fully accommodated by the above relative dwell weighting scheme.

Chapter 5 Summary and Conclusions

Since the first treatment of uterine cancer with ^{226}Ra in 1908 [Johns and Cunningham 1983], intracavitary brachytherapy has evolved to become the most-used tool for treating cervix cancer [Khan 2003]. This is because in brachytherapy the radioactive source is introduced into the uterine cavity in the vicinity of the tumor, which allows a very high central dose to be concentrated in the tumor, while there is a rapid dose fall-off in the surrounding normal tissue.

With the ready availability of CT and MRI, a modern treatment planning system, a single stepping-source PDR afterloader, and a CT/MRI compatible treatment applicator, the CCI embarked on a study of 3D image-based cervix cancer treatment planning in 2008, based on recommendations from a GEC-ESTRO working group [Haie-Meder *et al.* 2005, Potter *et al.* 2006]. The advantage of this technique is the possibility of employing the enhanced soft tissue resolution offered by MRI to delineate tumor and surrounding normal tissues, and adapt the dose distribution to the target volume for each individual patient. This allows an adequate dose to be delivered to the tumor volume while providing greater sparing of OARs, potentially producing greater local control rates than possible with the traditional Machester loading pattern which is based on a set of generic rules.

Two main aspects of the technique, as implemented at the CCI, have been addressed in this thesis. One is that the MR image of the applicator is usually distorted due to the large magnetic susceptibility difference between the applicator and surrounding soft tissue. Hence accurately locating potential dwell positions in the applicator on MRI is very difficult. One solution to the problem is to perform CT-MRI fusion to transfer the position of applicator from CT to the MR images, so that the applicator geometry can be defined nearly as accurately as for CT [Krempien *et al.* 2003]. To evaluate the geometric distortions of a titanium

tandem and ovoids intracavitary applicator imaged by MRI and the CT-MRI registration accuracy, a special phantom was designed for this study.

CT and MR scans of the phantom revealed that the applicator with its tandem source channel was clearly visible on all CT images, while on the MR images the tandem appeared deformed, and the source channel itself was not visible. Image fusion of the CT and MR images was performed and the registration error was evaluated using four pre-defined reference points on both sets of images. The fused images showed that there was a longitudinal extension of the tandem at its tip present in the 3T MR image with respect to CT, having a value of approximately 5 mm, which provides one measure of the MRI distortion. In the transverse direction there are also distortions observed in the MR images of the tandem, but these do not affect the applicator geometry defined by the tandem midline. Given the fact that the applicator geometry remains fixed from CT to MR, it is recommended to use the tandem midline combined with the external surface of the uterus as guides to clinical CT-MR registration. The use of the external surface of the uterus ensures that the registration will be most accurate in the volume of greatest clinical interest. The EMBRACE study dummy run conducted at the CCI using this registration method also agreed with our phantom experimental results.

The experimental registration error was assessed to be less than 0.8±0.9 mm, suggesting that the definition of reference points is reliable and the image registration procedure is accurate and acceptable, though in a clinical setting, registration error is expected to be greater because of organ and tissue motion and deformation. Nevertheless, from a visual inspection of the CCI EMBRACE dummy run images, using the tandem midline and the external surface of the uterus as guides to CT-MR registration appears to be a feasible approach. The phantom studies offered the possibility to correct for applicator distortion if necessary.

The other aspect of 3D image-based cervix cancer treatment planning addressed in this thesis is the development of a clinically robust dose optimization program. As the simulated annealing algorithm has been widely used for optimization problems, especially complex problems involving many variables, this method was investigated in this study. For PDR cervix brachytherapy treatment planning, the optimization process is aimed at determining the dwell time configuration for the applicator based on a set of constraints related to target coverage and OAR sparing, so that the dose distribution can be fitted to the target volume. For this investigation, a computer simulation model was constructed including structures representing the HR-CTV, bladder, rectum and sigmoid, and a clinically relevant set of model parameters was created by incorporating measurements of structure size and location obtained from patient images displayed in BrachyVision. With the model, we investigated the influence of OAR size and distance from the HR-CTV on SA optimization. Optimization results showed that when the OAR sizes and distances from the HR-CTV are in a normal range, the SA method can effectively optimize the dwell times. When the size of an OAR increases, or the distance between the OAR and the HR-CTV shortens, it becomes more difficult for the SA method to optimize the dwell times to meet the prescription criteria of delivering a high dose to the HR-CTV while sparing dose to the OARs.

For the clinically derived simulation model data, optimization starting from three different initial dwell times showed that for “easy” cases (e.g. smaller HR-CTV volumes with good separation from adjoining OARs), there exist multiple solutions to achieve the prescribed dose-volume constraints. Choosing longer initial dwell times tended to lead to relatively longer optimized dwell times which resulted in relatively higher doses to the HR-CTV and OARs. When dose constraints were stricter for the structure model (e.g. a larger HR-CTV volume immediately adjacent to one or more OARs), the different solutions tended to approach one solution (true minimum of the objective function), and the DVH parameters of the slightly different plans were close to each other. This is a feature of the SA method as we discussed in Section 4.1.4.

As mentioned in Chapter 4, it is not practical to let the optimization program determine the actual number of dwell positions, hence we investigated optimizations starting from a different initial number of dwell positions for the "easy" cases. Results showed that the SA algorithm generated plans using all available dwell positions, and that these plans still satisfied the dose constraints. The difference between these plans is not easily detectable by inspecting the DVH parameters reported, but can be seen to directly affect the isodose distribution in the irradiated area. Generally, although plans with a greater number of dwell positions tended to have shorter individual dwell times, they had greater total dwell times- and unnecessarily larger reference volumes. Considering that individual dwell times do not differ much, a plan with fewer dwell positions is preferable, since it has a smaller reference volume and is usually associated with a higher COIN value.

Compared with traditional Manchester plans, in general, optimization led to a reduction in the dose to normal tissue around the target while providing adequate coverage of the HR-CTV by the prescribed dose. A second difference distinguishing an optimized plan from a traditional one is that the former often resulted in a higher point A dose. Correspondingly, a Manchester plan delivering a typical prescribed brachytherapy dose of 35 Gy to point A often did not meet the specified dose-volume constraints. A third significant difference is that most of the optimized plans had significantly reduced ovoid dwell times compared to standard Manchester loadings, indicating that the most appropriate ovoid dwell time may not necessarily be as long as that used in a standard Manchester loading.

As for the evaluation tools, the DVH parameters help to evaluate the clinical sufficiency of treatment plans compared with prescription parameters, while the COIN value helps in comparing different treatment plans. COIN takes into account not only the coverage of the HR-CTV by the reference dose, but also the

excess radiation delivered to normal tissues outside the HR-CTV and specifically to the critical OARs.

Note that an upper limit for target dose was not introduced in this study. Consequently, in some cases D90 was much higher than the prescribed dose of 35 Gy. For such cases, it might be appropriate to consider introducing an upper limit for HR-CTV D90 having a high importance factor.

As shown in the present study, 3D dose optimization for 3D image-based cervix brachytherapy can achieve better target coverage while sparing dose to OARs compared to the traditional Manchester loading. As the present work in optimization is mainly based on computer simulation models, the logical next step is to apply the optimization program directly to clinical structures drawn by physicians on CT/MR images. Since the current software works on simulated structures having regular shapes (cylinders and spheres), when it is adapted to investigation of clinical structuress, the program needs to be revised in the aspect of boundary searching for contoured structures. Future work will also require transferring 3D DICOM image data from the BrachyVision system to a research computer.

A clear benefit of applying the optimization method directly to clinical anatomical structures is that the optimized dwell times are practicable for the corresponding patient, and can be fed back into BrachyVision. This would enable direct comparison of the dose distributions and dose-volume parameters obtained with the SA method and the Nelder-Mead simplex optimization method integrated into the treatment planning system.

References

Johns HE, Cunningham JR. *The physics of radiology*. 4th ed. 1983, Springfield, IL: Charles C Thomas. 453-97.

Haie-Meder C, Potter R, Van Limbergen E, Briot E, De Brabandere M, Dimopoulos J, Dumas I, Hellebust TP, Kirisits C, Lang S, Muschitz S, Nevinson J, Nulens A, Petrow P, Wachter-Gerstner N. Recommendations from Gynaecological (GYN) GEC-ESTRO Working Group (I): concepts and terms in 3D image based 3D treatment planning in cervix cancer brachytherapy with emphasis on MRI assessment of GTV and CTV. *Radiother Oncol* 2005; 74(3):235-45.

Khan FM. *The physics of radiation therapy*. 3rd ed. 2003, Baltimore: Lippincott Williams & Wilkins. 358-400.

Potter R, Haie-Meder C, Van Limbergen E, Barillot I, De Brabandere M, Dimopoulos J, Dumas I, Erickson B, Lang S, Nulens A, Petrow P, Rownd J, Kirisits C. Recommendations from gynaecological (GYN) GEC ESTRO working group (II): concepts and terms in 3D image-based treatment planning in cervix cancer brachytherapy-3D dose volume parameters and aspects of 3D image-based anatomy, radiation physics, radiobiology. *Radiother Oncol* 2006; 78(1):67-77.